UNIVERSITÀ
DEGLI STUDI
FIRENZE

DOCTORAL PROGRAMME IN INDUSTRIAL ENGINEERING
DOTTORATO DI RICERCA IN INGEGNERIA INDUSTRIALE

XXX

Steering feeling characterization by means of a hardware in the loop approach

ING/IND-14

Doctoral Candidate
Francesco Vinattieri

Supervisors
Prof. Renzo Capitani

Ing. Claudio Annicchiarico

External Referees
Prof. Massimiliano Gobbi

Prof. Massimo Guiggiani

Dean of the Doctoral Programme
Prof. Maurizio De Lucia

Years 2014/2017

A Carlo

Summary

Nowadays, the steering systems dramatically affect several aspects of passenger vehicles: performance, safety, driving pleasure and others suffer this influence. Additionally, differently from other systems, the driver's perception of the vehicle is greatly possible thanks to the steering wheel; therefore, it explains the more and more interest in their development, having the human factor as the central point. Moreover, the growing diffusion of electric power steering systems, mainly for reasons of efficiency, has contributed to sustain this interest. Indeed, removing the hydraulic circuit in favour of an electric actuation, the energy losses are reduced and consequently the global efficiency of the vehicle increases. In addition, specific control logics can be deployed for different functioning conditions, allowing a perfect integration with ADAS – Advanced Driving Assistance Systems. Unfortunately, all these benefits are counterbalanced by a longer and more demanding process of tuning.

Typical developing approaches that make use of test drives have been confined to the last phases of the verification, gradually introducing alternative methodologies, whose core are driving simulators. The reasons lie in the greater complexity, in the higher costs, in the lower level of repeatability and in the time-consuming process of the classic approaches.

Driving simulators are complex systems created with the main purpose to exploit and combine the features of advanced software for the characterization of the vehicle dynamics, with the human factor. Typically, the steering behaviour is transmitted to the driver using a so-called *feed-back unit,* which is a mechatronic device capable of reproducing the resisting torque using an electric motor. To guarantee this result, an advanced steering model must be used because, although the apparent structural simplicity of the steering systems, the inertial and hysteresis effects complicate the modelling phase.

In this context it is placed the proposed project, which aims at designing and realizing an experimental test bench for steering systems, capable to introduce a real steering unit in the loop of simulation. The main purpose of this apparatus is the reproduction of the force profiles generated by the tires in contact with the road surface at the tie rods, allowing also the rotation of the uprights around their vertical steering axis.

In parallel, a specific steering model has been created, to define a reference point for comparisons to verify the actual benefits brought by the proposed test rig. Furthermore, it was born with a second aim: considering the difficulties in replacing a physical part of the steering rack installed on the test rig, a novel procedure was conceived to speed up the process. It makes use of the model to vary some steering features with a software procedure, which changes the request of tie rods forces without replacing any physical part. It represents a brand new approach for the state of the art.

Table of contents

List of figures

List of tables

Acronyms list

DFT	Discrete Fourier Transform function
DoF	Degree of Freedom
EPS	Electric Power Steering
EPSiL	Electric Power Steering in the Loop
FSM	Finite-State Machine
HiL	Hardware in the Loop
HPS	Hydraulic Power Steering
I/O	Input/Output interface
IMU	Inertial Measurement Unit
ISO	International Organization for Standardization
KDE	Kernel Density Estimation
KPI	Key Performance Index
MNF	Modal Neutral File
MPC	Model Predictive Control
NVH	Noise Vibration and Harshness
PDF	Probability Density Function
PID	Proportional-Integral-Derivative controller
PLC	Programmable Logic Controller
RT	Real Time
SBW	Steer by Wire
SMC	Sliding Mode Control
VGR	Variable Gear Ratios

Research question

The world is witnessing an authentic revolution of the automotive market, which is rapidly moving towards autonomous technology. In light of this change, what answer is provided by the academic and industrial worlds to adapt the development framework to the new specifications?

The driving is going to be intended as a perfect fusion among the driver and advanced driving assistance systems, with a remarkable interest in the steering systems. In this sense, is it possible to find a novel solution that allows a combination of these new methods with a precise characterization of the steering's perception?

Introduction

Passenger cars have experienced an outstanding and inexorable evolution from their appearance. This has covered different fields, pulled by the requirements of improving safety, comfort and driving pleasure. A notable role has been played by the steering systems: nowadays, these are much more than simple assemblies in charge of modifying the vehicle direction but have a significant influence on all the most remarkable aspects mentioned. Furthermore, the introduction and the expected spread of Electric Power Steering (EPS) systems have given an additional weight to these aspects, considering their capabilities of affecting the vehicle handling and the direct integration with the safety systems. Figure 1 shows the outlook on the steering systems allocation in the near future and demonstrates the key role of this new technology.

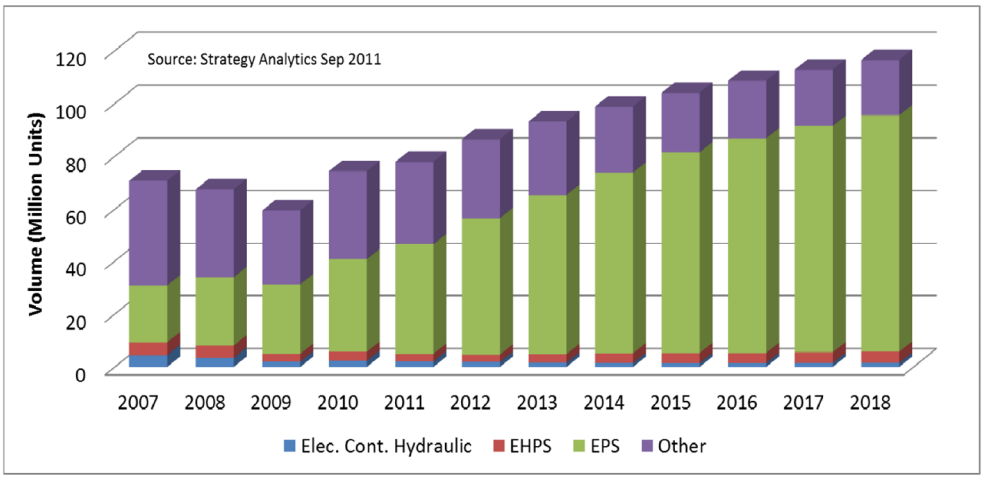

Figure 1 – EPS outlook [1]

However, in this context the challenging requirements of the market have been followed by a decisive reduction of the development time that had required a strong improving of the efficiency of the developing processes. As for almost all the aspects of the vehicle dynamics, the steering systems are currently developed with a process based on subjective assessments, mainly exploiting the advanced skills of experienced test drivers.

For all these characteristics, the research in the automotive field focuses on two main driving aspects. Concerning the subjective testing procedures, their role is crucial for lots of

vehicles' assemblies included steering systems, therefore cannot be abandoned. Nevertheless, the possibility to define clearer and stricter correlations with the objective parameters will result in an easier and quicker interpretation of the outcomes. In this sense, a plenty of scientific publications have analysed this issue and have proposed interesting solutions.

The second point focuses more on the test organizations: campaigns with real vehicles are extremely demanding and time consuming. Thus, the tendency is changing in favour of a new technology: it refers to the introduction of advanced driving simulators that allow testing in completely virtual environments, exploiting the potentialities of specific software to characterize the vehicle dynamics.

Driving simulators have faced different obstacles to reach a good level of realism required to sustain subjective campaigns, but referring specifically to the steering interface the challenge is still opened. The common solution consists of the adoption of feedback units to provide a realistic feedback, utilizing a numerical model that simulates the dynamic behaviour of the steering. Although their diffusion, they are characterized by some limitations hard to bypass: the complexity is enclosed in the representation of hysteretic and backlash effects that are always demanding to numerically model. Nevertheless, most of the time a complete characterization of the steering assemblies is not possible and this worsens the situation.

Some researching groups have proposed alternative solutions to overcome the problem, considering the use of real steering systems installed on specific test rigs.

Research purpose

The introduction of a steering test rig in a driving simulator environment increases the costs and the complexity of the structural layout, but can bring numerous advantages in the steering characterization enhancing the realism. Unfortunately, only few of the presented systems are capable of interfacing with a human being mainly for safety reasons and this represents a serious limitation. In the next chapter the issue will be investigated more deeply, but it can be anticipated how steering systems require a subjective evaluation besides an objective one.

Focusing the attention on those ones which furnish a human interface, the available solutions are limited and few publication can be found from a literature review. However, a large part is not implemented in driving simulators and almost all make use of a single actuator that simplifies the layout and reduces the system complexity but with a remarkable reduction of the efficacy ([2]–[5]).

Therefore the research question addressed at the beginning of the project was: is it possible to conceive an alternative test bench, with the aim of introducing it in a driving simulator in the place of the feedback unit and of providing a realistic response of the steering wheel at the same time?

Research process

The current paragraph is dedicated to a brief introduction of the process followed during the research project.

Before the work was approved, a preliminary stage was faced to verify the feasibility of the project. It entailed two steps: firstly, an analysis of a realistic steering system's performances was carried out to examine in depth the level of performance required. Then, a target driving simulator was identified to understand the actual possibilities of introducing this kind of device: this was selected establishing a collaboration with a company of the automotive field.

Since the answers were satisfying, the project was officially approved. The same results acquired for the preliminary stage were adopted to describe, in terms of objective metrics, the requirements of a generic steering system installed on a passenger car. Then, the designing phase began, with the creation of the most appropriate but also reliable layout; this can be considered as the first part of the project and it was presented by the author during an international conference, in a specific session dedicated to steering systems [6].

The second section entailed the realization of the first prototype of the test rig. It required a characterization of its behaviour which was divided in two parts, one realized before and one after the installation. All the information were then exploited to prepare a control algorithm necessary to compensate the unwanted inertial and friction contributions introduced and transmitted to the rack by the test rig. This process covered a long period due to the experimental nature of the procedure and included the development of a virtual part necessary to speed up the setting.

The first release of the compensation algorithm was the theme of a second scientific publication presented during a national conference [7].

Once the test bench tuning was concluded, the validation phase began. The basic feature to be satisfied was the generation of a force profile at the tie rods calculated by the control unit, therefore the analyses focused on this topic. This part was indicated as objective validation. However, as mentioned, the solution was proposed to enhance the steering feel, hence a subjective campaign was considered as necessary. During the planning, it was decided to realize a specific numerical steering model to compare the dynamic behaviour of the test rig with that of a feedback unit. Indeed, a part from the validation, there was the will of proving the real benefits that the solution could have brought.

Moreover, the creation of the model was the trigger to experiment a novel method to partially reduce a limitation of the test rig: since it considers the installation of a real steering, it was hypothesized a procedure based on the numerical model to virtually variate the response of the test rig, as if a physical part was replaced.

The main results about this last part are will be outlined on a scientific journal publication which is currently in conclusion.

Dissertation outline

- *Chapter 1:* introduces the steering systems, providing all the necessary information to understand the purpose of the project. This can be thought as divided in two principal sections: the first one presents a historical review of these assemblies and a physical description of the main components. The second one describes the physiological features that characterize the steering feel and subsequently gives the attention to the objective and subjective methodologies reviewed. This second part should endorse the importance of the proposed project to improve the current state of the art.

- *Chapter 2:* focuses on the test rig project. Since an optimal design is based on accurate data, the process starts from the analysis of data acquired with instrumented vehicles on the track. The information are post-processed and guide the definition of the layout. Furthermore, these help to select the actuation system typology and size, together with the sensors. The structural evaluation by means of static and dynamic analyses conclude the chapter.

- *Chapter 3:* deals with the numerical model of the steering system. A short analysis of the state of the art is required to describe the main features of the system and to select the most effective friction model too, before the creation of an adequate model. Its parameters are selected with an experimental procedure: this allows to get information mainly about the assist system and the friction model. As last point, the model is validated with track results: this permits to underscore the model benefits compared to the others available on literature.

- *Chapter 4:* describes the test bench installation and setup. In detail, after the assembling, the test rig is integrated with the driving simulator. At this point, the experimental campaign starts and the main features are characterized: friction and inertial components. All the information are then combined in the control logic previously defined: the tuning phase of the controller covers a large part of this chapter. The validation of the compensation logic concludes the process, while the chapter finishes after the presentation of the reverse steering model, necessary to modify some features of the mechanical steering system installed.

- *Chapter 5:* proposes an analysis of the main results obtained in online simulations. Both objective and subjective evaluations are shown, comparing the outcomes of the numerical model. The results highlight the benefits of this proposed solution.

- *Chapter 6:* concludes the dissertation summarizing the entire process and highlighting the advantages brought by this solution. A specific paragraph is dedicated to the possible developments.

1. Steering systems

The first chapter of this dissertation is dedicated to the core of the entire project: the steering system. If the introduction describes to the readers the main purpose and the structure of work and the dissertation, this has the role of providing the basic concepts necessary to comprehend the importance of the project.

A global characterization and an overview about its evolution during the years, anticipates a brief introduction about the subjective aspects of this assembly: how the driver interacts with it, which sensations are perceived and which aspects must be taken into account to provide a good steering feedback in driving simulators. Several methodologies available from literature give a framework to characterize the steering system: the main procedures will be presented before the end of the chapter. These clarify where the current work is placed in the state of the art.

The main information presented in the first part, belong to M. Harrer and P. Pfeffer steering handbook [8].

1.1. Definition and historical review

One of the main common feature that identifies a road vehicle is its attitude to proceed over a trajectory imposed by the driver without any constraints of following a pre-defined track, as for the trains. This is guaranteed by the possibility to steer the vehicle using a proper chassis assembly: the steering system. It belongs to an exclusive group of systems which appeared on the road cars since the first prototypes because backbone of a vehicle. Obviously, during the decades the evolution has strongly modified them and brought more effective solutions.

With the steering system was born the lateral dynamics as intended today, which is the capability to control the attitude of the vehicle to change its direction of motion. In other words, one of the basic feature of the vehicle was born with the introduction of the steer.

This provides to the driver the capability to influence the lateral dynamics having the possibility to directly interact with one of the main source of forces: if the aerodynamic effects are neglected, all the forces acting on the vehicle come from the contact of the tires with the road surface. The lateral dynamics of the vehicle is largely controlled with the steering system that defines the wheels orientation in respect to the vehicle body. Indeed, the deformation of the tire structure generates lateral forces that create the lateral momentum and a consequent variation of the path.

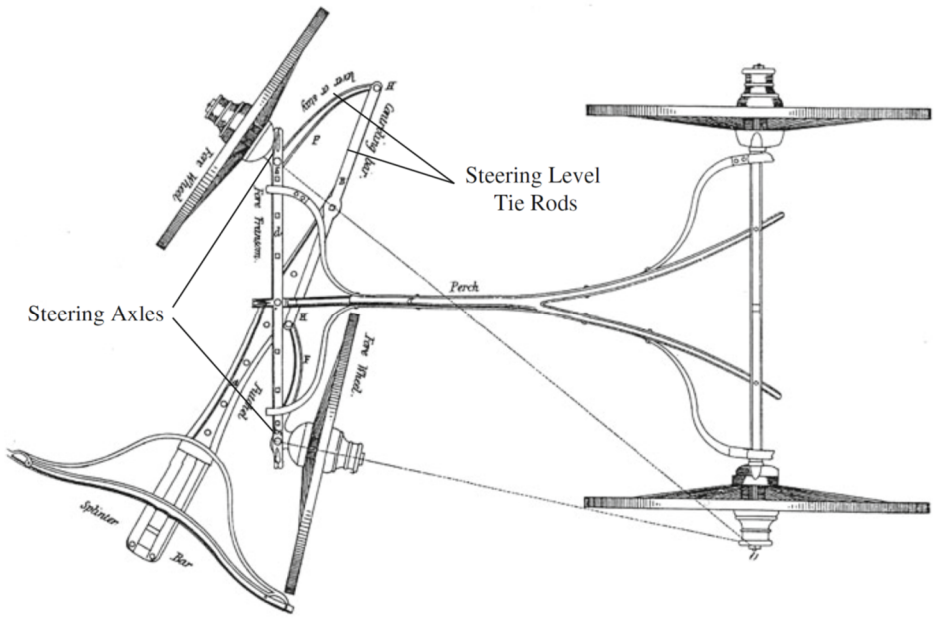

Figure 2 – Ackermann steering system [8]

The first versions of motor vehicles had completely different solutions to steer, inherited by the old carriage pulled by humans or animals, where the driver did not apply any direct action on the directional system. The drawbacks clearly revealed when the human beings started to feel the effort and the discomfort of a direct action on the steering systems, pushed to a deep revision of them.

The forefather of the modern solution was patented in 1818 by Rudolf Ackermann, but the original idea is associated to its friend Georg Lankensperger (Figure 2). This was designed for royal carriage and had the characteristic feature to allow an almost kinematic turn, as visible from the picture. The wheels of the steering axle used independent rotating joints with vertical axis; using a smart system of levers, turning the inside wheel follows a smaller radius than the external one reducing the slip. Nowadays this concept is still at the base of any steering system but it is made use of a steering wheel instead of a steering tiller.

Steering wheels appearances dated back the first years of the *XX* century, with the introduction of mechanical steering gears that facilitated the positioning and the use of the hand wheel. Several solutions were introduced and patented during the years (Figure 3).

The presence of a reduction ratio between the steering wheel and the wheels brought the benefit to reduce the driver's effort required. This aspect has become more and more important during the years, considering the evolution of road cars: heavier vehicles, larger tires and contact patches, higher levels of grip and so on, raised the value of the steering wheel torque required up to an unreasonable level. Hence, at the beginning of the fifties, the first version of power assisted steering system was presented: based on hydraulic system (HPS), it was capable to reduce the effort increasing the level of comfort of the vehicle.

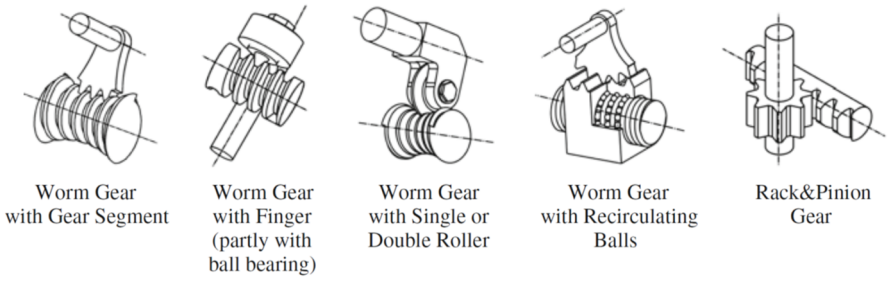

Figure 3 – Basic design of steering gears [8]

Besides the specific versions and their evolution, the HPS has maintained the basic structure and only during the nineties a completely novel solution has been presented: Electric Power Steering system. Basically, the hydraulic circuit was substituted by an electric motor which assists the driver: a suitable control logic uses the information about the vehicle state and the steering angle and torque (measured by a specific torsiometer) to define the request of torque. The possibility to decouple the driver actions from the assist actions has brought several advantages, mainly in terms of comfort, safety and drivability.

Figure 4 – A modern steering assembly [8]

The modern steering systems for passenger cars have some principal and fundamental components: steering wheel, steering column, steering gear and tie rods (Figure 4). The driver acts on the steering wheel and the rotating movement is transferred to the steering gear by means of the steering column. This is composed of several shafts connected with Hooke's joints to allow suitable adjustments of the wheel positioning and, at the same time, an optimal

kinematic movement. The steering gear has evolved during the decades to a common solution, which is nowadays the most widespread: rack and pinion drive. Hence, the rotation is translated into a liner motion of the rack, which carries the spherical joints of the tie rods at its ends. In turn, the tie rods apply a reaction to the wheels' upright forcing them to rotate around the steering axis (physical or virtual). In the end, the rotating effort of the driver is translated to a rotating movement of the front wheels.

Starting from this basic solution, the assembly has evolved introducing new features. For example, to exploit better the system in different driving conditions, Variable Gear Ratios (VGR) were introduced. The additional degree of freedom is used differently depending on the characteristics of the vehicle. For instance, sport cars can have a quick reduction of the steering ratio (the ratio between the steering angle and the average angle of the wheels) to enhance the effect of the feedback torque and consequently the driving precision. On the contrary, the passenger cars can increase the ratio in the central zone to reduce the demand of torque for a parking manoeuver without modify the total rack stroke.

Their evolution for luxury cars has materialized in superimposed solutions; this mechatronic system inserts a heterodyne gearbox between the steering column and the pinion rack gear. The heterodyne, working with the inverse principle of the car differential, is capable to combine the steering wheel angle with the rotating movement of an electric motor to obtain the pinion angle as their combination. Therefore, without mechanically decoupling the assembly, it is possible to intervene and variate the driver's action (Figure 5).

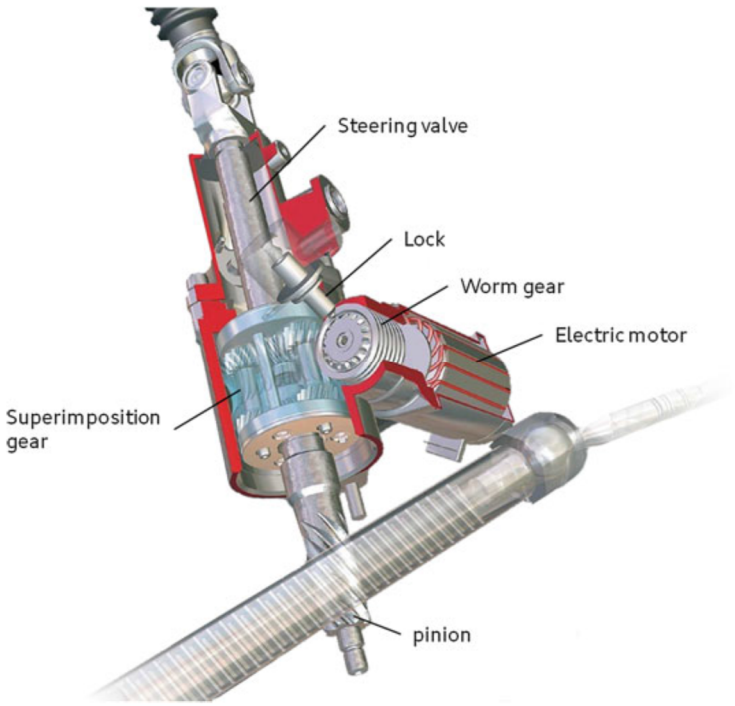

Figure 5 – Cut-away view of the actuator of an active steering solution [8]

This solution is the intermediate step between completely mechanical steering systems and the Steer by Wire (SBW) systems, where not any physical connection between the steering wheel and the rack is required. The driver command is electrically transmitted from an operating element (steering wheel) to an actuator that executes the actions on the rack. Considering the relevant importance of the feedback, a special actuator mounted below the steering wheel, gives a haptic response. In this field, the research is still active to create easier and cheaper solutions, meeting the safety and reliability requirements.

1.2. Steering requirements

As mentioned above, the steering system has the main purpose to control the lateral dynamics of the vehicle. The best solution balances the necessity of a precise and agile behaviour with the request of comfort, where the latter is intended as the capability of the driver to cope with all the driving situations without a great effort.

Moreover, a great attention should be paid on the drivers' prediction of the vehicle response. The steering wheel is the driver interface with the tires that communicates how the forces are generated. A suitable functioning should guarantee that the self-centring steering wheel torque is precisely perceptible and that increases with the lateral acceleration to describe the percentage of tire's lateral grip exploited.

For safety reasons, a reduction of the aligning torque should indicate the achievement of the handling limits. Additionally, the steering wheel returnability is necessary at the end of the manoeuver, without any overshoot. In this sense, the assist units should help the driver reducing the effort without altering the perception of the forces' generation process at the tires.

The importance of the steering feel, which will be described thoroughly in the following paragraph, raises from this concept and it is considered one of the key point during the design of the system. Nevertheless, the complex layout and the high technological level of the modern vehicles require the engineers to pay attention to a large number of contrasting factors but maintaining these basic principles ([9]–[11]):

- *Package:* as said, in modern vehicles all the assemblies have a limited space available and their shape should be optimized for a perfect integration with the others.
- *Weight:* the increasing demand for efficient vehicles brings to impose constraints for the weight reduction. In this sense, the main features that characterize the mass are the type of assist system and the power per mass index. In general, modern EPSs reach higher index values than HPSs.
- *Cost:* the great development of HPSs has brought to standard solutions, optimized in all the main aspects, cost included. The new challenge considers the cost reduction of the newest technologies that consider the electrifications of the steering systems.

- *Quality:* it refers to two main aspects. From one hand the reliability: considering the safety features of this assembly, it must maintain the complete effectiveness for the whole life. Moreover, this considers the quality perceived by the customers, which is significant for the decision to buy one car or another.

- *Efficiency:* as for many other assemblies, the strict constraints for the CO_2 emission's reduction has pushed towards the electrification of the systems. In this sense, EPSs can achieve good results, cutting the energy wasted in the hydraulic circuit.

- *NVH:* acronym of Noise Vibration and Harshness, this term indicates the study of the noise and vibration characteristics of a vehicle, where harshness is a qualitative index of the human impression. The increasing demand of comfort inevitably requires a reduction of them.

1.3. Steering feedback

The subjective characterization of the steering system is at the base of the steering assessment. Commonly, the driver perception is summarized in the steering feel concept, whose knowledge is crucial.

Following the theory well described in [12], the steering feel is thought as a layered structure with two levels: steering feel in a narrow sense and in a broad sense.

The inner layer (steering feel in the narrow sense) is completely related to the physical interface between the driver's hands and the vehicle by means of the steering wheel. In other words, at this level only the steering wheel torque and angle have the capabilities to change the perception, because the feel is completely unrelated to the vehicle: any variation of the vehicle dynamics does not cause any relevant reaction.

The outer layer, as visible in the scheme in Figure 6, defines the steering feel in a broad sense that encapsulates the steering feel in a narrow sense and the vehicle's reactions to the driver. Introducing the concept of generic driving task, the human being operates to modify the steering system and to nullify the difference between the present state of the vehicle and the driving task. In turn, this brings to a vehicle response perceived by the driver and again compared to the driving task. Therefore, the steering feel is the holistic perception, sum of visual, vestibular, haptic and acoustic sensing, of the vehicle lateral dynamics ([13], [14]). A clarification: for vestibular sensations are considered all the perceptions provided by the vestibular apparatus, part of the auditory system of the human being in charge of generating the perception of spatial orientation and balance necessary to coordinate the movement.

A complete dissertation about the physiological aspects defining the human perception in a vehicle falls outside the main goal of this work, but some brief comments are fundamental. Figure 7 describes a driver sat in driving position, holding the steering wheel and pressing the pedals; in addition, all the human perception paths are sketched. Taking a cue from several works identified during a literature review, it is interesting to understand how a human being

perceives the vehicle motions, as well as the feedback of angle and torque at the steering wheel during its actuation.

Referring to Table 1, generally the vestibular and haptic perceptions are faster than the visual signals; more in detail, the information are used together to detect the rotation movements, while a strict separation appears for the identification of the translation movements.

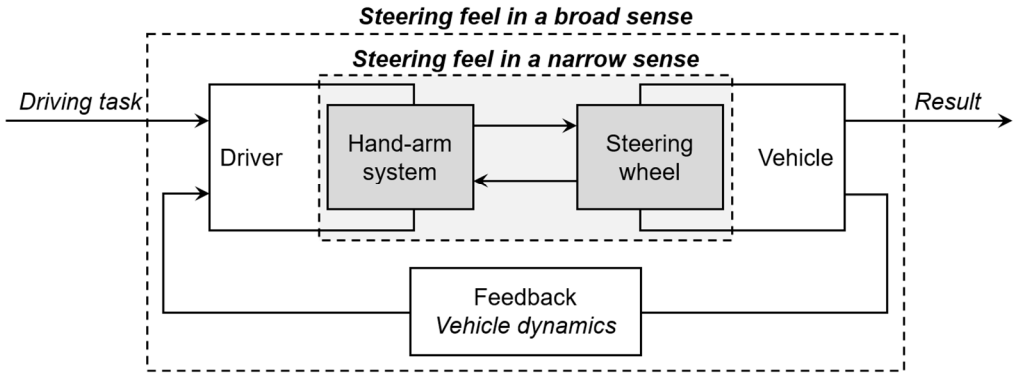

Figure 6 – Definition of the steering feel with two distinct layers

Referring to the haptic system, it plays a crucial role for the steering where only a limited influence of the visual system is demonstrated for the angle identification. Anyway, the driver perception of angle and torque is similar, therefore it raises the question: which information are used by the driver to generate the steering feel?

The answer is both: the driver associates the idea of steering feel to the perception of the vehicle lateral dynamics features, therefore all the haptic sensations are useful to fulfil this task. During the steering feel assessment, the driver decides a quantitative rating about the vehicle dynamics felt in comparison to its main idea of the reference steering system in those conditions. Thus, it is the result of a subjective comparison between the expected perception and the sensed perception.

To give an idea about the expected perception, consider that these are produced by some internal model of the driver, based on several information: from the vehicle segments, to the DNA of the vehicle, from the tires used to the weather conditions and so on.

As a corollary of this concept, it is explained the entire process adopted by the driver to control the steering wheel. As already describe above, the human being is a controller that compares the driving task with the actual state of the vehicle: neglecting for a moment the other control elements at the driver's disposal, the steering wheel is actuated to reduce this difference.

To achieve this goal, commonly a target of angular position is generated and the driver uses a torque open-loop controller, which is based on the internal model of the driver. The controller's feedback is the vehicle behaviour, while the direct feedback torque is useful to dynamically update the driver's internal model of the steer system behaviour.

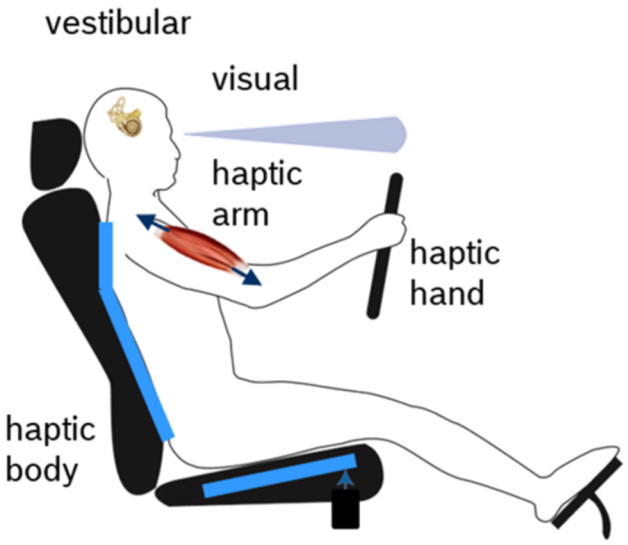

Figure 7 – Human perception path with relevance to vehicle guidance [12]

This brief introduction about the physiological aspects of the steering feel assessment has the main aim to underscore the complexity of the subject. Furthermore, the main indication about the steering that can be extrapolated is that a good characterization of the steering systems is basically based on two aspects: a proper mimicking of the system behaviour both in terms of angle and torque, supported by an accurate description of the vehicle dynamics required for a suitable feedback.

Table 1 – Human ability to perceive vehicle movements and steering wheel behaviour during its actuation [12]

Motion		Visual	Vestibular	Haptic			Perception threshold
				Hand	Arm	Body	
Longitudinal	$u\ /\ \dot{u}$	++					$90\ mm - 0.06\ m/s$
	$\ddot{u}$		+		o	++	$0.02 \div 0.8\ m/s^2$
Lateral	$u\ /\ \dot{u}$	++					$75\ mm - 0.054\ m/s$
	$\ddot{u}$		++		o	+	$0.05 \div 0.1\ m/s^2$
Vertical	$u\ /\ \dot{u}$	++					$215\ mm - 0.145\ m/s$
	$\ddot{u}$		++		o	+	$0.02 \div 0.05\ m/s^2$
Yaw	$\theta\ /\ \dot{\theta}$	++					$4\ deg - 0.6 \div 0.9\ deg/s$
	$\ddot{\theta}$	+	++				$0.05 \div 5\ deg/s^2$
Roll	θ	++	+				–
	$\dot{\theta}\ /\ \ddot{\theta}$	+	++				$0.2\ deg/s - 0.1 \div 0.2\ deg/s^2$
Pitch	θ	++	+				–
	$\dot{\theta}\ /\ \ddot{\theta}$	+	++				$0.4\ deg/s - 0.1 \div 0.2\ deg/s^2$
Steering wheel	θ	+		o	++		$0.2 \div 2\ deg$
	T_θ			+	++		$0.5 \div 1.5\ Nm$

u / $\dot{u}$ / $\ddot{u}$ = position / velocity / acceleration
θ / $\dot{\theta}$ / $\ddot{\theta}$ = angle / angular velocity / angular acceleration
++ = primary perception path
+ = secondary perception path
o = subordinate perception path.

1.4. Subjective characterization

The evaluation of the steering features coincides with the characterization of the lateral vehicle dynamics that includes two aspects: the subjective and the objective components, respectively feeling and performance [15].

Referring to the first point, the previous paragraph has introduced the subject: the steering feels are fundamental to characterize a vehicle response and to judge the global level of comfort. Since the global assessment of a vehicle can pass through the steering, the efforts made to precisely describe and enhance the steering perceptions are explained.

All the methodologies available to date can be clustered in two main classes: subjective evaluation of the steering feel and objectification. In the first case only information provided by the drivers are considered while in the second one the subjective information are combined with objective measurements.

Commonly, a pure subjective evaluation method is based on a sample group of non-professional drivers with different skills, who assume the task to drive the vehicle in different driving conditions and to observe it. As mentioned, the subjective assessments are affected by the personal experience, therefore these methodologies always require a sufficient number of test drivers.

Specific instructions to realize the manoeuvers are provided and an accurate survey is prepared to facilitate the task of the drivers. The most common rating criteria refer to a ten-points scale, where ten is the optimum. Although the surveys' questions are not rigidly defined, some characteristics criteria can be listed in accordance with [8]:

- *Steering wheel torque magnitude and tendency during a parking manoeuvre*
- *Steering wheel torque at the centre*
- *Centre feeling – Centring*
- *Steering wheel torque curve*
- *Steering wheel torque when cornering*
- *Response properties upon straight driving*
- *Response properties under lateral acceleration*
- *Straight driving*
- *Accuracy*
- *Steering wheel angle demand during the parking*
- *Steering wheel angle demand when lane changing*
- *Steering return*
- *Remaining angle after cornering*
- *Steering dynamics.*

The list of criteria can change, while the methodology to prepare the test and to acquire data are similar. On the contrary, there are changes concerning statistical and mathematical tools introduced to process the information: the basic idea is to define reasonable correlations between the different ratings, useful to understand how to intervene.

The second group of possible assessment techniques attempts to turn subjective driving perceptions into objectively measurable parameters, combining the drivers' information with the data acquired during the manoeuvers. Two examples can be described:

- *Characteristics-based correlation analysis*: using the knowledge acquired during the years and/or the correlations described on scientific publications, the objective parameters are extracted from subjective ratings using specific correlations. In this case, the data are directly acquired during the same standard manoeuvers used to evaluate the steering. It is the most spread method, as witnessed by the large amount of publications which adopt it ([16], [17]).

- *Vehicle model based objectification*: similar to the first method, it uses almost the same correlations, but in this case the objective measurements are gained from a car model. Although the identification process is demanding, the reduction of costs is evident avoiding real car measurements [18].

The steering development is still largely based on subjective assessment, but these approaches have several drawbacks. The assigned scores are tightly correlated to the drivers' experience, therefore often the results are scarcely coherent. Moreover, the process is extremely time-consuming and costly, especially after the introduction EPSs that have a greater number of tunable parameters [19].

To reduce the costs, during the last years a smart solution has spread and has progressively substituted the physical test on actual vehicles: it deals with the introduction of driving simulators. Basically, they reproduce a real vehicle (eventually with the actual cockpit) where all the interfaces are available to the driver, but do not control the real vehicle. On the contrary, the information are exchanged with a real time computer that describes the actual vehicle dynamics through a numerical model. The feedback is given to the driver in the form of haptic and visual sensations, the latter using different kind of visual devices. Beyond a specific description of the driver simulator, which will be faced in the next chapters, it has to be noticed that the possibility to use this solution is subordinated to the capability of precisely reproducing the vehicle dynamics and, furthermore, of replicating the steering behaviour.

A driving simulator is a perfect example of Hardware in the Loop (HiL) technique: this indicates a set of different testing procedures to assist the developing of an electronic or a mechatronic device, providing effective system parts that interact with the mathematical representation of the *plant* model ([20], [21]).

The last years have witnessed to a quick diffusion of this technique, pushed by the enhancement of the hardware possibilities but also by the increment of the mechatronic devices that gain the major benefits from the use of the method: the high level of reproducibility, the possibility to speed up the tuning process, the safe testing environment, together with a reduction of costs and time.

In some conditions, as for the driving simulators, human beings are involved because the human factor is crucial to characterize and develop the device or because the model requires a human interaction. Usually, the process takes the name of Human in the Loop. Once in the loop, the human being influences the outcome in a way difficult or impossible to reproduce exactly in an artificial way. Referring to the driving simulator, since the driver is immersed in the event, good results are obtained only reaching a very high level of realism.

1.5. Objective characterization

Most of the time a subjective characterization is not enough, because the actual steering behaviour can be very different than how the system is felt. Therefore, an additional step is required. Objective methods respond to the demand of describing the handling and steering qualities providing objective parameters independently from the driver. This is convenient for the application of the method in comparison to subjective tests: a list of specific manoeuvers have been produced during the years to cover the entire range of functioning and to gather all the information required.

These are divided in *Open-Loop* and *Closed-Loop* tests: in the first case the driver executes vehicle commands (accelerator and brake pedals, steering wheel and gear shift) following a defined time history, independently from the vehicle behaviour. On the contrary, the other imposes a driving task and the driver has to control the vehicle to fulfil it: in this case the vehicle behaviour is influenced by the driver's corrections.

Clearly the second approach limits the objective characteristics of the method, therefore its use is limited to few important tests as the Double-Lane Change for instance.

Referring to open-loop ones, commonly each manoeuvre is standard and described in all the aspects; since an accurate steer profile is required, the driver is substituted with a steering robot. A steering robot is an advanced actuator specifically designed to manage the steering wheel and to replicate whichever manoeuver deployed on its driver unit (Figure 8).

From each test different parameters are gathered, following a structured procedure. The most demanding aspect is the correlation between metrics and steering requirements, which is mainly based on the past experience and on the subjective information acquired in other experimental campaigns with test drivers. However, once the procedure is well defined, it is affected by a lower level of approximation than the previous one. The results can be easily documented and compared with other outcomes, even coming from a simulation environment since the test can be reproduced with a numerical model.

Nevertheless, the procedure has a drawback related to the validity of the information gathered: these describe the behaviour of the tested vehicle in the specific test conditions. It means that a global characterization demands a long list of manoeuvers and these tests must be performed each time some modifications to the vehicle occur.

Figure 8 – Example of steering robot ***(source AB Dynamics)***

The recommended open-loop manoeuvers are summarized in three tests:

- *Step steer*
- *Sine sweep*
- *Weave test.*

In Appendix A the procedures to realize these are described item by item, but in this paragraph a special attention to the last manoeuver is given. The weave test covers almost all driving conditions which are experienced in daily life and therefore represents a crucial aspect for passenger vehicles' steering systems [22]. Indicated as *on-centre handling*, it is described by norm ISO 13674-1 [23] as below:

> *"On-centre handling represents that part of the straight-line directional stability characteristics of the vehicle existing at lateral acceleration levels, typically, no greater than* $1\ m/s^2$*. On-centre handling is concerned primarily with features that directly influence the driver's steering input, such as steering system and tyre characteristics. Thus test schedules for the evaluation of on-centre handling behaviour seek to minimize other factors that influence the wider aspects of straight-line directional stability, such as disturbance inputs due to ambient winds and road irregularities".*

Even if the norm prescribes a superior threshold of lateral acceleration equal to $1\ m/s^2$, normally the tests consider the maximum acceleration of $4\ m/s^2$.

This is distinguished from the *off-centre handling* that characterizes the higher lateral acceleration driving conditions; the interest for the latter is however limited because it refers to handling limits conditions usually not intentionally reached if not for emergencies situations.

In accordance with [24], good on-centre handling features are reached if the vehicle requires minimal corrections, if the steering wheel transmits to the driver the amount of correction to apply and if the command is accurate enough.

Several scientific publications dealt with the objective qualification of it, defying a list of basic parameters and metrics ([25]–[27]). In accordance with A. Balachandran, among the most important can be mentioned:

- *On-centre feel*: is the steering wheel torque gradient among $\pm$ 0.5 g of lateral acceleration.
- *Returnability*: defines the vehicle lateral acceleration at zero hand wheel torque. If the vehicle continues to have a lateral acceleration despite the steer torque is null, the level of returnability is low.
- *Torque linearity*: is the ratio of the steering torque gradient between $\pm$ 0.15 g and the value described in the on-centre feel. It is useful to understand the contribution of the power assist in comparison to the feedback torque made by the tires' forces.
- *Effective torque stiffness*: is the torque gradient measured between $\pm$ 20% of the maximum steering input. It characterizes the stiffness felt by the driver when turning: the greater is the value the heavier is the hand wheel.
- *Steering sensitivity*: is the steering wheel angle enclosed by $\pm$ 0.2 g of lateral acceleration. A more sensitive system increases the responsive feel.

All these are extracted from two main plots that are the steering wheel torque versus the vehicle lateral acceleration and the steering wheel torque versus the steering wheel angle (Figure 9).

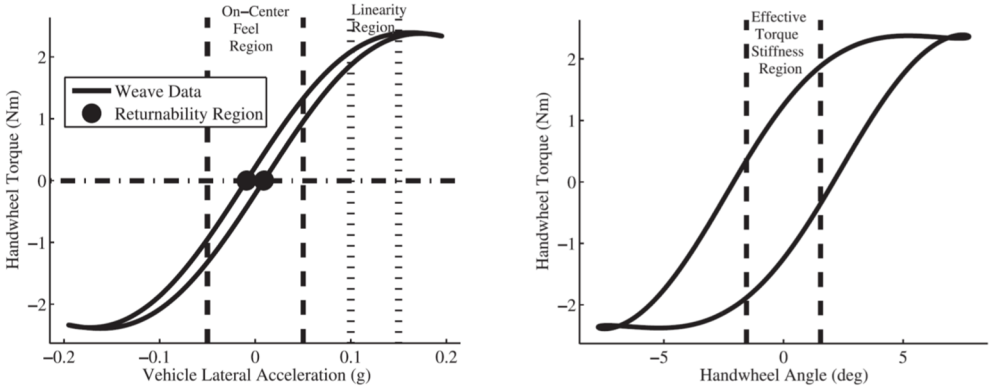

Figure 9 – Example of on-center handling graphs [27]

In conclusion, this chapter has demonstrated the importance of the steering feel in the process of the steering systems characterization but also the necessity to follow subjective and objective procedures to completely describe the steering functioning. In both the cases, and especially for subjective techniques, a reasonable and smart alternative to tests on real cars consists in the employment of driving simulators. But their use is possible if some requirements are guaranteed: the vehicle dynamics should be realistic as well as the steering response.

If the first point is related to the accuracy of the numerical model of the vehicle, the second one depends on how the feedback is created. This highlights the key importance of this project, which sets the goal of raising the realism to a higher level than the current one.

2. Test bench design

In chapter 1 a general overview about the steering systems and the problems related to their development have been introduced. In the same chapter, have been described the methodologies adopted to characterize them, from an objective and a subjective point of view.

The following chapter describes the design process of the steering test bench, which hereafter will be indicated as EPSiL, acronym of Electric Power Steering in the Loop. The name is the perfect fusion of two terms: Electric Power Steering system and Hardware in the Loop method. The first term gathers together all the solutions of steering systems electrically assisted, which are the newest and most advanced nowadays. EPSs represent the future of steering systems and bring to life new challenges that require adequate answers using new techniques; this explain the direct inspiration of EPSiL from these systems, which the entire project (with its choices and principles) was mainly based on.

The chapter is divided in two subsections: a first part deals with the specification of the proper technical requirements to design the experimental test bench. The following presents the most suited layout created for this application.

The project has been widely supported by a partner company; for this reason, some confidential information are protected by non-disclosure agreements and, thus, cannot be revealed or can be reproduced in a normalized format only.

The activity described in the following chapter were presented at the *Steering and Suspension Technology Symposium* during the *SAE World Congress* [6].

2.1. Load case definition

The design phase started from the load case definition. A first attempt conducted has considered a literature review, but with negative results: the principal motive is the lack of data published, especially in terms of environmental and vehicle information. To clarify, the design of an experimental test bench requires a large amount of information not limited to steering systems, but related to vehicle dynamics, suspensions layout and test conditions too; while, quite all the scientific publications do not provide extensive representation of all the data.

Also, another point is the EPS: as said, this project was based on these newest steering systems, but obviously the availability of dedicated literature is limited. Both the reasons pushed towards an experimental phase.

Therefore, the process began from a careful observation of the phenomenon, planning a series of experimental track tests with instrumented vehicles.

All the information have been used for three main points:

- *Selection of the actuation system:* type and size strongly depend on the load and velocity requests at the steering rack.
- *Definition of the mechanical features of the test bench:* characteristics as maximum resistance, local and global stiffness or frequency response, used during the design phase, were specified in accordance with the steering system behaviour.
- *Analysis of the influence of the toe link direction:* as will be thoroughly discussed below, the misalignment of the toe link from the rack direction is origin of friction effects.

2.1.1. Data acquisition

Three different vehicles, ranging from a sports hatchback to a high performance GT sports coupé, have been used for the testing procedures: all the cars were equipped with an EPS. Their relatively high grip performance and large tires' footprint ensured that the data acquired would be on the higher end of what is required (in terms of force, velocity and power) to specify the components of the test bench.

The tests performed were:

- *Double & Severe double lane change (ISO 3888)* [28]
- *Step steer (ISO 7401)* [29]
- *Sine sweep (ISO 7401)* [29]
- *Different test tracks lap*
- *Parking cycles*
- *Low speed curb impact.*

These last two manoeuvers, which are the most critical ones, were selected because pivotal to judge the comfort of steering systems.

Each car was instrumented with transducers described in Table 2. The measurement system includes:

- *Body dynamics sensors:* using mainly Inertial Measurement Unit (IMU) and laser sensors, the body behaviour (if considered as rigid) was completely described.
- *Steering system sensors:* steering wheel data (angle and driver torque) were gathered by specific sensor mounted behind the steering wheel. Another potentiometer was used to acquire the rack position profile. A torsiometer on the electric motor monitored the assistance effect of the power steering.

Finally, special tie rods equipped with strain gauges measured the axial loads flowing through the rack.

- *Suspensions position:* linear potentiometers parallel to damper elements described the vertical movement of the wheel, since the characteristic curves of the suspensions were known and available. In detail, this quantity was used to investigate the tie rod misalignment effect.

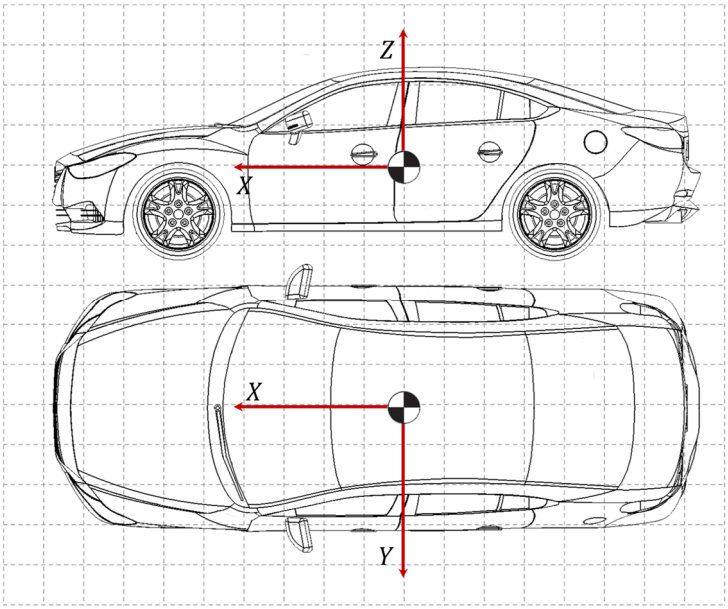

Figure 10 – Vehicle axis system [30]

Table 2 – Measurement equipment

Sensor	Measurement	Unit of measurement
Inertial Measurement Unit	Longitudinal acceleration	m/s^2
	Lateral acceleration	
	Vertical acceleration	
	Roll velocity	rad/s
	Pitch velocity	
	Yaw velocity	
Speed laser sensor	Vehicle speed	kph
	Side slip angle	rad
Measurement Steering Wheels	Steering wheel angle	rad
	Steering wheel torque	Nm
Torque sensor	Electric motor torque	Nm
Strain gauge	Tie rod force	N
Linear damper potentiometer	Damper displacement	mm

2.1.2. Data post-processing

Appendix A describes how each manoeuver has been performed, following the ISO rules; other results here presented are related to tests not regulated by any rules but traditionally considered to characterize these aspects of the vehicle: these will be described before the graphs.

The main purpose of this paragraph is, instead, the illustration of the post-processing method. Indeed, considering the large amount of data acquired, a crucial point is how to transform them in condensed usable parameters and this entails not using time-based graphs of the main quantities.

In this specific circumstance, the first step implied the definition of the main channels to be analysed, some of which *math channels*, so calculated in the post-processing phase:

- *Rack speed*
- *Steering wheel angle & speed*
- *Tie rod forces*
- *Total rack force*
- *Assist force.*

Since a crucial point is the level of noise introduced during the acquisition, it is important to process the quantities to cancel any possible source of error in the interpretation of the data. So, a zero-phase low pass filter (forward-backward filtering [31]) was used: this method avoids a phase shift which is common for the low pass filter used. The cut-off frequency was set to 4 Hz.

Finally, each manoeuver was analysed individually to obtain mainly information to be used for the structural analysis of the test bench and to select the suitable typology and size of the actuation system. This resulted in creating scatter plots of the total rack and assist forces versus the rack velocity: the peak values gave an idea about the maximum thrust and velocity requested at the actuation system.

In addition, some other curves are visible in the graphs: these constant-power lines indicate the necessary level of power for the different functioning conditions. This is a positive aspect of this kind of graph, which simplifies the selection of the electric motor size. As already introduced, the graphs are all normalized according to the same full-scale.

The standard manoeuvers chosen and analysed in this dissertation are the double lane change, the sine sweep and the step steer: the results are shown in the following graphs (from Figure 11 to Figure 13). These are affected by a characteristic behaviour in terms of rack speed: all the points are placed at fixed intervals. The reason is the sampling process: the rack speed originates from the derivative of the steering wheel angle with respect to time. Because of the low resolution of the steering wheel encoder these inaccuracies are generated.

Focusing the attention on the results, the graphs show a similar tendency in terms of force: the values are quite the same for rack speed near zero. Regarding the request of rack speed instead, in the sine sweep manoeuver is greater. The reason is clear: the tests were pushed at high values of frequency (even beyond the limits suggested by the norm) to explore the behaviour of the cars closer to the limits. Thus, high frequencies drive to high rack speeds.

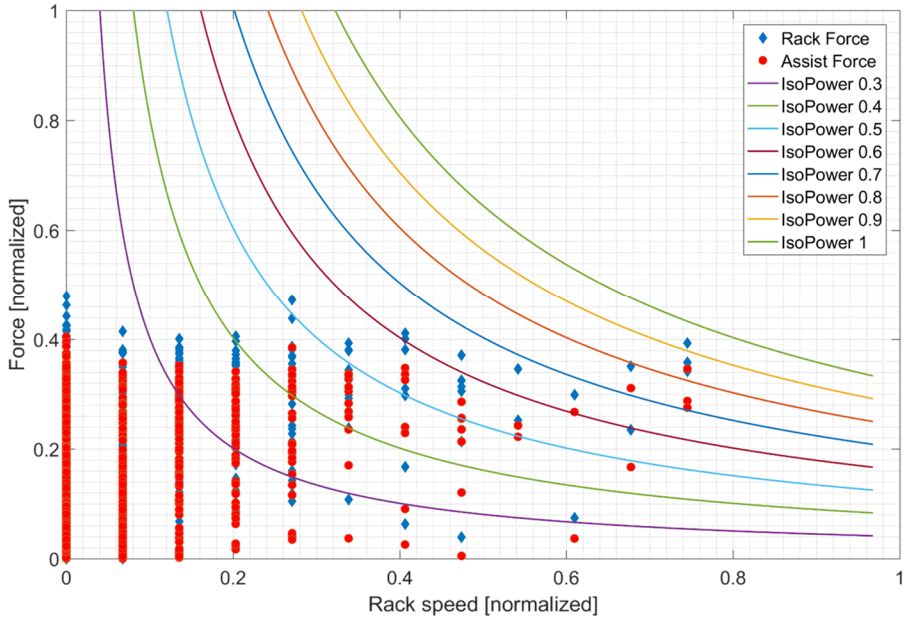

Figure 11 – Lane change manoeuver at 200 kph

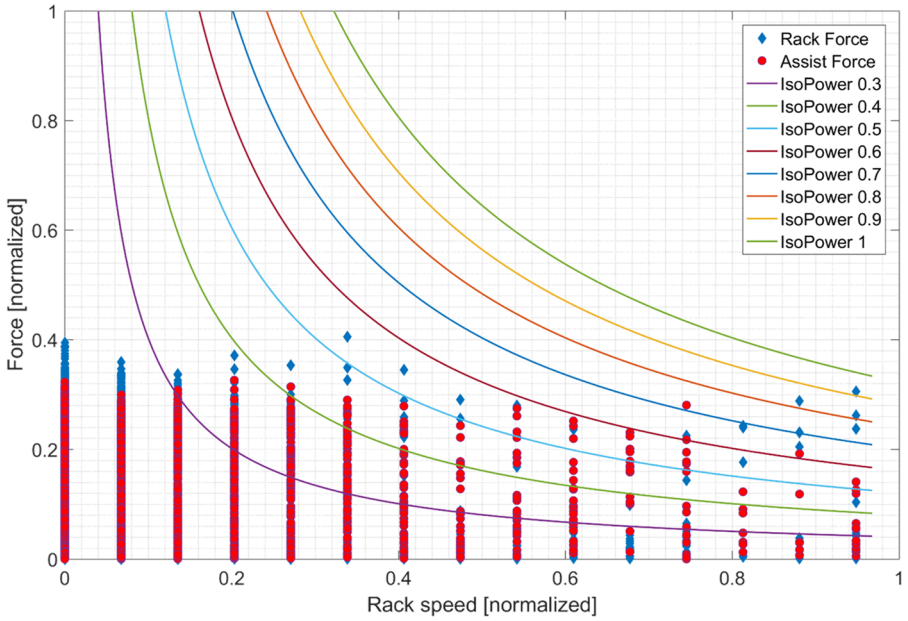

Figure 12 – Sine sweep manoeuver

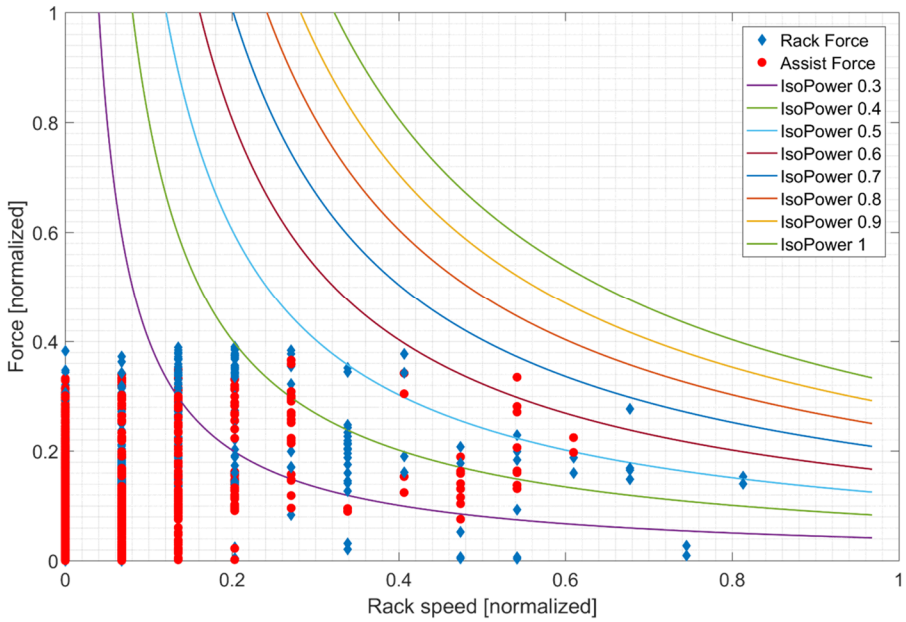

Figure 13 – Step steer manoeuver

More differences are visible in Figure 14, which includes results from different parking manoeuvers and misuse tests (i.e. steering wheel rotation after putting a tire in contact with the sidewalk). It has to be highlighted that these belonged to another experimental campaign previously realized with other objectives; however, the results were used for this analysis as well. The difference appeared clear considering the graph, which is not affected by the sampling problem visible in the others.

Regarding the data, although the level of force measured is higher, the power request is similar due to the lesser rack speed.

Figure 15 concludes the analysis: for reasons of clarity, the results of four different tracks are described by means of the envelope curves. Despite the differences between the circuits, the rack speed requests are similar, sign that it represents a sort limit acceptable for the driving conditions on the track. On the contrary, the requests of rack force are variable: the results are placed among the superior limit defined by the parking manoeuvers and the values of the other standard tests.

All the data attached in this chapter represent a precise selection of a larger amount of data acquired and processed during the experimental campaign, since the main purpose it is not the analysis of the data but a general overview about the method chose to use them.

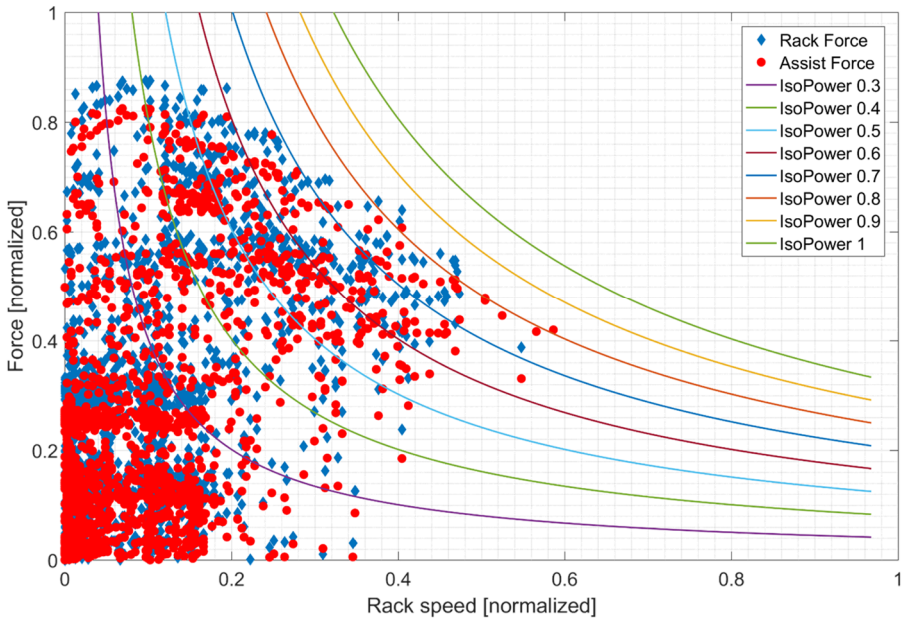

Figure 14 – Misuse & parking manoeuvers

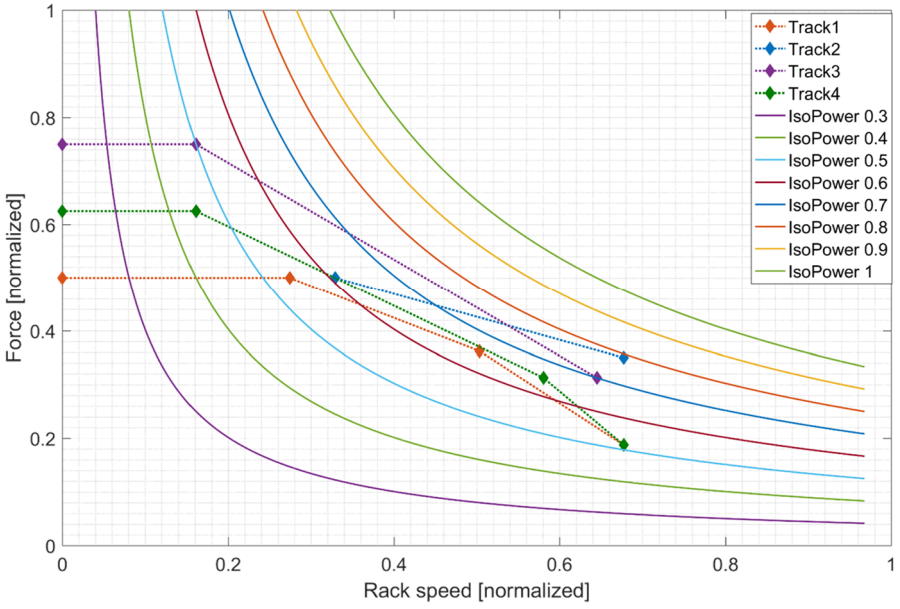

Figure 15 – Track tests

As mentioned before, the information acquired during this phase helped to decide the proper actuation system. Below (Figure 16) the graph shows the comparison between the tests' envelope curve in red (outer limit of the points of all the other plots) and the characteristic curves of the actuator selected for the test rig in blue, transported to the rack using a proper motion ratio.

About the actuator, the dashed line delimits the transient functioning area (where the system achieves the peak of torque) while the continuous one indicates the continuous functioning.

The selected solution fits well the performance requested by the test bench, because the continuous duty range of the actuator covers almost the entire working area. Only a limited part, at low speed and high force, is covered by the intermittent duty range only; anyway, it is not a problem because that area mainly refers to the parking and misuse conditions that are not the main goal for the test rig.

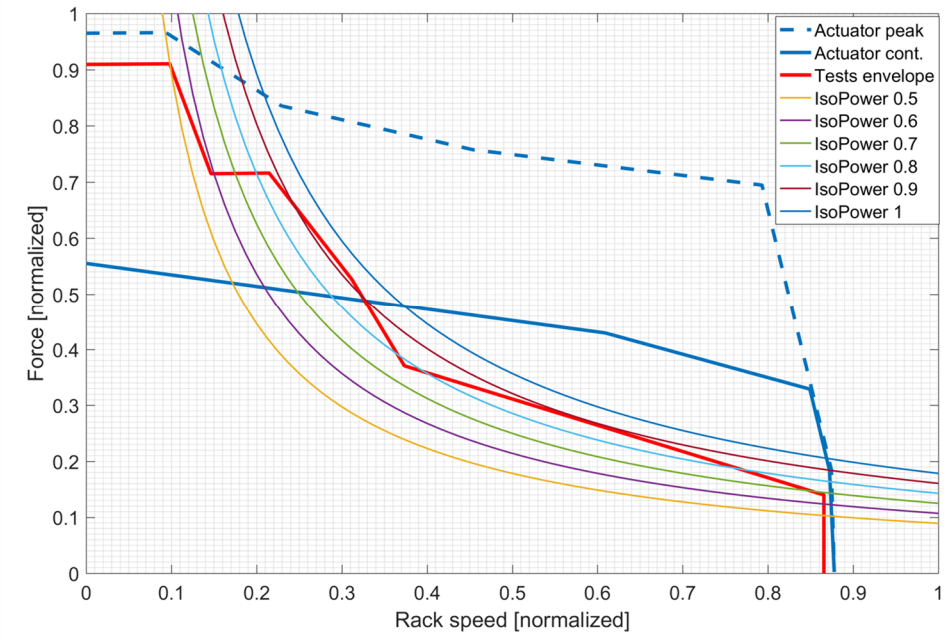

Figure 16 – Comparison between actuator capabilities and rack force/velocity requests

2.1.3. **Rack friction investigation**

At the start of the project, the question was raised about the influence of the movement of the wheel in the vertical direction and around the steering axis on the steering feel coming back to the driver. In particular, the vertical movement of the wheel imposes a radial component of the rack force due to the toe link to rack misalignment and this introduces friction in the sliding bushings which may be felt by the driver. Hence, it was questioned

whether this component of rack force and consequently the steering torque was significant in terms of perception by the driver and therefore important to replicate in the test bench.

For this reason, the experimental campaign previously introduced was organized to acquire the suspension position during the manoeuvers. Moreover, other kinematic calculations were run in parallel: this was possible knowing the exact suspension geometry as well as the rack characteristics.

This allows to know the toe link angle with respect to the rack at any time step, as a function of the steering angle and wheel suspension travel.

The target of this investigation was the understanding of the magnitude of this *misalignment friction* effect on the driver's hand wheel torque. Using this geometric information, as well as the load cell data from the toe links, the following calculations were carried out to define the equivalent driver hand wheel torque which arises from rack sliding friction effects.

- The position of the outboard toe link joint, in the chassis system of reference, was determined by a two-dimensional kinematic lookup table. Each coordinate (XYZ) was described as a function of the wheel damper travel and the steering wheel angle, as illustrated in Figure 17.

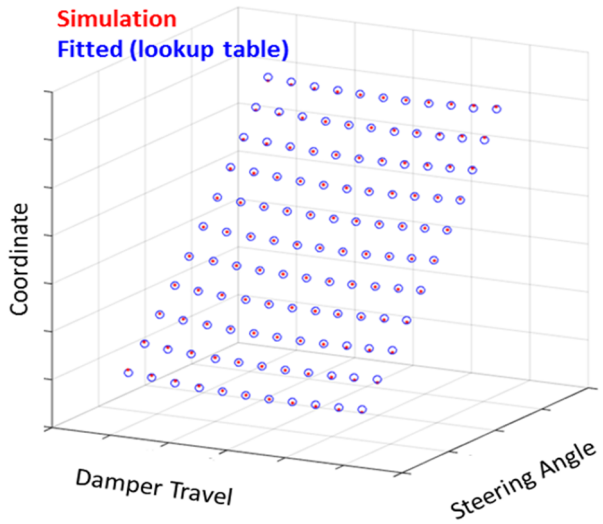

Figure 17 – Example of outboard toe link joint position (generic coordinate) as a function of the wheel travel and the steering wheel angle

- The position of the inner toe link joint (which translates laterally across the chassis) was calculated using the steering angle and the rack ratio.

- A link orientation vector (r_{link}) was defined as the unit vector pointing from the inner toe link joint to the outer joint and composed of three elements: $[r_{long}, r_{lat}, r_{vert}]$.
- The steering rack radial forces were then calculated as the longitudinal and vertical components of the toe link forces. These were found by multiplying the toe link forces from the load cells by the r_{long} and r_{vert} elements of the orientation vector r_{link}.
- The rack bushing friction force was then calculated from the total radial rack force multiplied by an assumed coefficient of friction of 0.35 (brass on steel). It was oriented (in a left/right sense) using the steering rack velocity.

It is possible, due to the parametric nature of the lookup table, to view the individual components of the rack friction force, which are:

- The component coming from the static misalignment of the toe link (in the design condition).
- The component coming from the suspension vertical travel.
- The component coming from the steering input.

The calculated rack friction force together with its components are shown in Figure 18.

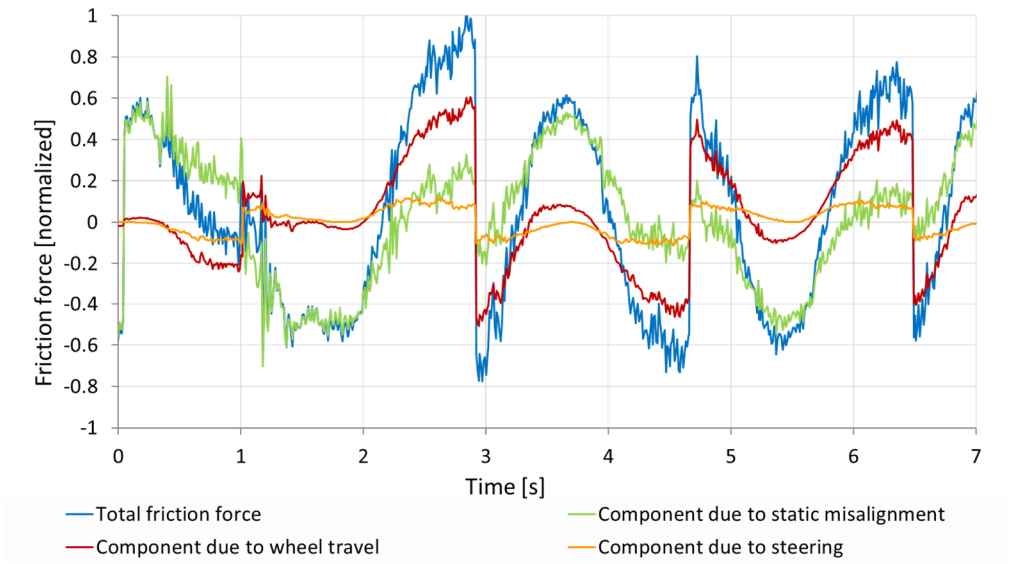

Figure 18 – Rack friction forces due to toe link misalignment

To estimate what these forces translate to in terms of a steering wheel torque after being attenuated by the power steering system, the gain of the power assistance was calculated based on a free body analysis of the steering rack (Figure 19).

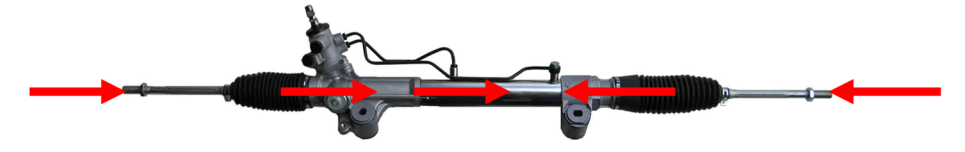

$$\Sigma F_y = F_{ToeLinkLeft} - F_{ToeLinkRight} + F_{Pinion} + F_{Assist} - F_{GuideFriction} = 0$$

Figure 19 – Analysis of the forces acting on the rack

The assist force could be solved as a function of the other previously derived forces:

- $F_{ToeLink}$: are the axial components of the toe link forces found using the toe link kinematics.
- $F_{GuideFriction}$: is the bushing frictional force found above.
- F_{Pinion} : is the meshing force of the pinion and it is equal to the steering wheel torque divided by the pinion radius.

From this, the assist gain (F_{Assist}/F_{Pinion}) was estimated to understand how much the rack forces are attenuated by the steering assist before reaching the driver.

Although the assist gain is not constant due to the nonlinearities of the hydraulic assist, a linear assist level was assumed for these calculations given that the target was to determine the order of magnitude of the friction forces rather than their precise behaviour.

The rack friction force ($F_{GuideFriction}$) was divided by the linearized assist gain (found to be 6 from the experimental data) and the result is an estimation of the component of the driver's hand wheel torque which comes from rack sliding friction effects.

The rack friction component of the steering torque can be plotted on a normalized scale (Figure 20) with the total (measured) steering torque, which shows that the peak-to-peak range of the friction component is approximately 5% of the peak-to-peak range of the total steering torque in this test.

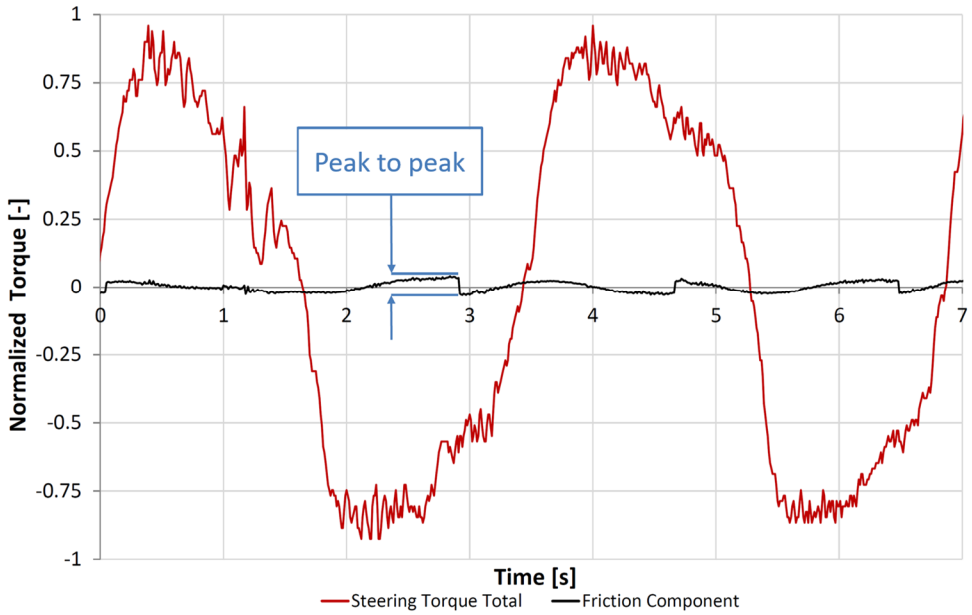

Figure 20 – The steering torque and its friction component shown on a common normalized axis

From this investigation, it was understood that the friction torques are quite small but not insignificant. As a result, it was decided that the first layout of the bench would be designed with a static adjustable misalignment of the toe link to introduce these friction forces; instead, the vertical movement would not be replicated.

This allowed the retention of the misalignment friction effect but limiting the complexity of the bench to a minimum level, by avoiding the need of two actuators for each unit. In other words, it was thought that the relative increase of the accuracy was not worth by the increment of cost and complexity of the structure.

2.2. Layout

As discussed in the previous paragraph, this detailed investigation provided information to design the steering test bench, as for example the use of a simplified solution without any system to reproduce vertical movements of the wheels. Therefore, the structural layout should be considered as a direct outcome of the preliminary analysis conducted.

An important point is the complex nature of the structure which combines together hardware, software and electronic parts to realize a Human in the Loop system.

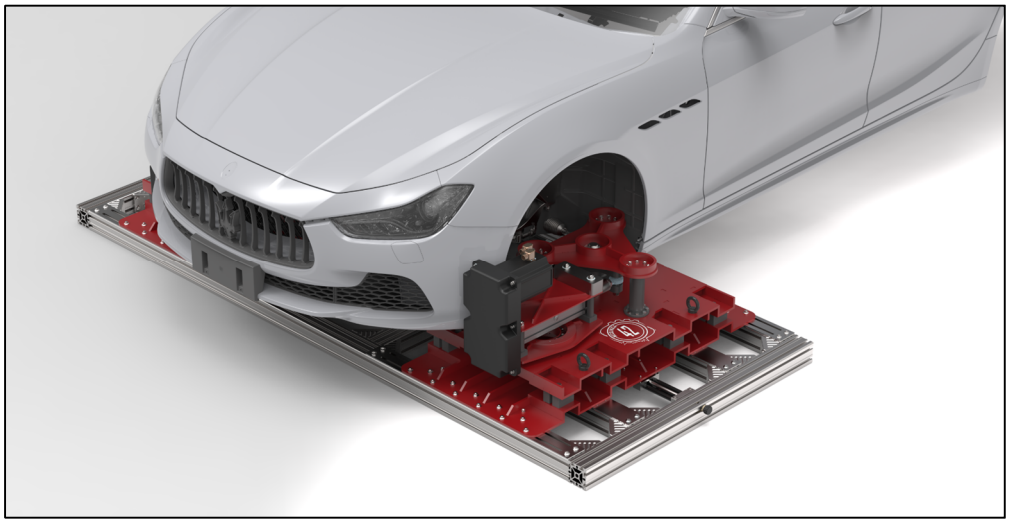

Figure 21 – Preliminary render of the final layout, coupled with the driving simulator's cockpit

2.2.1. **Mechanical structure**

Starting the description from the mechanical structure, this consists of two symmetrical units, one for each front wheel. Each one has a single degree of freedom only, which is the revolution of the wheel around its steering axis. For the reasons explained above, the second degree of freedom (the heave) is not permitted. The description of the test rig will refer to the structure of the left unit, illustrated in Figure 23.

The structure was designed according to the requirements of the driving simulator, in terms of overall dimensions and interface, to simplify the integration. From this point of view, Figure 21 gives a perfect idea about the restricted area allocated to the test rig installation: the zone under the cockpit engine compartment and the zones besides the wheel arches. The engine compartment is deprived of the powertrain, but the entire chassis sub frame is mounted, while outside the vehicle bodyworks, the test rig components must remain invisible to the test driver during a simulation. Hence, the available space is limited.

Furthermore, following the technical specifications, to create a solution usable for a large number of steering racks, considerable adjustments are feasible. In fact, the test rig was specifically designed for the vehicle incorporated in the static driving simulator, which is equipped with an EPS system, but this may be used for different classes of vehicles. Referring to the frame of reference already described, the most significant adjustments are along y and z axes.

The longitudinal adjustments are guaranteed by the longitudinal shift of the base frame (the bottom element of the assembly) over specific guideways, which is laterally fastened to the ground.

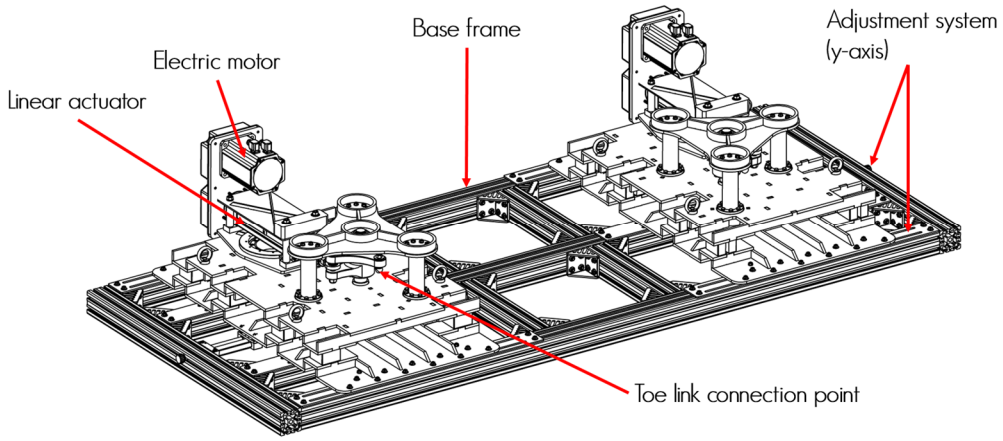

Figure 22 – Test bench structure

Above the base frame, two symmetrical units are placed. Each one has a steel alloy structural frame, which supplies the adjustments along the other two directions. Moreover, it hosts the heart of the whole system on the top, which is the resistance loading system with its main element: an electric linear actuator.

The choice of this solution, consistent with those of other research groups ([3]–[5]), derives from the superior features of electric actuators in these fields, in addition to a higher level of cleanliness. Such a solution is easier to control, with a low response time. The only weakness is the larger physical dimensions in comparison with a hydraulic system of equal power.

For this reason, a specific investigation of the actual loads acting on the steering rack was made to find the best trade-off for the linear actuator's size and performance (2.1.2).

Besides the linear actuator, the kinematic chain includes other two main elements: a rotating table and a rocker. As illustrated in Figure 23, the rod end of the actuator, which is fastened upon the rotating table, is attached to one end of the rocker.

The other rocker end is then connected to the toe link of the steering system: the choice of this solution originates from the possibility to emulate the actual toe-torque of the vehicle by mimicking the wheel rotation around its steering axis.

This allows the consideration of all the effects connected to the steering rod inclination, impossible to be investigated with a direct connection of the actuator to the rack.

Another possible solution, adopted by other authors and manufacturers, utilizes a rotary actuator: even if it eliminates the rocker, this solution is characterized by a greater weight and overall dimensions due to the required motor performances.

The rocker is arranged such that two attachment points lie in a common horizontal plane with the steering rack. This eliminates vertical force components from the toe link that increase the test bench stress; also, these components can create friction forces, which affect the ability of the system to reproduce the simulated toe link loads.

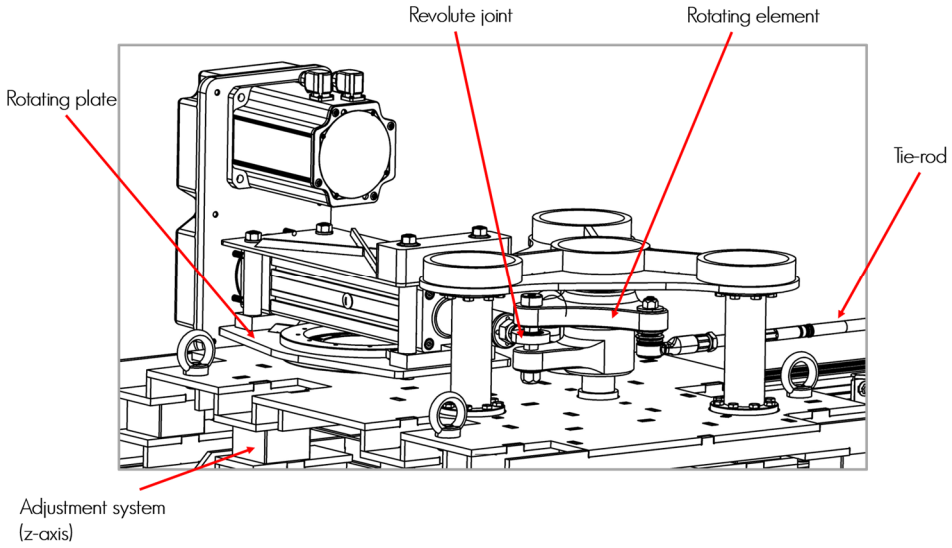

Figure 23 – Test bench structure – Single unit (zoom)

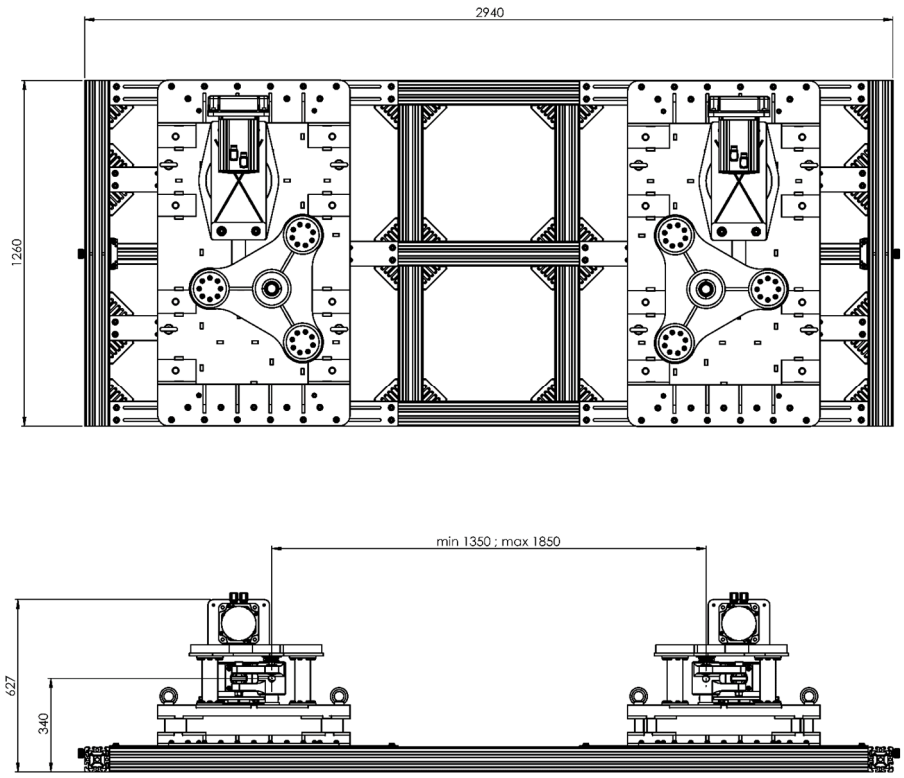

Figure 24 – Test rig overall dimensions

2.2.2. Actuation and control system

Being a mechatronic system, the mechanical part is joined with an actuation system. The solution is a couple of electromechanical linear actuators composed of an electric motor connected to a ball screw cylinder using a toothed belt.

Two electrical drivers, one for each motor, command their actuation. In Table 3 the main features of the actuators are summarized.

2.2.3. Sensors

The test rig is equipped with sensors. According to Table 4, the steering wheel has a special sensor that simultaneously monitors angle and torque applied by the driver.

On the rack another sensor (optical) is installed to calculate the rack displacement: this could appear as a redundant measurement, but it is necessary because of the elasticities and backlash effects of the kinematic chain; the rack speed and acceleration is calculated as the derivative of the position signal with respect to time.

Two axial load cells are mounted on customized tie rods to measure the forces applied by the actuation system. Since the requests for these cells were strict in terms of range, accuracy and frequency response, a custom solution has been chosen. As will be highlighted in a following chapters, a control system is necessary to guarantee the perfect functioning of the test bench and it uses a feedback controller based on this channel. Thus, the more accurate is the acquisition the better is the accuracy of the controller.

Both the electric motors have a digital encoder (relative but with zero position indicator) to monitor their position and their velocity.

Lastly, two Hall's effect magnetic sensors are used as safety devices to switch off the system in case the linear actuator goes out of functioning range. Specific details about the main sensors are described in Appendix D.

2.2.4. Integration with the simulator

As declared in the introduction, the EPSiL project was conceived to be integrated into a static driving simulator. Therefore, the design phase was subjected to dimensional constraints.

The test rig has a single base frame necessary to guarantee the alignment of the two symmetrical units, but this frame has a low profile required to position and fasten the simulator's cockpit in the middle of it.

Similarly, the two units have a compact structure to avoid any interference with the wheel arches. Adjustment methods are available to allow the right positioning of the steering system that, at the same time, is fastened to EPSiL and connected to the cockpit's sub frame. Figure 25 shows the actual configuration after the coupling.

Definitely not the least important one, it is the description of the communication system represented in the flow chart of Figure 26: starting from the left side, the entire simulator is managed by a Real Time (RT) operating system on a RT hardware that schedules all the tasks at a fixed time step. A commercial software (Vi-Grade *CarRealTime*™) is used for modelling and simulating the vehicle in real time.

Table 3 – Main characteristics of the actuators

Applied Loads - Linear actuator (single)	
Peak thrust (kN)	20
Continuous thrust (kN)	2
Maximum speed (mm/s)	300
Nominal speed (mm/s)	50
Maximum power (kW)	2.7
Actuator stroke (mm)	200
Maximum rocker rotation - with a 120 mm lever arm (deg)	40
Force control bandwidth - mechanical limit $[-3\ dB]$ (Hz)	30

Electrical features	
Two programmable electrical drivers (with PLC)	-
Current/drive monitoring (MHz)	1
Internal position/speed loop (kHz)	8
Power Supply Voltage (V)	150÷500
Peak current $(Arms)$	30
Interface	EtherCat
Additional digital/analogue input-output	-
Digital encoder (incremental)	25 bit

Table 4 – Test bench sensor list

Sensor	**Measurement**	**Unit of measurement**
Measurement Steering Wheels	Steering wheel angle	rad
	Steering wheel torque	Nm
Axial load cell	Tie rod force	N
Laser distance sensor	Rack displacement	mm
Electric motor encoder	Electric motor rotation	rad
Hall's effect magnetic sensors	Safety switch	$Boolean$

An Input/Output (I/O) interface connects this computer to other devices, mainly through serial communication using EtherCat protocol. The network is divided in two branches: one is dedicated to the simulator and all its tasks, while the other to EPSiL.

Concerning the latter, the system can be thought as composed of four main parts: the driver units, the linear actuators, the sensors and the mechanical part of EPSiL with the steering system.

The core are the drivers, which operate as network nodes: they acquire the sensors signals, control the electric motors, monitor the test rig and constantly communicate with the RT system.

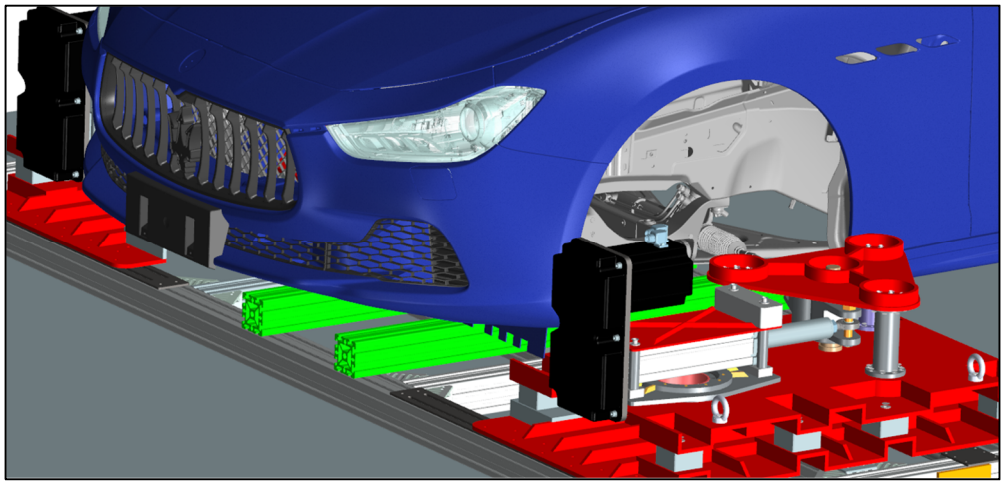

Figure 25 – Integration of EPSiL with the static driving simulator

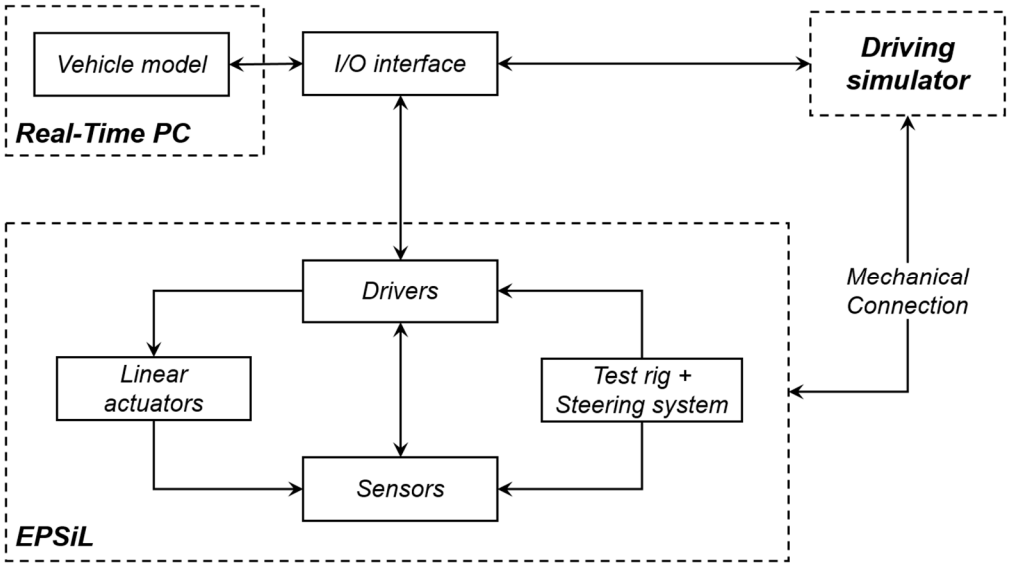

Figure 26 – Simulator flow chart

What happens at each time step it is described below to clarify the process. The vehicle model calculates the forces on the two tie rods; the values are converted in a serial message and sent to each electrical drive. The driver combines these information with the signals coming from the sensors and input them to the control algorithm; the output is the current level

to be generated, which the drivers provide to the electrical motors. The electrical power is converted to motor torque and then to longitudinal force applied to the rack.

The results are acquired by the sensors which send these information back to the real time hardware; among these measurements, the rack displacement read by the optical sensor is used to describe the vehicle dynamics at the following step. In this manner the loop is closed.

2.3. Kinematic studies

The relations describing the kinematic chain of each unit are the subject of this paragraph. Approached in an early phase of the design process, the outcomes of this analysis were useful in more than one occasion: during the definition of the layout, they were used to verify the interference of movable parts; for instance, the rigorous dimensional constraints forced to a specific investigation of the table's rotation to avoid any sort of possible contact. The results, together with the maximum stroke required by the technical specifications, were used to select the nominal length of the actuator's rod.

Also it has been analysed the evolution of the torque applied to the rocker during its rotation with a constant force exerted by the linear actuator. The misalignment between the force vector applied by the actuator and the tangential direction of the rocker has a double effect: it reduces the actual torque created and increases the mechanical stress of the bearings. This last kinematic relation was also introduced in the control algorithm, to modify the force target as a function of the rocker rotation angle.

To be precise, since the rocker angle is not monitored by any specific sensor, the kinematic relation (1) is used to indirectly acquire it by means of the measurement of the rod displacement. Figure 27 helps to describe how this relation was defined.

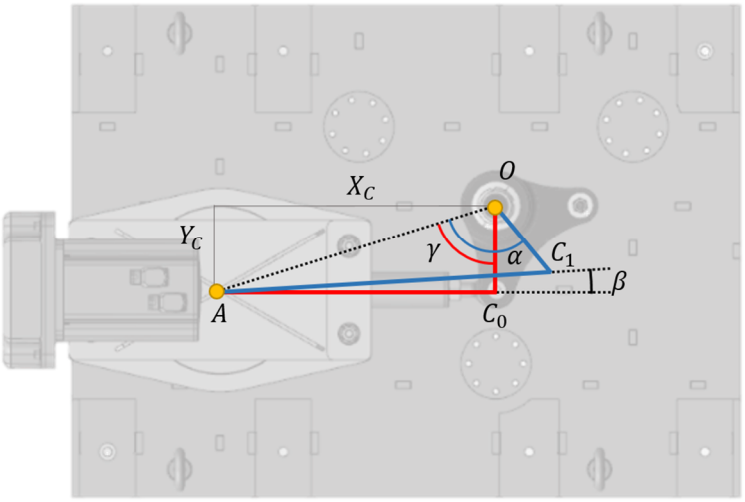

Figure 27 – Kinematic relation: rod displacement as a function of the rocker angle

$$X_{Act}(\theta) = \left(\sqrt{R^2 + (X_c^2 + Y_c^2) - 2R\left(\sqrt{X_c^2 + Y_c^2}\right)\cos(\gamma + \theta)}\right) - L \qquad (1)$$

where:

$OC_0 = 0C_1 = R = Rocker\ arm$

$L = AC_0 = Rest\ position\ distance$

$X_{Act} = Actuator\ rod\ displacement$

$OA = \sqrt{X_c^2 + Y_c^2} = Rotating\ center\ distance$

$\gamma = \cos^{-1}\left(\frac{OC_0}{OA}\right) = Rest\ position\ angle$

$AC_1 = \sqrt{OC_1^2 + OA^2 - 2\,OC_1 OA\cos(\alpha)} = L + X_{Act}$

$\theta = \alpha - \gamma$.

The planning of this activity occurred at the beginning of the design process, as said, during which the continuous variations of the layout required specific methods to verify pros and cons and to analyse even the less significant aspects.

Considering the results valid for the definitive version of the structure, presented in Figure 28, it is clear how even great rotations of the rocker do not imply consistent angles of the table or variations of the rod displacement to rocker angle ratio (the difference relative to the linearization curve is minimal). Despite that, Figure 29 proves that a reduction of the rocker torque occurs during the rotation, thus a correction function is necessary.

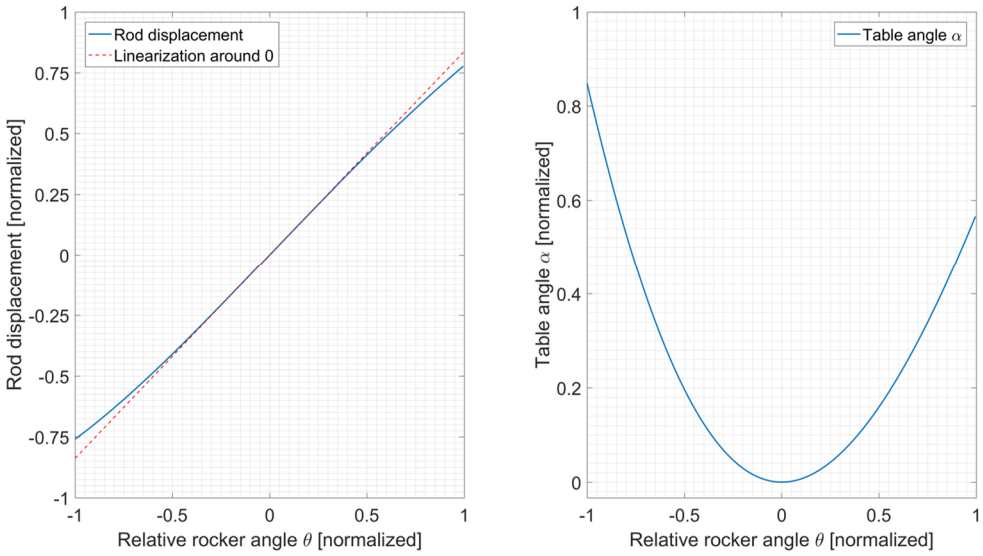

Figure 28 – Rod displacement and table angle versus relative rocker angle

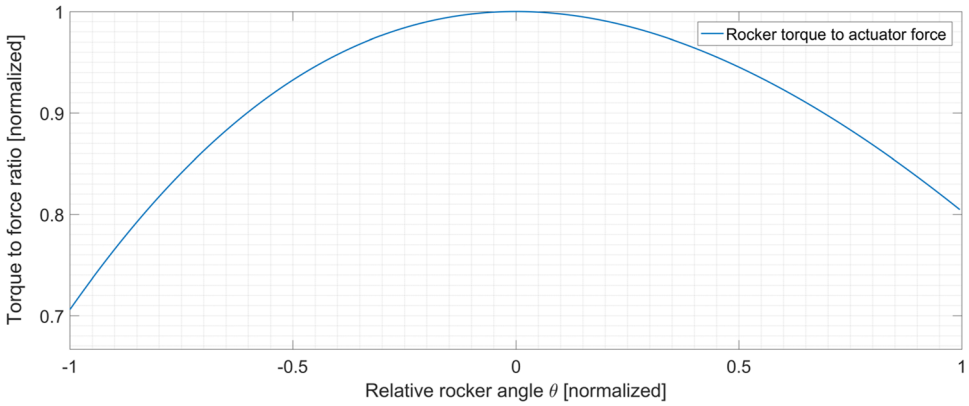

Figure 29 – Rocker torque to actuator force versus relative rocker angle

2.4. Structural analysis

The main structural requirement was an adequate stiffness, because for a correct functioning, the position of the rocker must remain fixed during the application of the loads. This means a careful analysis not as much in static conditions, but rather in dynamic ones to check possible interferences between the load spectrum and the frequency response of the test bench.

Regarding the first point, some finite element analyses of the main deformable elements of the structure helped to verify the static conditions. Instead, the dynamic conditions required a specific method consisting in a multibody approach with a flexible frame.

Ideally, the analyses could have been realized with a finite element method but with a lower level of efficiency. Indeed, despite an undeniable complexity of defining the actual load conditions to be applied, this method provides specific information about the structural stress for each single node, which however is not interesting. On the contrary, the mixed approach gives the required information about the displacements reducing the degrees of freedom.

The process has seen several consecutive steps. In the first instance, the frame structure has been built up in a finite element environment. This facilitated a modal analysis, which helped in the preliminary phases of the project, for example to decide the disposition of the aluminium extrusions. Furthermore, this represented the basis to generate a Modal Neutral File (MNF), which can be imported into the multibody environment ADAMS/View™. It contains all the information about the flexible parts as the inertial matrix, a selected set of mode shapes and frequencies of the model and the position of the chosen interface nodes.

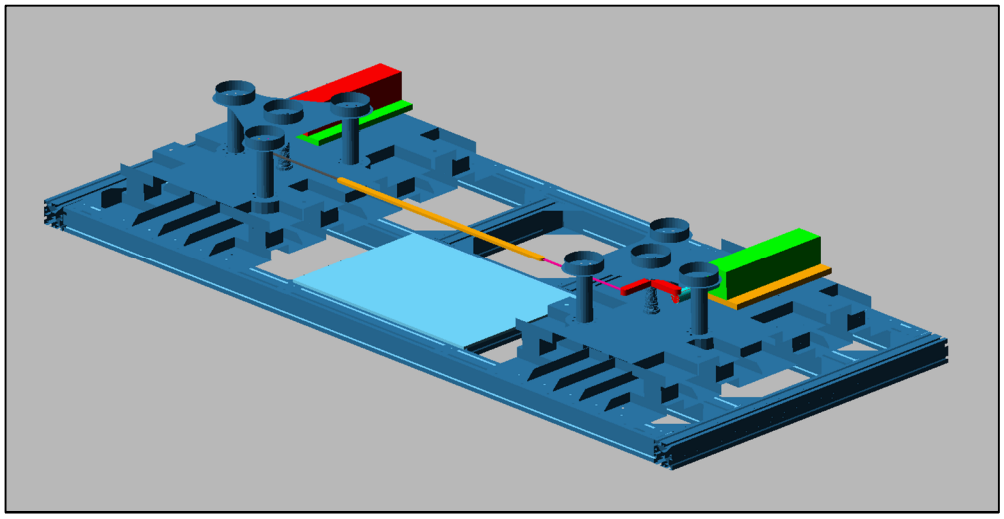

Figure 30 – Flexible multibody model of EPSiL in Adams/View environment

In parallel, a multibody model of the test rig was prepared simplifying the structure. Great attention has been paid to its inertia that would have severely altered the steering torque feedback: the inertial components of all the main elements that compose each actuator were represented as an equivalent translating mass attached at the end of the actuator's rod.

To investigate this effect one of the design conditions was selected: the steering wheel has been actuated following a sinusoidal input and the resisting forces opposed by the linear actuators were modelled as simple linear viscous actions. The two graphs below (Figure 31) show the inertial effects distinguishing the forces acting on the rack's ends in two components: axial and radial. On the right ordinate the total axial and radial forces are shown, whereas on the left ordinate the inertial component of the same force. All the curves are normalized with respect to the same maximum value.

Considering the results, although the effects of the inertial components could appear limited, their influence on the steering torque is dramatic. Therefore, the outcomes of these graphs recommended the deployment of a specific strategy to compensate the inertial effects.

At the end, the data from the two models have been combined: the MNF file was input to the multibody model and the simulations have been run again to compare the results and to point out the influence of the structural flexibility. Again, the resisting elements have been modelled as viscous dampers (with a constant damping coefficient) and a sinusoidal input, sweeping a defined frequency range, has been imposed to the steering wheel.

The process was aimed at verifying the proper working range of the test rig, evaluated through a comparison with the rigid equivalent structure. A suitable condensation of data is illustrated in Figure 32, where the magnitudes of the axial forces at different frequencies, obtained using the Discrete Fourier Transform function (DFT), are illustrated. In account of this, in order to reduce the number of tests, a logarithmic progression of the frequency with base two was adopted.

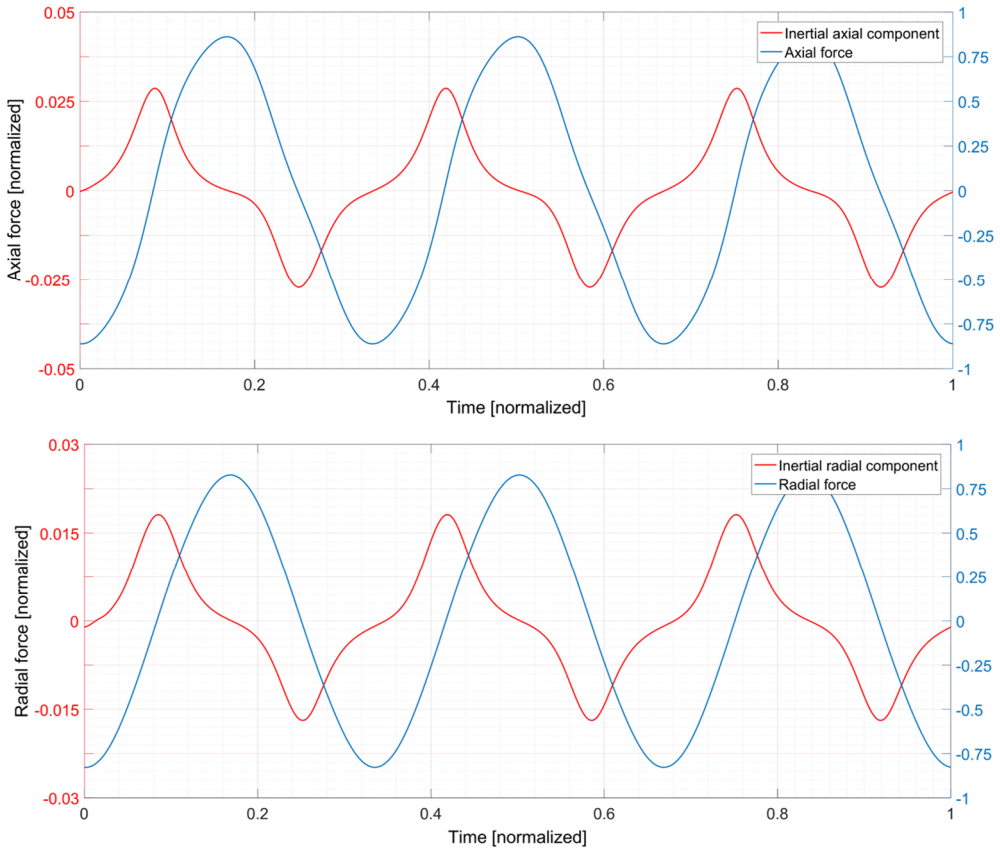

Figure 31 – The effects of the inertia on the axial and radial forces

As may be seen, after a certain frequency, the curves' tendency is different: it means that the flexibility of the structure changes the resisting load values and, consequently, modifies the steering torque. In other words, this indicates the functioning limits of the test rig, which, however, matches the target range of frequencies indicated in the specifications. Thus, the stiffness of the structure accomplishes the goal set, despite the apparent difference in comparison with other solutions characterized by massive frames. The keystone is represented by the aluminium extrusions that are able to reach high stiffness to mass ratio, with equal dimensions: it is an important difference that catches the eye at a first comparison.

Furthermore, this consideration is supported by the shorter height of the proposed test rig: limiting the height there is a reduction of the possible deformation effects, therefore also the size of the structure can be lowered.

In addition to the study of the test rig frequency bandwidth, were considered the effects of the radial force changing with the frequency (Figure 33). As already said, this component is directly related to the friction effects, which contribute to the resisting torque generation.

This study shows that below a certain frequency (of about 40 Hz) the radial component is substantially equal for the rigid and the flexible solution. Over this point, some fluctuations are present, due to the combination of the inertial and the structural deformation effects. Nevertheless, it might be deemed a good solution considering the functioning range indicated.

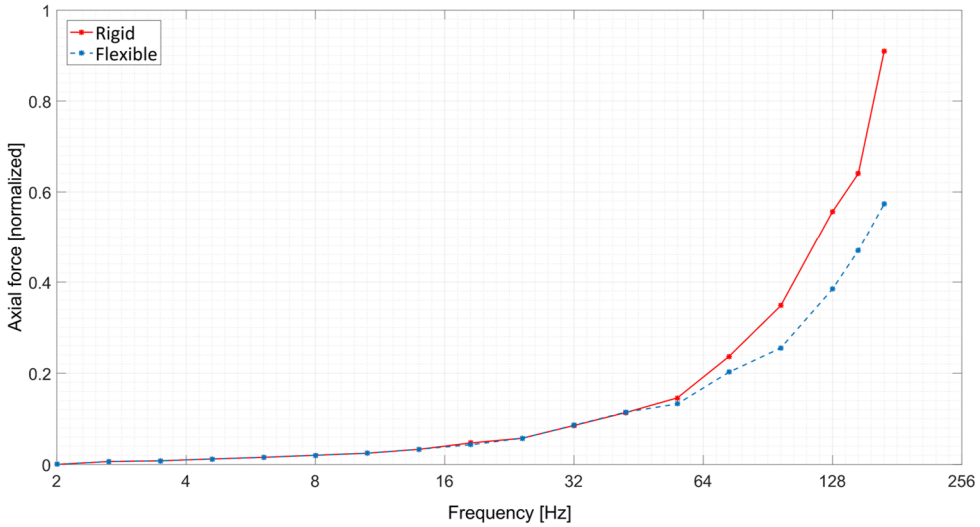

Figure 32 – Peak of the axial force normalized with respect to the actuation's frequency. The data in abscissa are spaced in logarithm progression with base two

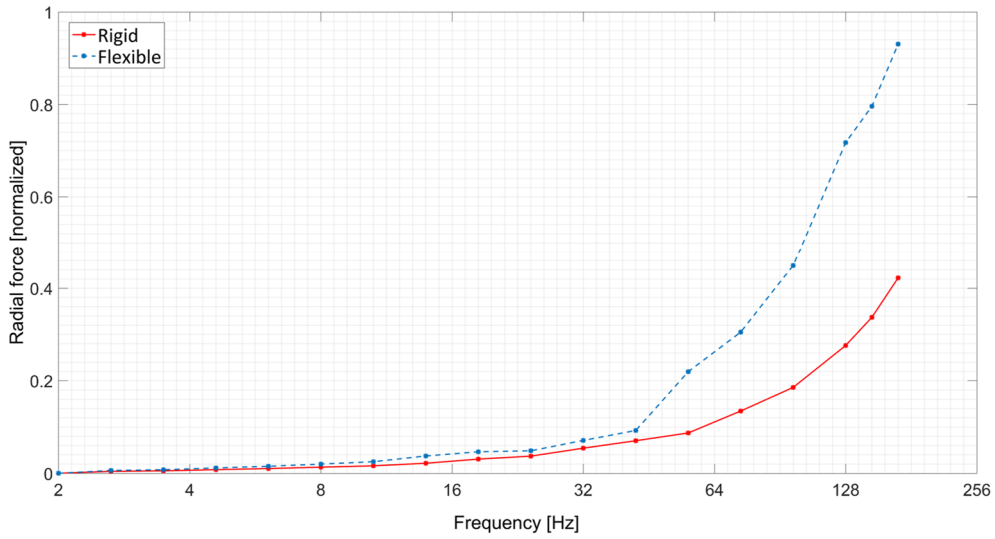

Figure 33 – Peak of the radial force normalized with respect to the actuation's frequency. The data in abscissa are spaced in logarithm progression with base two

3. Numerical model

Chapter 2 is dedicated to describe the design process of the steering test bench. This started from a preliminary experimental campaign to set the project's targets necessary for the following design phase. Then, once the final layout of the test bench was presented, a dedicated paragraph showed how it is integrated into the driving simulator, considering the description of the communication system used with the simulator.

Differently from the previous one, dedicated to an experimental apparatus, this chapter illustrates a parallel activity: it deals with the creation of a numerical steering system model. Despite it could be thought as an activity conflicting with the design of a steering test bench, it actually has an important role.

First of all, once verified, this represents the reference point to compare the effectiveness and the advantages of the test bench. In fact, due to the increment of complexity, to the higher costs and to the larger volumes required, the improvements in terms of steering feeling must be significant.

In addition, as will be exposed in the last part of this dissertation, this numerical model is part of a method proposed to overcome some limitations of the steering test bench: the impossibility to change any steering system features from one test to another without substituting physical parts.

Also, not least, referring to the improvements of the steering feedback, this model represents a good solution, especially to understand the main behaviour of a steering system in the preliminary design phase, when a real prototype does not exist yet.

3.1. Introduction to steering system models

A steering system is a complex element that influences many aspects of the driving and for that reason is hard to model. In general, a complete model must satisfy a large number of requirements, often even contrasting:

- Lightness, from a computational point of view.
- Accurate calculation of the wheel steer angle.
- Realistic feedback torque at the hand wheel.
- Numerical stability.

- Ease in the parametrization, without a difficult process to acquire data.

As said, because of the reciprocal conflicts, it is important to choose the correct model for the specific needs. In this sense, it is fundamental the introduction of the main classification of simulations: these are divided in *offline* and *online*. In offline simulations the driver is not involved and the vehicle model runs on the computer; for instance, it is used to study the actual dynamics of the vehicle, without introducing any human effect.

On the contrary, with online simulations are intended all the tests performed at the driving simulator with a driver: the cockpit's interface allows the introduction of the human being in the loop of simulation. From a computational point of view, the main difference is represented by the solver behaviour: for the online simulations it is mandatory the real time functioning, which defines the system response within specified time constraints.

As already mentioned, in offline simulations the steer model is important mainly to understand the vehicle's behaviour, therefore, the fundamental point is how accurate the angular profile is transmitted to the wheels. Because the feedback torque has a minor importance, the model should have the simpler structure possible, which brings benefits in terms of numerical stability.

On the other hand, for online simulations, the key points are the real time features, the numerical stability and an advance capability to emulate the feedback torque. This shows how a single model is not sufficient to cover all the possible cases.

A brief literature review unearthed a large amount of different models, with differences in layout and degrees of freedom.

The easiest one is the kinematic single degree of freedom model: considering a single track vehicle model, the steer angle at the front wheel θ_{Whl} is (instantaneously) equal to the steering wheel angle θ_{SW} multiplied for the pinion to rack ratio. The relation (2) describes the steering behaviour and the feedback torque applying the principle of virtual work. Extremely easy to populate and numerically stable, it shows great limitations to reproduce the steering torque: the main point is the absence of any sort of elasticity, backlash or compliances that are necessary to obtain reliable and realistic results.

Summarizing, this is the perfect model for both offline and online simulations only when the main focus is on the vehicle dynamics regardless the driver.

$$T_{SW}\,\partial\theta_{SW} = T_{Whl}\,\partial\theta_{Whl} \tag{2}$$

where:

T_{SW} = steering wheel torque
θ_{SW} = steering wheel angle
T_{Whl} = kingpin torque
θ_{Whl} = kingpin angle.

An interesting alternative has been presented by Cianetti et al. ([32], [33]), to extend the capabilities of the single degree of freedom model but maintaining all its benefits.

The model is still based on a single mass but the rack position used by the vehicle model is found with a different procedure. The first rack position (labelled as kinematic position) is obtained as the steering wheel angle multiplied for the gear reduction ratio (it can be fixed or

a lookup table to consider modern racks with variable transmission ratio). Calculating the difference between that value and the steering angle at the previous time step, with the hypothesis of a linear torsion bar, the steering torque is obtained. This is the feedback torque used in driving simulators. Concerning the rack position, this derives from the rack acceleration double integrated: the force contributions are the resistive forces coming from the tires, the torsion bar torque transformed in axial force, the friction force (calculated by means of a Maxwell model) and the viscous component.

Considering the ease of the model, the enhancements in terms of steering torque are remarkable, although it is still affected by some important issues: the proposed version lacks of any assistance system, which severely affects the results and the torsion bar dynamics is not modelled. This last point is crucial, especially for all those conditions of steering release when it is not possible to simulate realistic oscillations of the steering wheel.

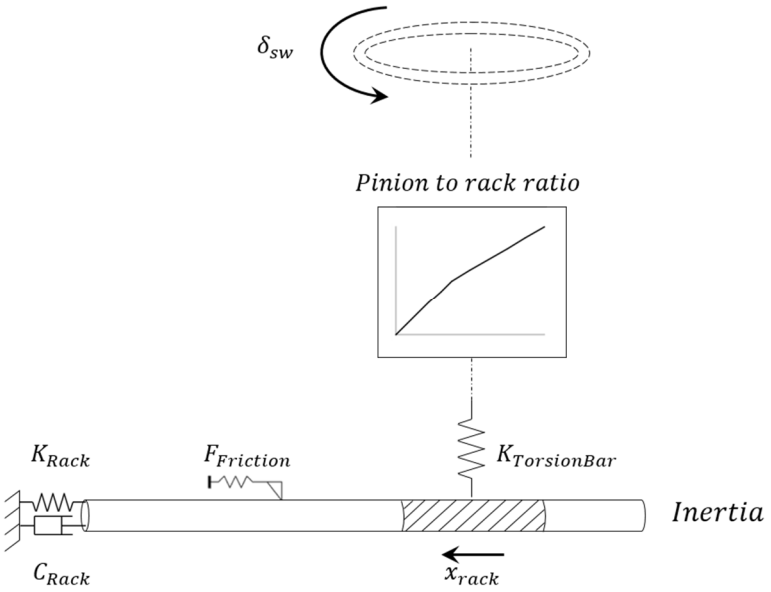

Figure 34 – Advanced single degree of freedom model [32]

The diametrically opposed solution was presented by prof. P. Pfeffer in its doctoral dissertation [22]. This is an advanced model able to reproduce precisely all the main effects, which is recognized to date as the reference model for steering simulations thanks to its completeness and accuracy.

This model receives the steering torque profile and the tie rod forces as input and returns the rack position and the steering wheel angle. It is composed by two sub models: mechanical and hydraulic.

Five different bodies, connected by springs and dampers, compose the mechanical model. As visible in Figure 35, starting from the top, the model's parts are:

- *Steering wheel and first shaft of steering column.*
- *Second shaft (among the Hooke's joints).*
- *Third shaft.*
- *Pinion.*
- *Rack.*

An important role is played by the friction model, which is a crucial point especially for feedback. The authors chose an Exponential Spring Friction model modified with a Maxwell element in parallel, as theorized by U. Neureder [34]. The mechanical system equations (22) are indicated in Appendix B.

Regarding the assist model (Figure 36), this refers to a physical hydraulic model to consider the effective model dynamics. It is based on the definition of quasi-static pressure curves $p = f(\theta_{TorsionBar}, Vehicle\ speed)$ with the addition of a first order delay introduced to emulate the latency typical of the actuation. Again, the extensive discussion of the matter is shown in Appendix B.

As demonstrated in Pfeffer's works, the results attained are realistic as not any other steering model in terms of feedback torque and dynamic response of the system. But the preparatory phase is demanding considering the long list of parameters to identify; therefore, the possibility of using this kind of model is limited to few cases that almost coincide with the steering system producers.

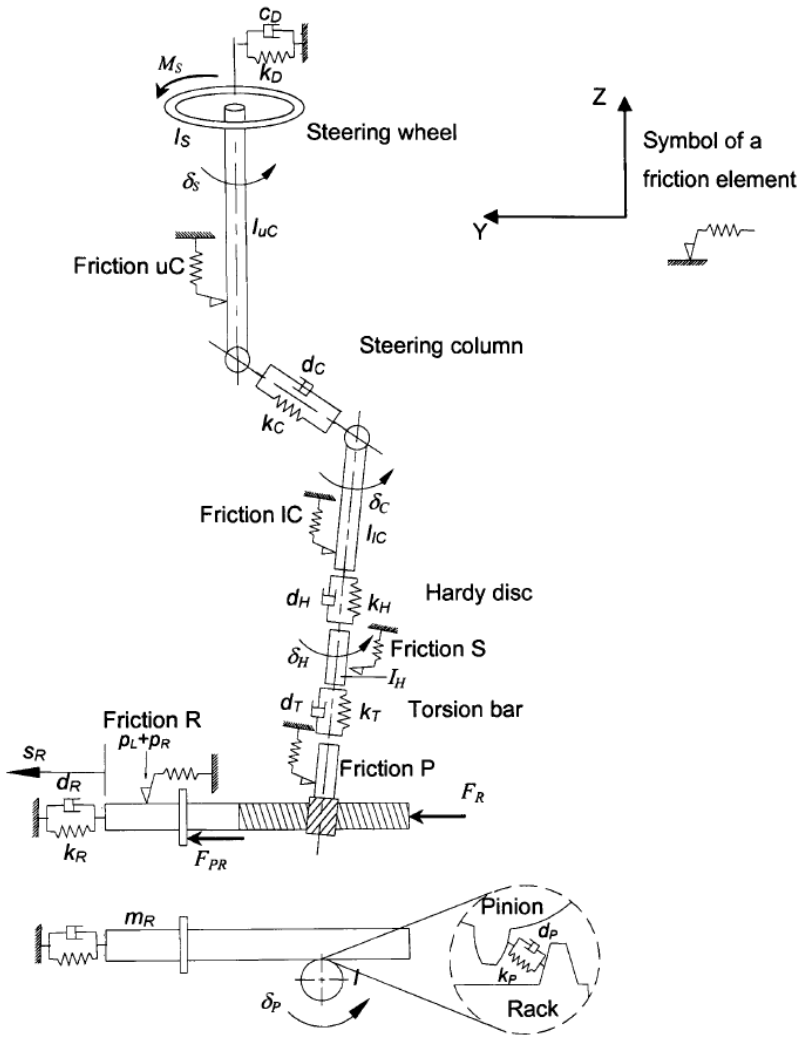

Figure 35 – Five DoFs model of steering system [22]

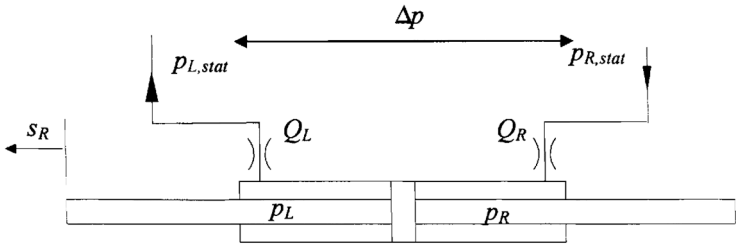

Figure 36 – Hydraulic model [22]

3.2. Two degrees of freedom model

Taking the cue from the literature review shortly shown in previous paragraphs, an adequate steering model for feedback units must emulate the most important effects of modern steering systems, included the assistance systems' effects, keeping a high level of numerical stability but without requiring detailed parameters as for the Pfeffer's model.

Hence, the proposed solution is a double mass model that has all the required features and that guarantees vehicle dynamics simulations (both online and offline), a suitable steering feedback and an accurate analysis of each single effect of the steer assembly. Additionally, reducing the degrees of freedom, the numerical stability increases because the high frequency instabilities are eliminated. Below the equations are introduced, but the final version of the model in the numerical environment is described in Appendix C.

As illustrated in Figure 37, the first body includes the steering wheel and the steering column up to the torsion bar, while the second one is composed by the pinion, the rack and the tie rods. The rotating inertia of the wheels around their steering axes, transported to the rack, are added to consider the inertial effects. The connection element is the torsion bar.

Thus, the model allows the dynamic characterization of the two bodies, which is an intrinsic advantage because manufacturers provide rack groups that are then connected to steering column groups; so, each main part of the assembly has a dedicated body, with its dynamics behaviour.

The system of equations, described in (3), considers two rotating elements connected by a torsional stiffness and a torsional damping:

$$\begin{cases} I_1\ddot{\theta}_1 + c_1(\dot{\theta}_1 - \dot{\theta}_2) + c_0\dot{\theta}_1 + k_1(\theta_1 - \theta_2) = T_{SW} + T_{f_1} \\ I_2\ddot{\theta}_2 + c_1(\dot{\theta}_2 - \dot{\theta}_1) + c_2\dot{\theta}_2 + k_1(\theta_2 + \theta_1) = T_r + T_{f_2} + T_a + T_h \end{cases} \quad \textbf{(3)}$$

where:

I_1, I_2 = bodies' inertia
θ_1, θ_2 = angular position of the bodies
c_0 = damping coefficient to model the losses of column bearings
c_1 = damping coefficient to model the losses of the torsion bar
c_2 = damping coefficient to model the losses of the rack
k_1 = torsion bar stiffness
T_{SW} = driver input torque
T_{f_1}, T_{f_2} = friction torque
T_r = rack force transported to pinion
T_a = assistance torque
T_h = rack end stop force transported to pinion.

The torsion bar stiffness k_1 rapidly increases at high values of the angle to simulate the end stop. Regarding the inertia, I_1 is kept constant, because the effect of the Hooke's joints were neglected (ratio near to 1). I_2 is instead variable: firstly because the rack can have a variable gear ratio, but also because the second body includes the wheels' inertia and this is

not constant with the displacement. Since often this values is not known, a good approximation is obtained considering the rotation around the vertical axis in the middle of the contact patch.

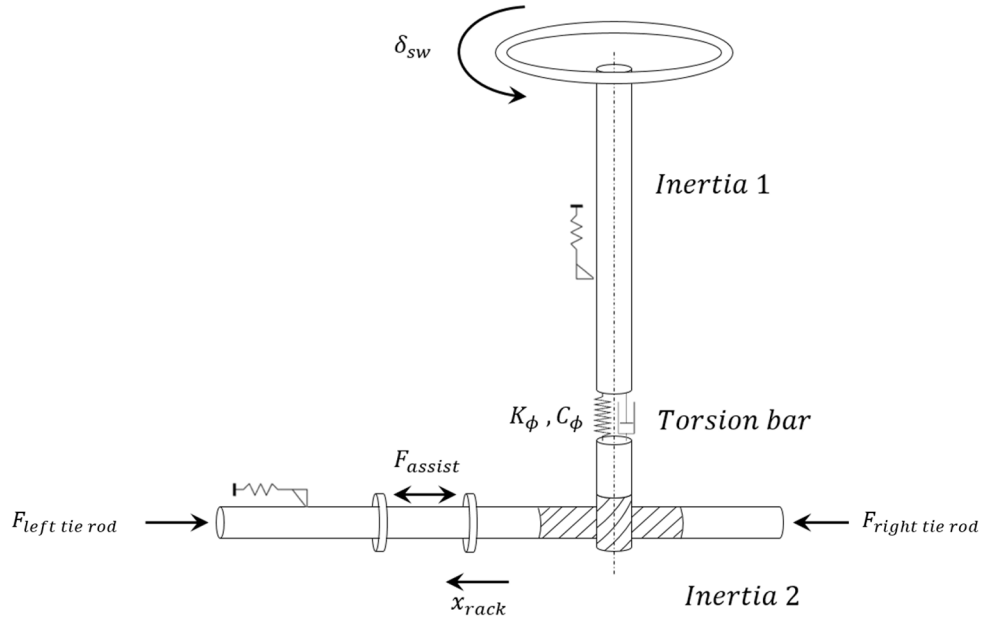

Figure 37 – Two DoFs steering model scheme

This model, which takes in input the steering wheel angle and the forces acting on the tie rods (forces due to the contact between the tires and road surface), calculates the steering wheel torque and the rack displacement (explicit formulation (4)).

This is not the only possible solution for the driver interface: the opposite version considers in input the driver torque. Although this is possible, the angle controller has more benefits: from a hardware point of view, an angular encoder is sufficient instead of an expensive torsiometer. In addition, the feedback unit control is easier due to the torque command and this guarantees more stability. Concerning the vehicle dynamics, deviations of steer angle are prevented, with a higher precision.

Furthermore, using this approach it is possible to use the same model for the offline simulation: it is easier to control the vehicle trajectory describing a steer profile, without the use of external angle to torque controller. In other words, this kind of controller is the best choice for driving simulators.

$$\begin{cases} T_{SW} = I_1\ddot{\theta_1} + c_1(\dot{\theta_1} - \dot{\theta_2}) + c_0\dot{\theta_1} + k_1(\theta_1 - \theta_2) - T_{f_1} \\ \ddot{\theta_2} = \dfrac{1}{I_2}\left(c_1(\dot{\theta_2} - \dot{\theta_1}) + c_2\dot{\theta_2} + k_1(\theta_2 + \theta_1) + T_r + T_{f_2} + T_a + T_h\right) \end{cases} \quad \textbf{(4)}$$

3.2.1. **Friction model**

Any steering model, to properly emulate the realistic behaviour must characterize precisely the hysteretic effects using advanced friction models. The main reason lies in the distinctive functioning conditions of these assemblies, which often move at low speed around the middle position.

A great number of different models are available from literature, most of which were born to be integrated in friction estimators or feedforward controllers mainly used in robotic field to compensate friction effects ([35]–[42]). After an analysis of the state of the art, a LuGre model was chosen.

This model was developed at the Universities of Lund and Grenoble (from which takes the name) as an improvement of the Dahl model to integrate the Stribeck effect, which allows an optimal description of the stick-slip effects. A nonlinear state equation of variable z (5) describes the model through the definition of a specific equation of the relative speed (6): here the Stribeck's effects are taken into account. Equation (7) defines the friction relation.

$$\frac{dz}{dt} = v - \sigma_0 \frac{|v|}{g(v)} z \tag{5}$$

$$g(v) = F_C + \frac{F_S - F_C}{\exp\left(\frac{|v|}{v_s}\right)^2} \tag{6}$$

$$F_f = \sigma_0 z + \sigma_1 \frac{dz}{dt} + \sigma_2 v \tag{7}$$

where:

v = relative speed
v_s = Stribeck's speed
F_c = Coulomb friction force
F_s = static friction force
σ_0 = equivalent stiffness of surface asperities (roughness)
σ_1 = micro-viscous coefficient
σ_2 = viscous friction coefficient.

Furthermore, another term was added to consider the effects of the force components perpendicular to the rack: each time the tie rod is not aligned to the rack direction, force components in x and z direction load the rack bearings creating a Coulomb friction. Once the friction coefficient is set (ω), the force can be calculated as in the following equations (8) - (9).

$$T_{f_2} = T_{f_{2R}} + T_{f_{2L}} \tag{8}$$

$$T_{f_2} = \omega\sqrt{F_{x_R}^{\ 2} + F_{z_R}^2} + \omega\sqrt{F_{x_L}^{\ 2} + F_{z_L}^2} = \omega\left(F_{\perp_R} + F_{\perp_L}\right) = \omega F_{\perp} \tag{9}$$

where:

$F_{\perp}$ = sum of the two perpendicular forces acting on the rack.

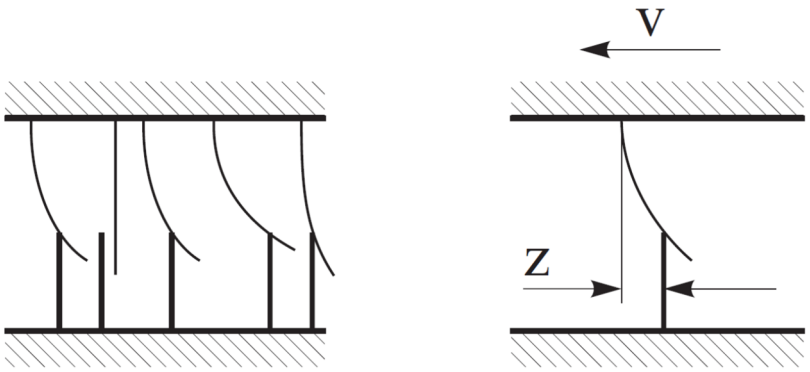

Figure 38 – Left: schematic picture of the contact model between the surfaces, with contact asperities modelled as bristles. Right: contact asperities accumulated to one bristle as in the LuGre model [35]

3.2.2. Steering assistance system

Generally, any assist system can be described by means of a physical or a functional model. The first one considers the modelling of the real system: in case of a hydraulic solution for instance, this means the pump, the pipe network, the distribution valve, the torsion bar and the cylinder. As might be understood, the solution requires the knowledge of the specific plant features; additionally, the necessity to cover a wide range of functioning, up to higher values of frequency than the functional model, leads to a complex layout with evident stability and convergence issues.

This explains the choice of a functional modelling that consists of a mathematical formulation, which guarantees the same behaviour of the real model. To do this, it is important to observe and characterize how the system works.

In this specific case, a hydraulic power assisted system was characterized, because the test vehicle available was equipped with this technology; hence, an experimental test procedure was defined using EPSiL.

Once the steering system was mounted, only a single tie rod was connected, using a load cell: the actuator was set to exert a resistive force. The tester moved the steering wheel following some sinusoidal profiles. In output the quantities acquired were the steering angle and torque together with the load cell signal. In fact, it is important to connect the assist pressure (obtained by dividing the force value for the piston section) to the applied steering wheel torque, because the latter is directly related to the relative angle of the torsion bar that, in turn, defines the valve opening.

This specific model has a solenoid valve that reduces the plant pressure at the increment of the vehicle speed, to have a great assist effect at low speed (e.g. parking manoeuvers) and more stability at high speed. An example is shown in Figure 39, where three (raw) curves are plotted at different vehicle speeds.

Curves as these have to be processed to extract the assist effect, subtracting the driver torque and the friction effects that cause the hysteretic behaviour.

Remembering the aim of modelling the assist effect, the use of the raw curves is discouraged. On the contrary, the definition of a parametric function is preferable, but has to be defined considering the average tendency of the curves. A careful observation of the curves highlights how each one is linear in the first interval while rapidly increases its slope (up almost to a vertical asymptote) at higher values of torsion bar torque.

Following this behaviour, the formulation has a linear and an exponential component up to a saturation limit that describes the upper pressure limit (10). Figure 40 shows the parametrized curves for all the current levels.

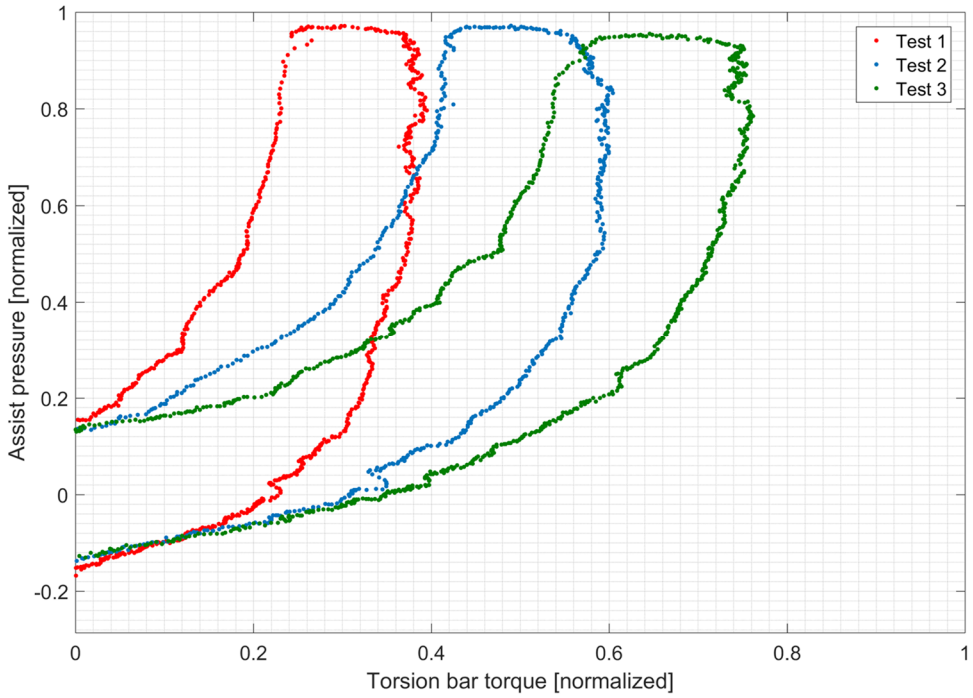

Figure 39 – Assistance curves example - Raw data

$$p(\theta, i) = \begin{cases} p_{sat}(i)\left(\dfrac{\theta}{\theta_{sat}(i)}\right)^{n(i)} + \theta k(i), & p < 120 \\ 120, & p \geq 120 \end{cases} \quad \text{where} \quad p_{sat}(i) = 120 - \theta_{sat}(i) \tag{10}$$

where:

p_{sat} = saturation pressure value
p = assistance pressure
θ = torsion bar angle
θ_{sat} = saturation of the torsion bar angle
i = current level
k, n = tuning coefficients.

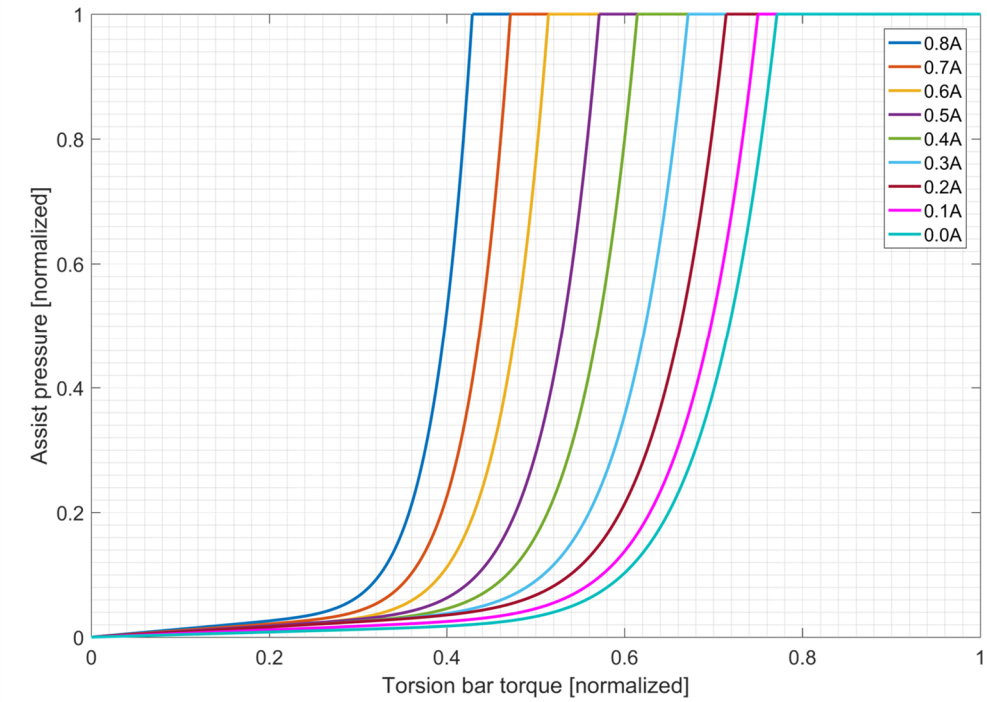

Figure 40 – Assistance curves

3.3. Vehicle model

The validation phase was based on data acquired on a real vehicle, whose model was created to run validation tests using a commercial software: Vi-Grade *CarRealTime*™. This is

conceived as a five masses model (one for sprung chassis and four for the unsprung masses) with lookup tables to consider the suspensions behaviour.

A key factor is the tire model which must be accurate enough to validate the steering model; in this case, the model used and parametrized thanks to values obtained with an experimental procedure, is the Magic Formula in its 6.1 version [43].

Figure 41 explains the method used for a simulation: the vehicle model runs in cosimulation with the steering model. An interesting detail is the solver time step: the vehicle model uses a fixed time step of 1 ms, required to maintain the real time conditions. Rather, the friction formulation inside the steering model needs a ten times lower time step, to avoid numerical issues. This is possible using *rate transition* blocks, which match the signals' rate.

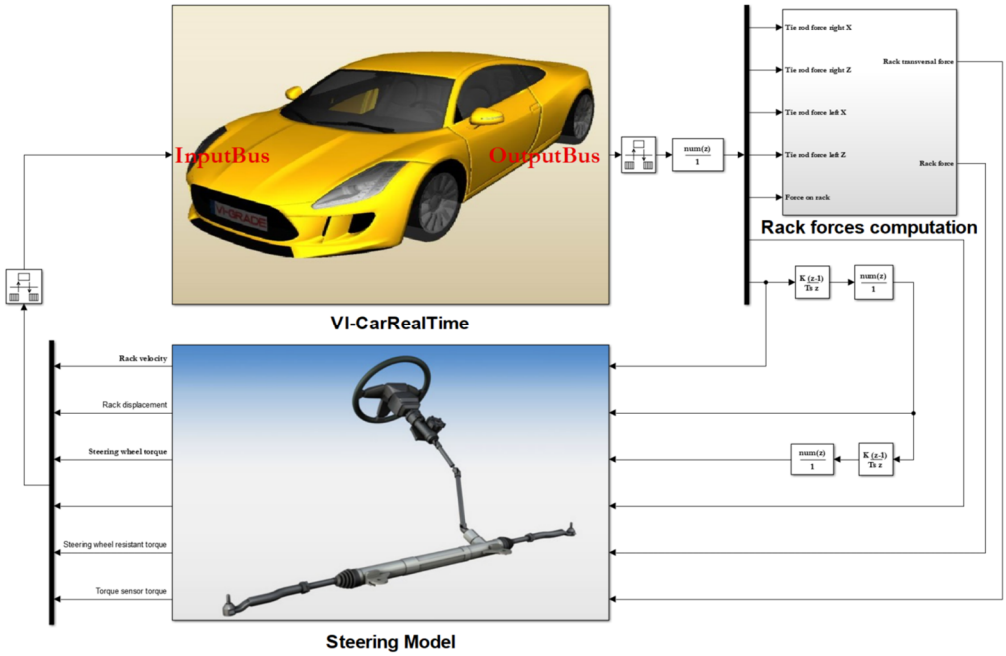

Figure 41 – Cosimulation model

3.4. Validation phase

In this paragraph the steering model validation, based on real data acquired on an instrumented test vehicle is presented. In detail, the same manoeuvres described below, were run and some Key Performance Indices (KPI) were compared.

- *Slow ramp steer*
- *Weave* 120 *kph*
- *Weave* 60 *kph.*

During the ramp steer the vehicle is kept at a constant speed of 100 kph and the steer is slowly rotated, at around 5 deg/s: this allows to characterize the behaviour of the vehicle over the entire range of lateral acceleration.

On the contrary, the weave tests help to define the low lateral acceleration range (lower than 0.15 g): the frequency is fixed at 0.2 Hz while the amplitude changes to maintain the same peak of lateral acceleration.

As already mentioned, a leading point of this project is the enhancement of the steering feeling perception, important for simulator's test drivers. This implies an evaluation of the performances both in objective and subjective ways, therefore the validation considers an offline simulation session followed by online tests helpful to receive driver's feedbacks.

3.4.1. **Objective metrics**

Figure 42 presents the main results for the slow ramp steer test: the torque at the steering wheel sensor versus the lateral acceleration. It has to be highlighted that the graph specifically refers to the torsiometer's values because it does not consider the not neglecting inertial contribution of the steering wheel: thus, what the driver feels is different but not directly measureable.

Concerning the results, those achieved by the model well follow the best-fit curve of the real case: the fitting is essential because of the different vehicle's response in right and left turns, proved by the visible span between the two curves.

Lesser similarities are evident in the results of weave test at 60 kph (Figure 43) where the under estimation of the steer torque is due to inaccuracies in modelling the power steering; the hydraulic circuit has a complex behaviour, especially in dynamics conditions. Limitations of the characterization process drove to these inaccuracies.

In a similar way, some discrepancies in the torque measurements are shown in Figure 44 that describes the weave test at 120 kph: in this case the effects of the hydraulic model are less important. The main error is concentrated on the unloaded curve after the inversion, caused by the friction: the LuGre model has limitations concerning the pre-sliding conditions that characterize this phase [40], here emphasised by the sudden change of assist torque.

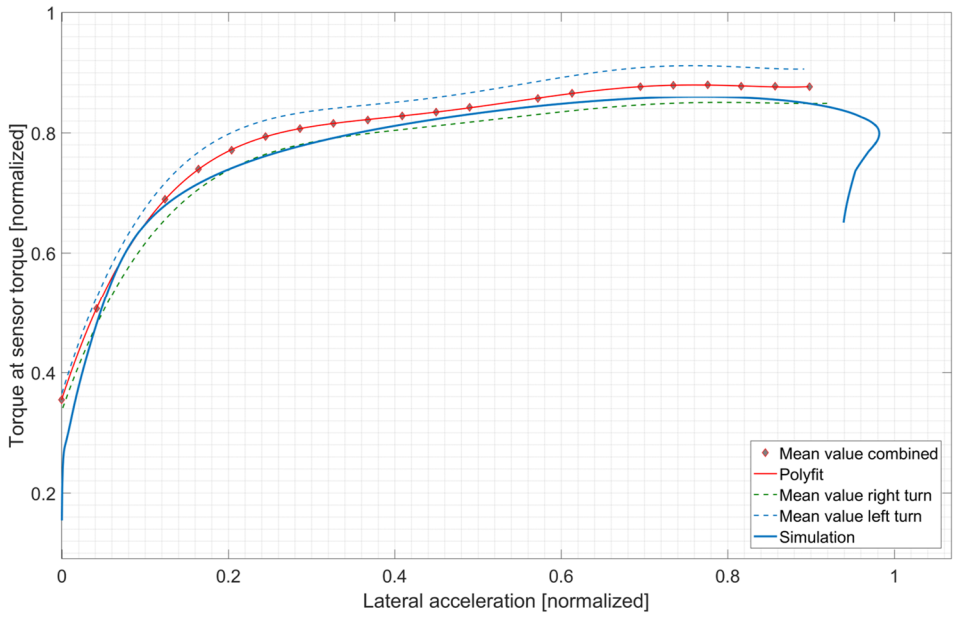

Figure 42 – Slow Ramp Steer test – Steering torque versus lateral acceleration

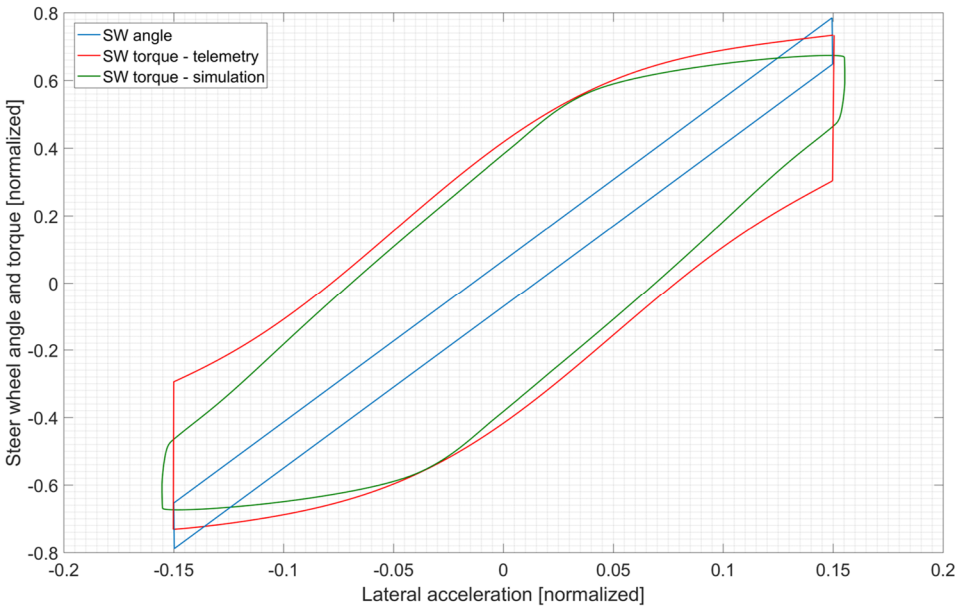

Figure 43 – Weave test (60 kph) – Steering torque and angle versus lateral acceleration

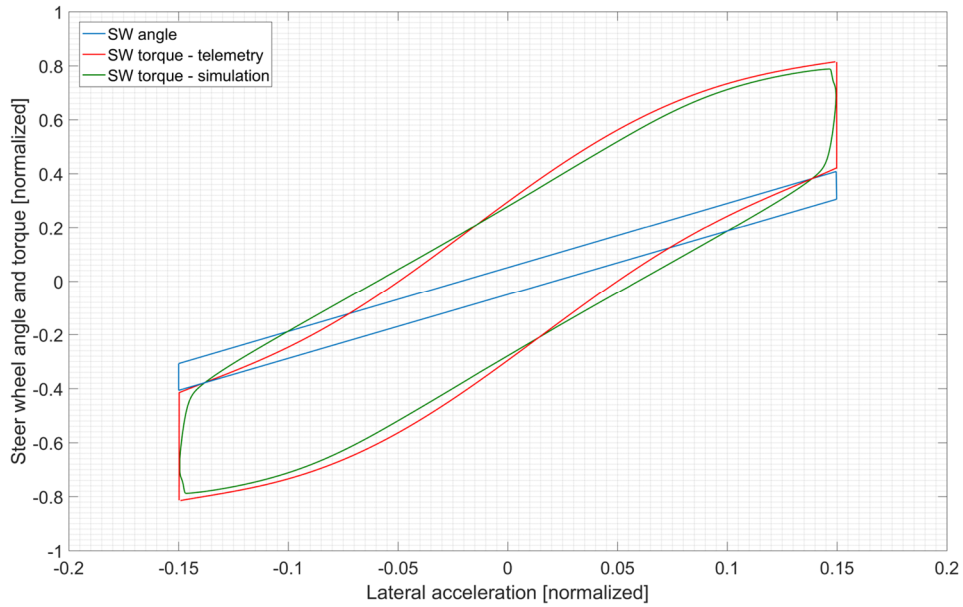

Figure 44 – Weave test (120 kph) – Steering torque and angle versus lateral acceleration

3.4.2. Subjective metrics

A campaign was organized to show the potentialities of the proposed model in comparison with the one degree of freedom steering model. The reason is simple: verify if the solution brings benefits without increasing the computational complexity as the Pfeffer's model does. Having different targets in comparison with the objective tests, the list of manoeuvers was prepared with the test driver, to exploit his experience. Unfortunately, for reasons of confidentiality, it is not possible to specify test details. All the outcomes, summarized below in few principal points, refer to different manoeuvers: a more detailed description of the subjective tests is presented in paragraph 5.2.1.

- *Steering torque to lateral acceleration gradient*

The proposed model creates an almost constant load in $0 \div 0.8\ g$ range. The original model instead shows a large linear variation, which is less feasible. In fact, Figure 42 shows how the steering wheel torque quickly increases in the first part and then saturates due to the assist effect.

To visualize more clearly this effect, Figure 45 compares the steering torque versus the lateral acceleration for the two models. In this case, the results were shifted to have the same peak of torque.

Another evidence that helps to explain the almost constant torque tendency, is visible in Figure 46: this illustrates how the hydraulic contribution is prevalent at higher loads, with an exponential growth compared to the steering torque applied.

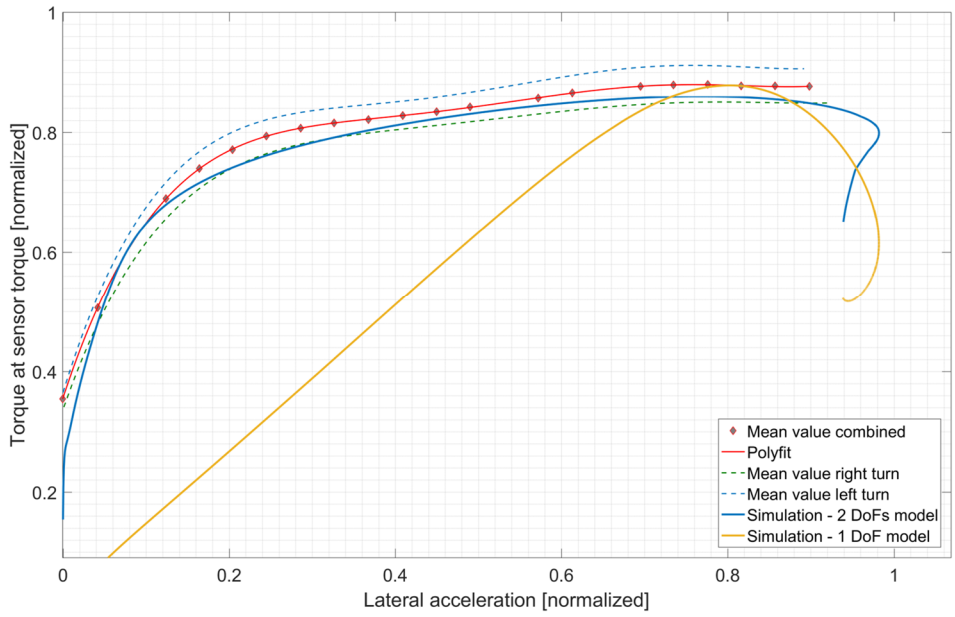

Figure 45 – Steering wheel torque for the single degree of freedom model

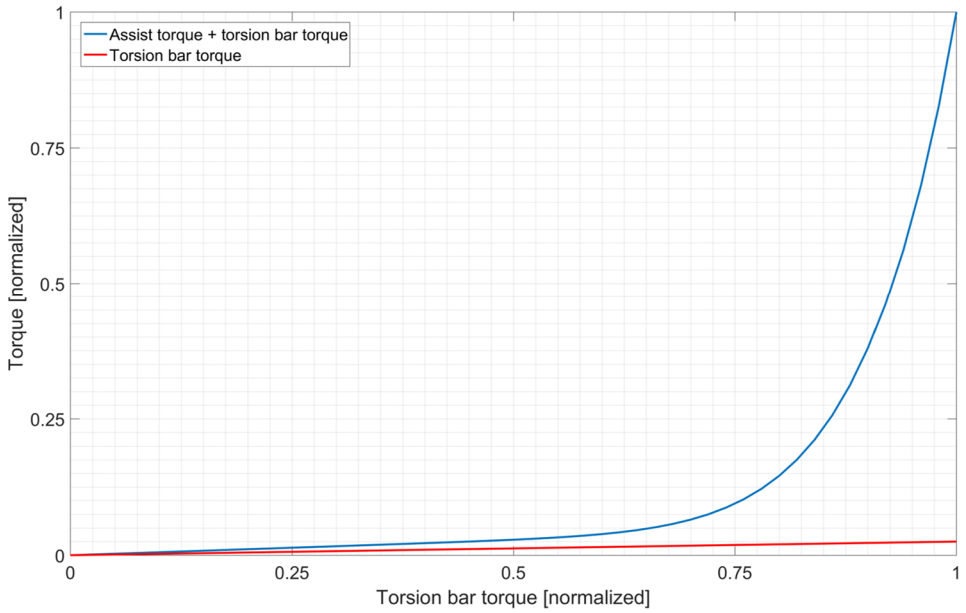

Figure 46 – Comparison between torsion bar torque and torsion bar plus assist torque during a ramp steer test

- *Steer angle rate*

This parameter describes the relation between the steer angle and the lateral acceleration, around the idle position. Indeed, in the on-centre zone, the desired functioning should be linear. The two degrees of freedom model has a progressive yaw response of the vehicle, which is an equivalent evidence of a good response. On the contrary, the basic model has a flatter response.

- *On-centre feeling*

The main benefit is the on-centre dead-band introduced, not obtained with the single degree of freedom model because modelled without any elastic element. Indeed, the effect of this dead-band is intense on the steering perception and it is absolutely necessary to have a realistic response.

- *High-speed reversibility*

The simpler model has a slower return with oscillations characterized by annoying overshoots as a spring-mass model. The proposed one has a more mechanical return. Given that, it may be noticed how this effect is strongly affected by the tire behaviour, more than for the other parameters; therefore, the comment has to be considered with caution.

3.5. Results and benefits of the solution

In conclusion, the proposed model complies with the initial project requirements. From an objective point of view the outcomes are close to real data, demonstrating a sufficient level of approximation. Certainly, this phase revealed two crucial aspects to obtain an accurate behaviour: the friction model and the assist system. The latter, in particular, creates some issues because the dynamic behaviour of the hydraulic circuit should be characterized with a dedicated test bench. However, despite this indicates an important future development, the model can be considered adequately accurate for the purpose of this thesis.

Similarly, the subjective performances increase, although this report format does not facilitate a direct comparison between the two models. The main features embedded, which definitely enhance the driver feedback, are a dead-band around idle position and a more step gradient of torque, which are both crucial to realistically emulate the on-centre handling conduct. In this sense, a decisive role is played by the torsion bar, which decouples the movement of the two equivalent masses. As a secondary effect, the returnability of the steering wheel improves thanks to a more natural free movement of the hand wheel due to an accurate inertial component.

As already mentioned, the reference model from a literature review belongs to prof. P. Pfeffer. Therefore, as a conclusion of this chapter, a comparison is appropriate. It was demonstrated how the proposed model can reach an optimal matching of objective results but using a fewer number of parameters. This is a key point not only in terms of performances, but also in terms of model pre-process: with the same results, the proposed model requires less parameters that suggests a quicker and less expensive parametrization phase. In addition, having a lower number of degrees of freedom, the stability margin is higher, with improvements in the simulation stability.

4. Test bench installation

In chapter 3 the numerical activity has been described; this concerned the definition of a steering model to fulfil two main targets: to create a robust and reliable reference point to compare the test bench results and to introduce a brand new methodology to change via software the physical features of real steering systems tested. The validation phase, which ended the chapter, confirmed the potentialities of the model.

This chapter symbolizes the combination of the activities introduced in the previous two chapters: the design of the experimental test bench from one hand and of the steering model from the other. Following the chronological order, firstly it will be described the installation process of the test bench, divided in several steps.

The first one entailed the characterization of EPSiL's main features, as resistive loads (friction effects) and inertial contributions. The information collected during the entire process were then used for the second phase: creation and testing of the control system, brain of the test rig. Whereas the first part made use of a simple mechanical connection between the two units of the rig, the second one needed the integration of a real steering system, mainly to have generic input from a test driver using the steering wheel. The entire process of control system's tuning comprehended this and a second phase, which took place after the integration of EPSiL with the static driving simulator.

The process ended with the introduction of the method that, using the numerical model, sets the goal of modifying the steering feedback as one or more physical elements were changed.

4.1. Installation phase

EPSiL was installed in a dedicated testing area, adequate to verify all the functionalities and to set up it before this was moved to the static driving simulator room.

The preparation considered the load cell amplifiers calibration and the linear actuators check: the amplifiers calibration is a common procedure done to set the right amplifier's parameters based on the load range, load frequency and resolution; for instance, the conversion constant between the axial force applied and the tension value measured (11). Together with (12) that characterized the linear actuator force exerted versus the measured current, is important to interpret the obtained results.

$$k_{LoadCell} = 1.47 \frac{N}{mV} \tag{11}$$

$$k_{LinearActuator} = 1570\frac{N}{A} \quad \textbf{(12)}$$

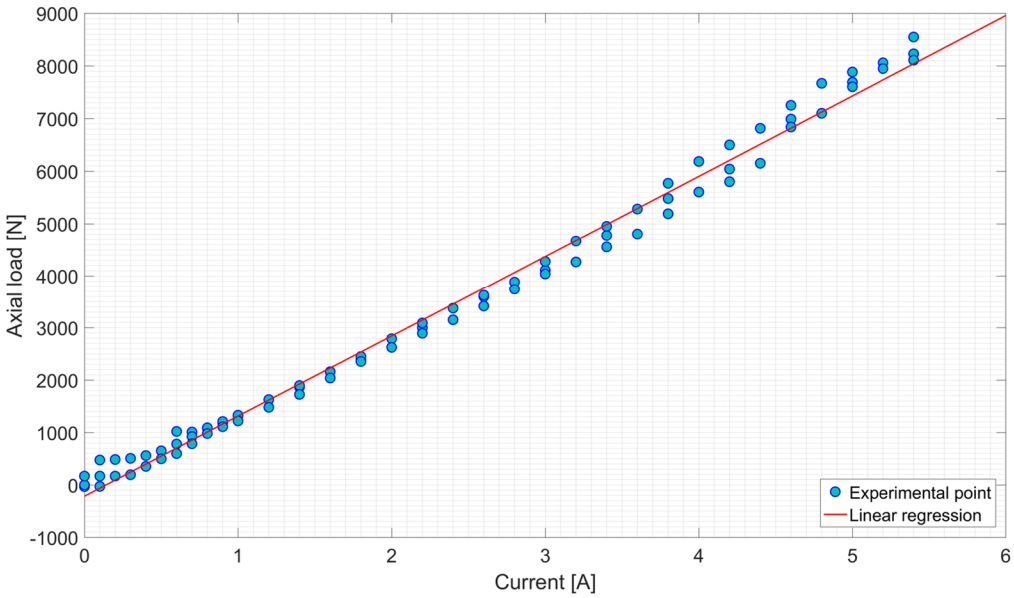

Figure 47 – Axial load versus current in linear actuator

Once the test rig was assembled, a rigid bar to connect both the rockers was inserted: in the middle a load cell was screwed between the two segments that composed the bar. For the first part of the work, it was supposed to use the two actuators differently: one was used to follow a position profile of the bar, while the other alternatively as a resistive load or as the compensation unit. Figure 48 illustrates the first assembly with the rigid bar and the load cell.

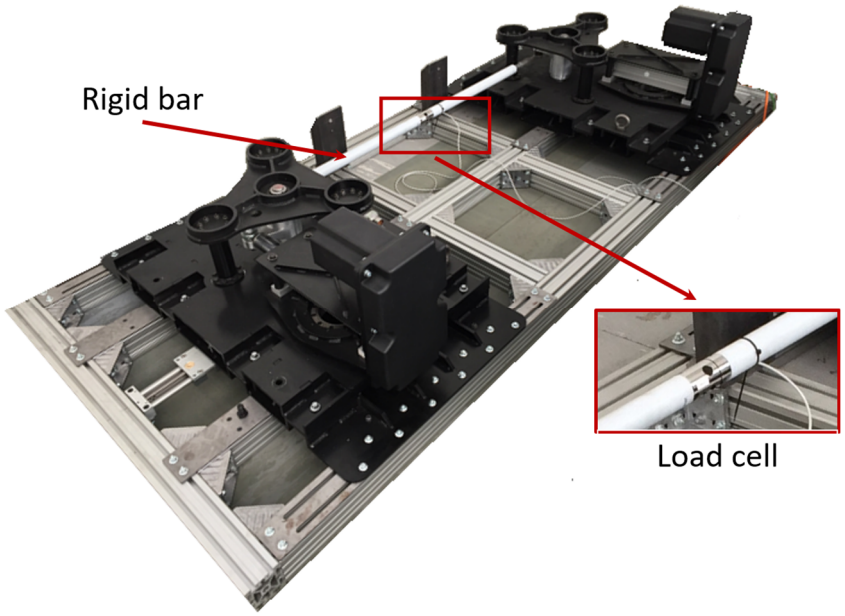

Figure 48 – Test rig equipped with the rigid bar and a single load cell

4.2. Test rig characterization

A reasonable characterization of the test rig must consider lots of different key aspects. Starting from the principal points, one concerns the mechanical part: as discussed during the description of the design phase, without a sufficient dynamic stiffness or with unwanted backlashes along the kinematic chain, the functionalities are compromised.

Thus, taking the cue from the flexible multibody analyses, similar tests were done, using an actuator as resistive load and the other as active. Not having specific tools to qualify the behaviour, only a visual check was realized considering the vibrations of the base frame. The test rig's behaviour over the working range was considered acceptable and without alarming backlash effects.

Once the mechanical structure was validated, the following parts focused on the kinematic chain's conduct. Since the principal task of EPSiL is to exert the requested amount of force at the tie rods, to have an optimal dynamic functioning the friction and the inertia components introduced by the actuation system must be completely compensated. However, this is possible only after a specific investigation, due to the large number of parameters that influence the phenomenon.

Generally, an enough accurate calculation of the inertia contribution is possible, knowing the inertia of each single part and the kinematic transmission ratio. Unfortunately, in this specific case some of the predominant components were unknown, hence an estimation was necessary.

From a literature review, it was possible to select some of the most promising methods: these are mainly used to characterize complex robotic or mechatronic systems. For example E. G. Papadopoulos [44] proposes to calculate the inertia replicating some specific movements: repeating several transient steps with different features and measuring the time constant of the system, an estimation of the equivalent mass is possible with small error. Based on the same principle, others make use of frequency response technique, recalling more generic methodologies used for rigid bodies ([45]–[47]).

Other authors prefer a simpler approach: describing the model as an equivalent mass undergone to driving and resisting forces, once all the external actions are known, the inertia is calculated from (13).

$$M_{eq}a = F_{DrivingForces} - F_{ResistingActions} \tag{13}$$

However, this can be used only if all the forces acting on the system are known; therefore, for the specific case, it means that it could be used after an accurate analysis of friction components. In addition, this method has a second backward: estimation errors sum together, increasing the error.

To avoid this negative aspect, the chosen method is based on a simple idea: use two measurement points to respectively cancel the unknown components [48]. More in detail, Figure 49 illustrates the basic principle: the system's controller must impose a triangular velocity profile with equivalent slopes, which means the same accelerations, in absolute values.

Then, measuring the required drive force on both the branches, at the same level of velocity, the equivalent mass contribution is extracted (14). Obviously, the controller must strictly follow the required profile without oscillations, otherwise the measurements' goodness decreases.

$$J_{eq} = \frac{C_1 - C_2}{2\dot{\omega}} \tag{14}$$

where:

J_{eq} = equivalent inertial contribution
C_1/C_2 = measured torque on the two branches (at the same ω)
$\dot{\omega}$ = acceleration level.

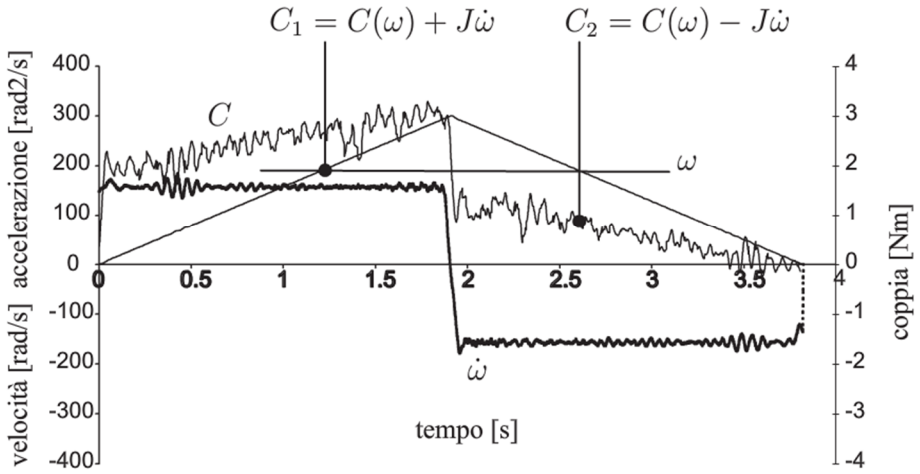

Figure 49 – Inertia estimation method [48]

Referring to friction, the problem is much more complex. Every mechanical assembly is exposed to different effects, therefore a universal method to identify all the factors is not effective. From the state of the art some generic suggestions can be found: a part from particular procedures that make use of DFT algorithm to understand which components are prevalent, which kind of effects they represent and which mechanical effects are referred to [49], all the others are based on phenomenon observation.

The basic idea simply considers to reduce all the effects to a mathematical model. Indeed, once a more or less simple model foresees the actual friction behaviour, the possibilities to compensate the effects increase. For instance: Figure 50 shows how the data acquired in different conditions are fitted by a Stribeck formulation [50].

The latest friction models emulate the effects with an incredible level of accuracy but, facing the reality, not all the contributions can be measured easily, so a proper definition of the friction model has to be done considering also this issue.

It may be remembered that friction in mechanical systems is a nonlinear phenomenon characterized by two separated regimes: the pre-sliding and the sliding zones [40].

The second one is easier to be described. According to several authors (an example is E. G. Papadopoulos [44]), the procedure considers the use of an actuator's controller able to keep in motion the system at a constant speed. Thus, if the acceleration is null and friction is the only resisting action, the force to move the system, in steady-state conditions, corresponds to the friction force.

Repeating the process over a specific range, it may be defined the viscous contribution, which is the dependence of the force from the velocity. Each measurement is replicated in different points to reveal a possible position dependency, plausible for ball-screw systems.

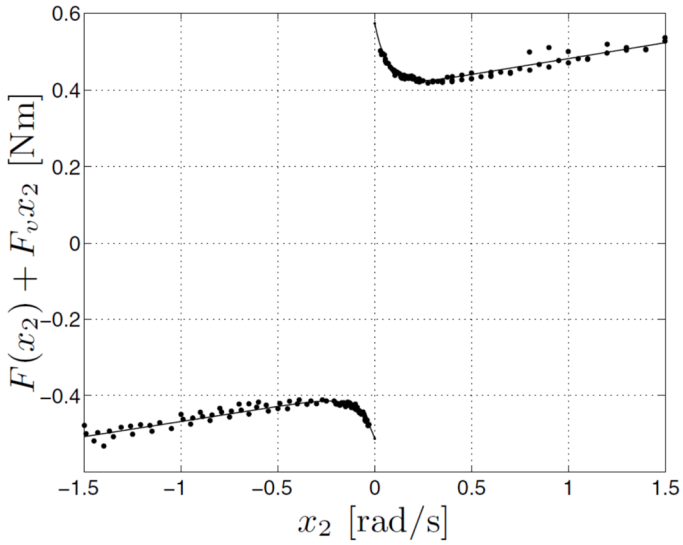

Figure 50 – Example of friction curve with measurement data (· ·) and fitted curve (-) [50]

Regarding pre-sliding regime, the characterization is harder. According to R. W. Daniel [51], breakaway friction tests are useful to investigate the area around null speed: starting in different positions, the electrical tension or the load applied by the actuator is increased until a movement is observed; the measured force corresponds to the friction value. All the tests are repeated in both the directions, to take into account the asymmetry effects.

Measurements are preceded by a warm-up phase, necessary to carry the mechanical system at the working conditions, because temperature is another decisive factor.

4.2.1. Inertial components identification

The triangular procedure, above introduced, was chosen as the primary method to properly identify the inertia. In detail, one actuator was commanded to follow the desired speed profile; in this way the entire inertia of the kinematic chain was estimated, included the inertia of the second actuator that was turned off during the process.

An example is visible in Figure 51: the rack speed follows a triangular shape, with the same absolute level of acceleration on both the branches. This is possible only using an accurate position control, which uses the motor's encoder channel as feedback. The measured quantity is the load cell force.

Some oscillations are visible, likely due to control fluctuations: indeed, although the speed profile is quite smooth, the load cell detects all the quick torque variations. Having said that, considering the average profile (dashed grey line in the plot), the inertial contribution is isolated and analysed.

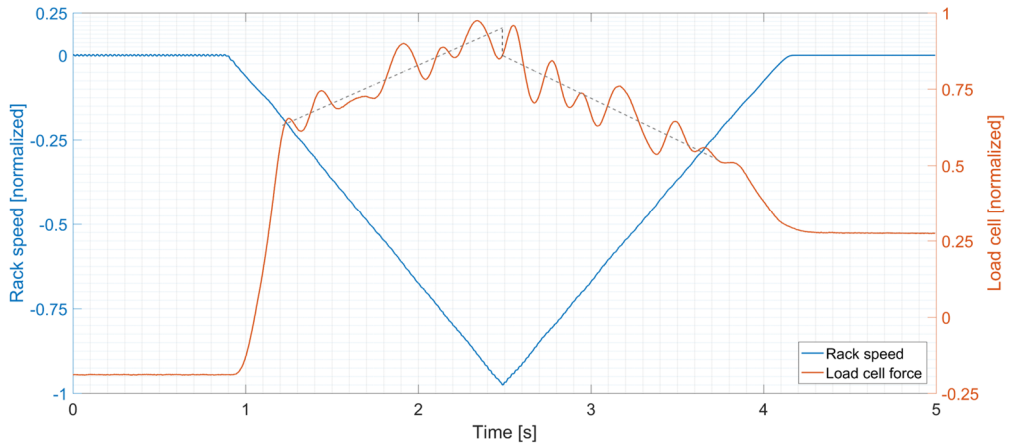

Figure 51 – Triangular test: rack speed and load cell force profiles

Considering the actuation geometry of EPSiL, the transmission ratio from the actuator's motor to the rack is variable; therefore, the equivalent mass varied depending on the position. This is an important aspect to keep in mind during the tests: the same method was replicated several times in different positions. Then, knowing the geometrical ratios, the results were corrected to have only one value of equivalent inertia.

Obviously, being an experimental methodology, each analysis was repeated with different levels of acceleration (Figure 52), to verify the presence of other components. In fact, as said, friction is a nonlinear phenomenon that can result in a different conduct during the acceleration or the deceleration phases. Anyway, the results were all located in a small neighbourhood, with a limited standard deviation that allowed to exclude this possibility.

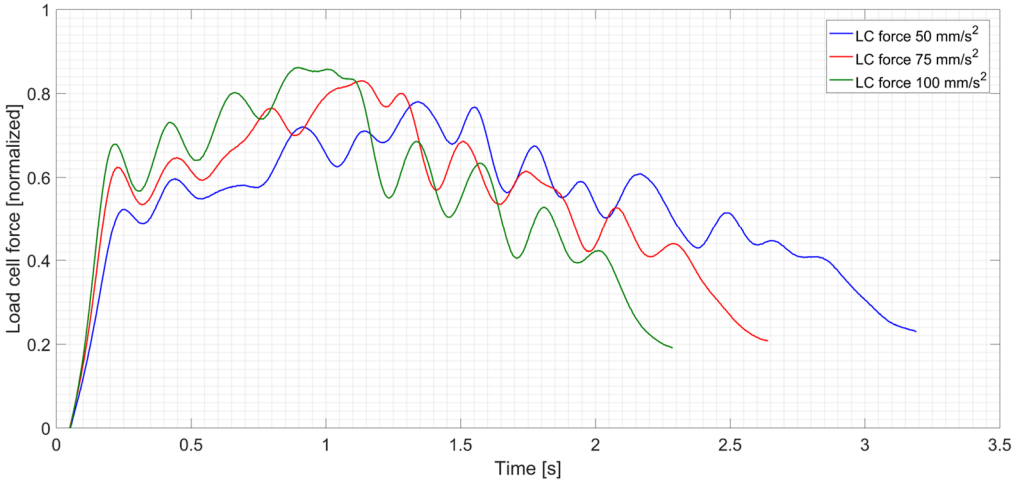

Figure 52 – Triangular test: different levels of acceleration

As a check, a different method was adopted: from the total measured force profile, the total friction component was subtracted. The latter, not directly measured, was estimated from the relation defined in paragraph 4.2.2.

Referring to Figure 53, all the different curves are visible: the resulting curve slightly oscillates around its mean value, due to some lacks in the evaluation of the friction components. However, considering the average value, the result is close to the previous one. Therefore, the values were recognized as enough valid and the triangular method as effective.

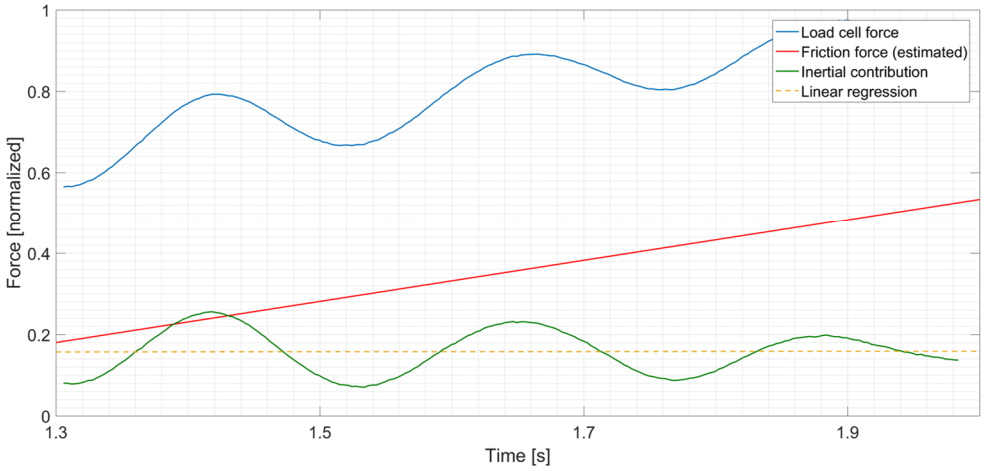

Figure 53 – Inertia estimation: alternative method

4.2.2. Friction components identification

Since this represents a preliminary phase of the project, a very early analysis was conducted before the complete installation, when the load cells were not available yet. As alternative of the measured force, the actuator driver's current was considered, having a linear relation with the motors torque. This procedure led to scattered results, mainly due to the high level of signal noise, characteristic of these electrical machines that do not use specific filters. The installation of load cells attenuated these problems and allowed to have more reliable results.

The process began analysing the speed dependency: a trapezoidal speed profile was defined, considering the maximum stroke available and avoiding violent accelerations and decelerations. Indeed, to gather reliable data, the stability of the speed values is crucial. The functioning speed range were equally split in several testing configurations.

An exception to this linear subdivision is the region around null velocity: in this area the number of testing configurations were increased, to better characterize the pre-sliding phase.

Figure 54 shows an example of trapezoidal profile used: as might be seen, the internal controller of the actuator introduces some unwanted fluctuations around the set speed. This effect rather gets worse considering the load cell force channel, instead of the speed value, because it directly perceives the torque oscillations.

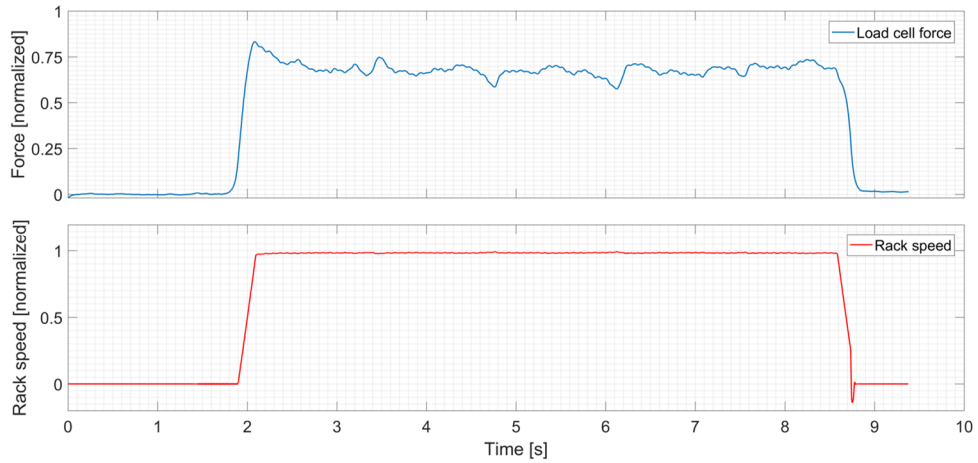

Figure 54 – Example of trapezoidal speed profile and load cell

Figure 55 illustrates three tests at different speeds: after the ramp, the values do not stabilise. It requires attention for the following phase, designated to measure the resisting force for all the speed levels. In general, since the signal is composed of a mean value plus a low frequency noise, the procedure consists of chopping a steady-state part of the signal and of acquiring its mean value.

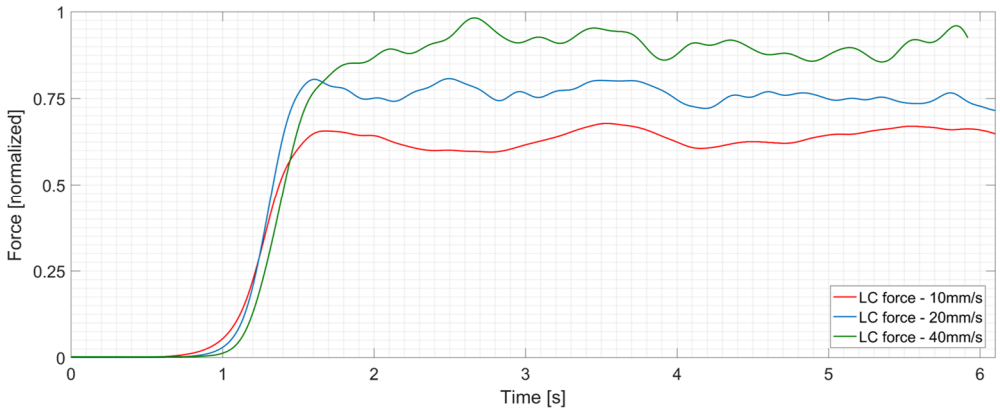

Figure 55 – Friction analyses: constant speed profiles

Repeating this method and keeping a point for each test, the graph in Figure 56 was created. It shows the characteristic behaviour of the system: as might be seen, the best fit curves are not exactly linear, but quadratic with negative gradient. Additionally, the values reached with forward and backward tests are slightly different; the reason is simply related to the nonlinearities of the mechanical system, for instance due to gaskets' shape of ball-screws. Although this could appear as an issue for the controller, actually the effect is compensated by the opposite unit of the test rig.

Referring to the quadratic trend of the regression curves, the reasons are less clear. If it was considered as a classical friction effect of contacting surfaces, such gradient reduction would be difficult to justify. Nevertheless, this way to represent the friction is ideal, because all the effects distributed over the kinematic chain are transported to a single point and related to its speed. Consequently, the only relevant point is to reproduce this behaviour as well as possible.

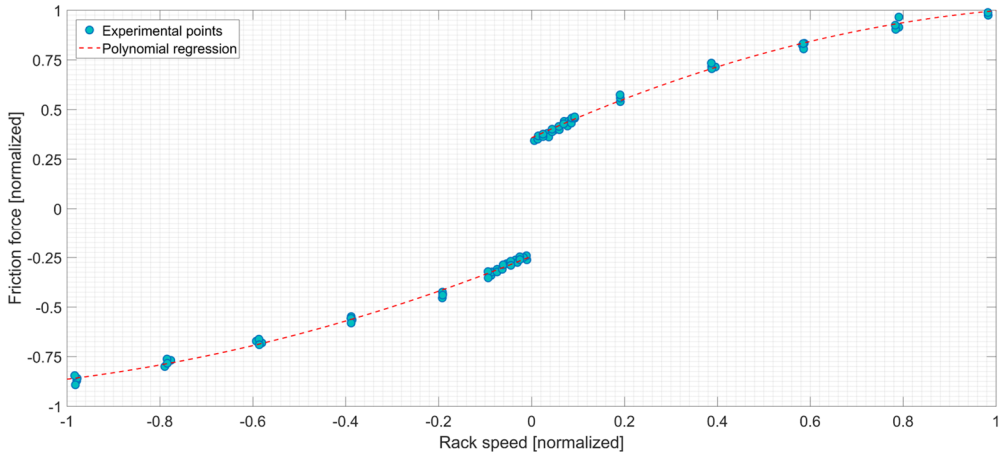

Figure 56 – Friction force versus rack speed: experimental points and regression curves

To characterize the pre-sliding phase, ad-hoc detaching tests were employed: Figure 57 shows an example. Starting from a static condition, the current was linearly increased until the rack began to move: correlating the position signal with the force channel, it was possible to characterize this region.

More than the other tests, these were affected by a large deviation, therefore it required more runs for every configuration. In addition, the starting position had an influence on the outcomes, maybe because the screw worked with a different number of spheres and geometric dispositions that changed with the relative rotation of the rocker. Since this transformed the force distribution, the friction effects changed too.

Other than a simple correlation with the force's peak, it is interesting to notice how the process evolves, being a perfect example of stick-slip phenomenon. In detail, referring to the rack displacement curve, the first part represents the elasticity of the asperities, the second one the stick effect of the same bristles once the deformation is completed and the conclusive part describes the sliding zone where the remaining force component is the static Columbian contribution.

As said, it is not a real explanation of the actual effects, but a connection to the behaviour of a simpler friction model. However, it is required for the feedforward controller used for the actuators and described in the following paragraphs.

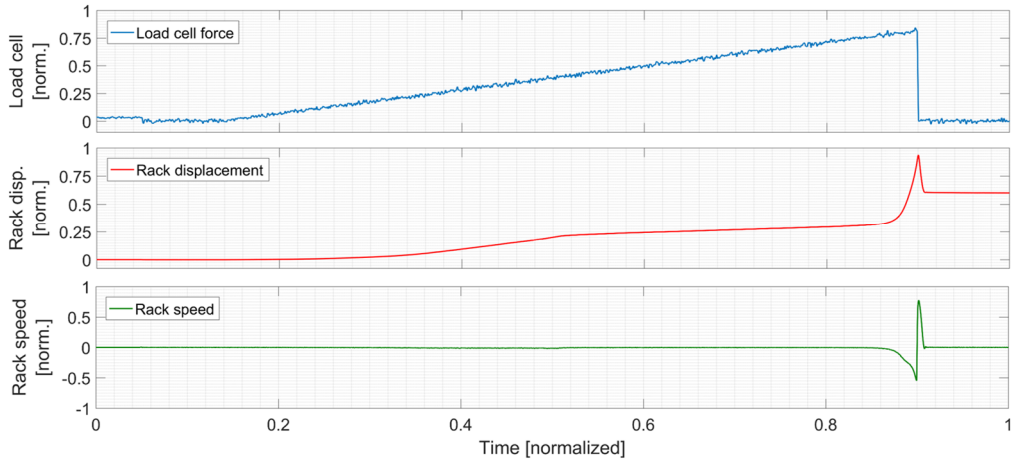

Figure 57 – Example of detaching test. From the top: load cell force, rack displacement and speed

4.3. Integration with the driving simulator

The first phase of the installation ended with the characterization of friction and inertial components, described in the previous paragraphs of this chapter. The following step concerned the integration of a human driver, which required a proper interface: the rigid bar was dismantled and substituted by a real EPS system, get from a passenger car (Figure 58 shows the rack fastened with its sub frame).

As mentioned, each tie rod was modified to insert a load cell: this allowed monitoring the actual force acting on them, which is the target from the simulation.

The steering system itself has its friction and inertial effects, especially in this electrical version: since these contributions are similar to the ones introduced by the test bench, the importance of EPSiL influence decreases. Rather, the steer acts as a filter of these effects. Few tests demonstrated the perfect functioning of the test rig and opened at the following step: the conjunction with the driving simulator.

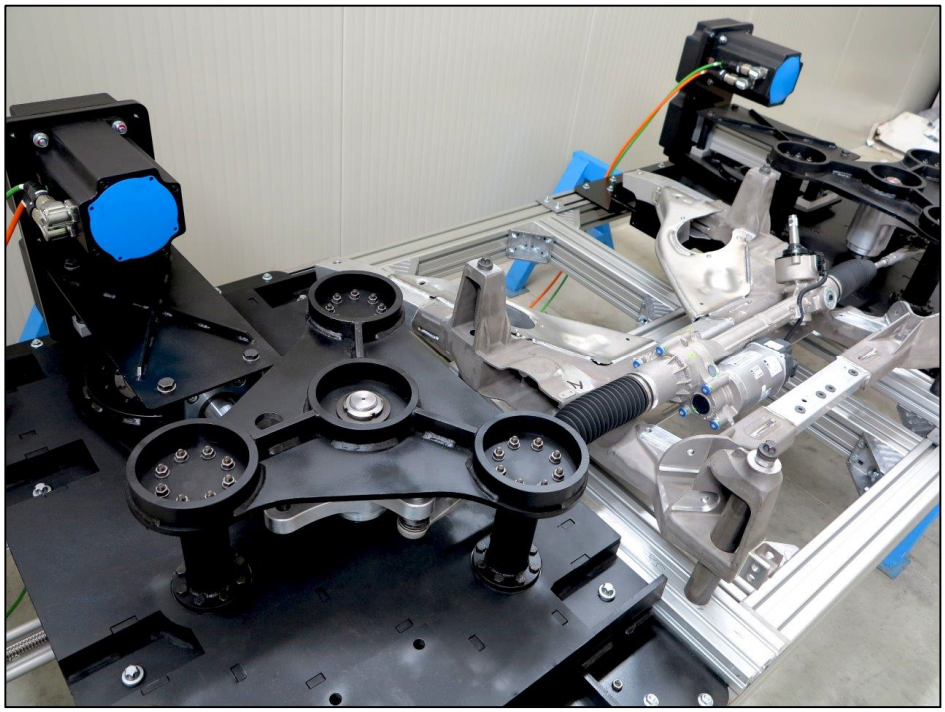

Figure 58 – EPS mounted on test rig, without the steering column

Driving simulators are widely used in automobile industry and research field for lots of different tasks, where the interaction with human being is crucial. S. T. Godley [52] highlights the importance of these tools to analyse how the drivers act in their natural environment, summarizing their advantages in two basic points known as *physical validity* and *behavioural validity*.

The first one, often indicated as simulator's fidelity, defines the physical correspondence between the reality and simulator's components, layout and dynamics.

The second level considers the correspondence between the real world and the simulator in the way the human operator behaves. Two different aspects together related. In this case, the introduction of EPSiL brings the physical validity to a higher level, drastically enhancing the steering dynamics.

Figure 59 – Static driving simulator – Property of Danisi Engineering

The presented project was supported by Danisi Engineering, owner of an advanced static driving simulator (Figure 59) used for the integration. Being based on a real car, the front part was modified to embed EPSiL with its steering system; in turn, this was connected to the hand wheel controlled by the driver. As discussed in chapter 2, the mechanical structure was conceived to be easily integrated in the simulator with the fewest possible modifications at the car's structure: in the end, only the front bumper was removed to avoid interface problems.

Additionally, another aspect was taken into account during the design process: to increase the level of realism perceived by the driver, all the elements of EPSiL were hidden at the drivers' eyes using a careful design. As might be seen in Figure 60, the level of integration is high, symptom of a good design process.

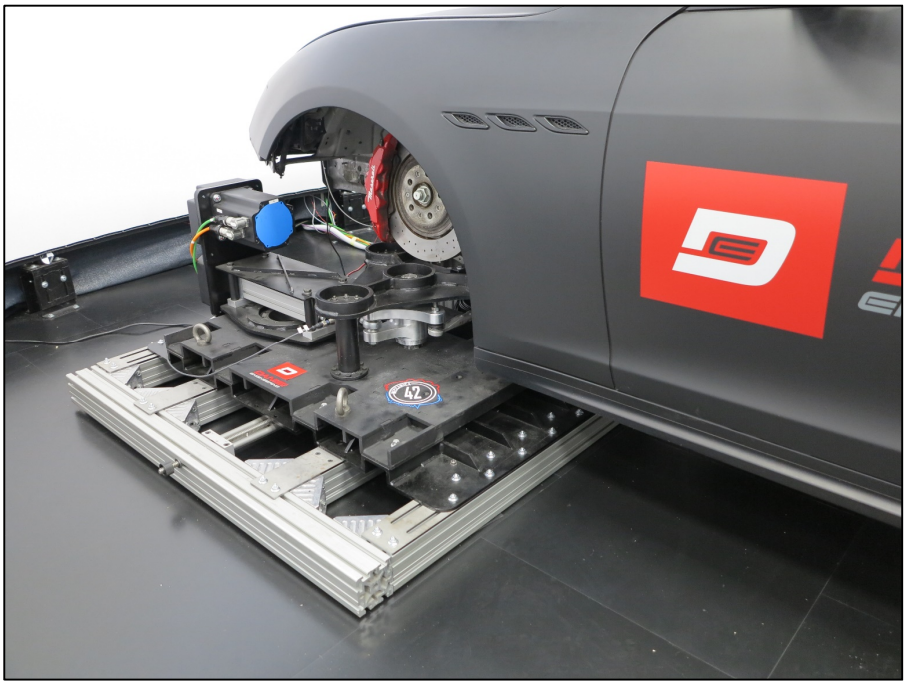

Figure 60 – Static driving simulator – Detail of left side of test bench

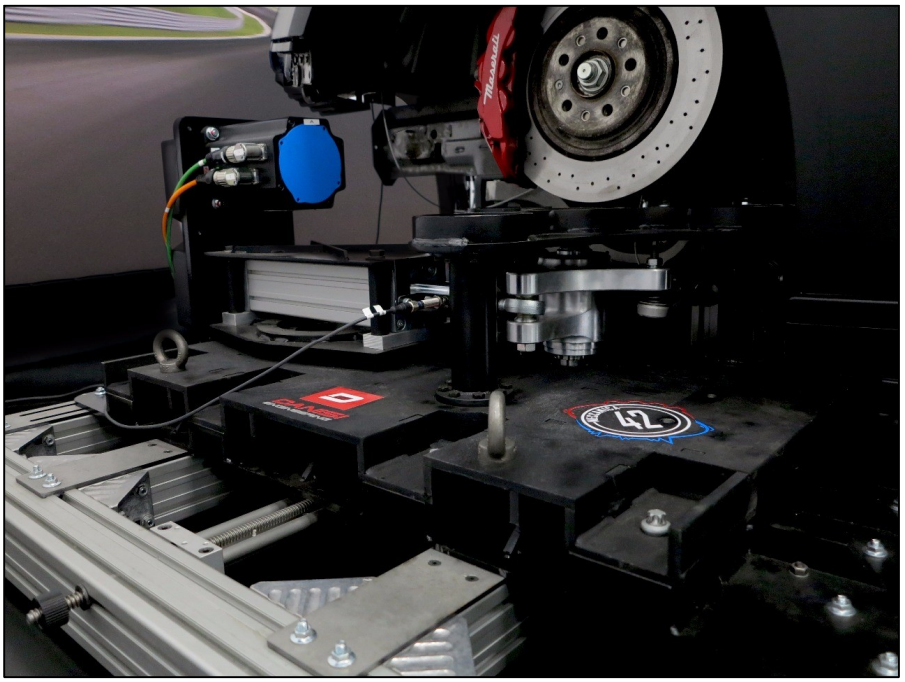

Figure 61 – Static driving simulator – Detail of the connection between rocker and tie rod end

Besides the load cells, additional sensors were installed as decided during the design phase (refer to paragraph 2.2.3). Firstly, for safety reasons, each unit has available a Hall's effect magnetic sensor, visible in Figure 61, to avoid any collision at the end of the rod stroke. Still on the rack, an optical sensor was fixed on the housing to monitor the rack displacement: it is hidden in the picture, because situated under the vehicle engine bay.

Lastly, to monitor and acquired the angle and the torque at the steer, a torsiometer was fixed behind the steering wheel (Figure 62): it is a specific sensor for automotive solutions, characterized by a high level of accuracy in torque and angle, for static and dynamics functioning conditions. Appendix D describes in detail the characteristics of each sensor used.

Figure 62 – Static driving simulator – Detail of the steering wheel with its torsiometer

4.4. Control system

The following paragraph is aimed at describing the control system issue. As mentioned before, the main purpose of the proposed solution is to increase the steering feedback with the use of a real steering system. It means that the main goal is to recreate the same force profiles defined in the simulation environment at the tie rod's ends.

The task has been entrusted to the actuation system, which exerts the forces on the tie rods by means of two rotating elements. Although it appears as a simple assignment, the secondary effects can cause a strong mismatch. This issue, clear from the early beginning of

the project, has been faced with a control system algorithm, which has to compensate the inertial and frictional components without affecting the force profile and, in turn, without conditioning the steer torque.

Concerning the approach followed, it can be considered as a good balancing among theory and practice. Indeed, as will be described in the following paragraph, the basic solution released has been studied with a simpler model in numerical environment. Then, the first easiest and safest physical tests were performed and the outcomes used to feed the numerical model and speed up the setting procedure.

The last phase was completely developed at the test bench to reach a fine tuning with the help of test drivers. It is important to highlight how the accuracy of the controller in applying the required force profile had the same importance of keeping a stable controller for safety reasons: this was considered as a key point during the tuning phase. Together with the characterization, this represented a demanding phase that required a long process of tuning.

4.4.1. Controller framework

The process started from a literature review about compensation algorithms. In this sense, great expertise has grown in the robotic field, where commonly the control systems require a compensation of side effects; in particular the compensation of all those which limit the accuracy in positioning because position controls are the most popular. Despite the different target of the application, which requires a force control, some journal articles were used as starting point.

Putra et al. [50] and T. Dietz in its master thesis [35] describe similar control techniques, based on a closed-loop system with an observed-based friction model that calculates a term to compensate the friction effects.

Another illuminating paper was presented by Zschäck et al. [39]: this introduces the combination of a simple feedback controller (PID) with a feedforward one based on an advanced friction model (Generalized Maxwell Slip model). Additionally, to raise the effectiveness, they propose an online adjustment of the linear model's parameters used to define the friction contributions.

The control algorithm proposed for this project was inspired by this publication and by a successive paper presented by B. Bona and M. Indri [53]. They compare some solutions, all based on a close-loop controller with an algorithm to compensate the friction effects. They claim that, although the controller's methods are different (simple PD, PID and nonlinear PID), the actual difference is made by the friction compensation technique, which should be selected considering the system's layout, the control law target and the hardware/software features, as the sensors' accuracy for instance.

Getting the idea from these publications, the system was conceived with a feedforward and a feedback part. The first one, also known as open-loop controller, provides a control action which is independent from the output of the controlled system; it is an advanced control scheme that is well-suited for processes which are affected by a known source of disturbances. Therefore, if an accurate model of the disturbance is realized, this control architecture enables quick adjustments, reducing the negative effects. The more accurate is the model, the more effective is the controller: with a perfect model the error is almost null.

Actually, too many factors affect the system functioning, therefore the possibility to consider all of them is minimal. This explains the necessity of a second term: a feedback controller. Therefore, the founding idea was to compensate the unwanted effects using a

model-based control system (feedforward) and placing a second control beside (feedback) to compensate the residual error [54].

Focusing on the specific application, the feedforward term includes two blocks to calculate inertia and friction forces: the latter based on LuGre model. As mentioned previously, a long process of characterization provided all the parameters to calibrate this friction estimator. To be more precise, during the test phase, the model was slightly variated with the aim to make it more adequate to the specific application and to simplify the structure for an easier future implementation in the control unit. The alternative solution described in (15) is the final result of an optimization process based on an experimental stage.

Referring to inertia, the calculation is simply based on the acceleration measured at the rack and on the estimated equivalent mass.

$$F_f = \sigma_1\, u^3 - \sigma_2\, u^2\, sign(u) + \sigma_3\, u + \sigma_4\, z$$
$$dz = \sigma_5\, (u - abs(u)\, z) \tag{15}$$

where:

F_f = friction force estimated
σ_i = i-th constant coefficients
u = rack speed measured
z = state variable.

The feedback control is based on a well-known Proportional-Integral-Derivative (PID) linear controller, considered the most widespread technique for the perfect combination of performance and ease. The generic formulation is briefly described in equation (16):

$$u(t) = K_p e(t) + K_i \int_0^t e(\tau) d\tau + K_d \frac{de(t)}{dt} \tag{16}$$

where:

$e(t)$ = error value, difference between a desired set point and a measured process variable
$u(t)$ = control variable
K_p = proportional term
K_i = integrative term
K_d = derivative term.

Several other more effective methods could have been selected, but this choice can be attributed to two main reasons. Firstly, the necessity to realize the fine tuning directly at the test rig, which requires a physical correlation between the controller's parameters and its response. Indeed, advanced methods as Sliding Mode Control (SMC) or Model Predictive Control (MPC) are characterized by matrices containing weighting coefficients, where a manual intervention is hardly possible.

If this is a conceptual reason, a further operative reason pushes towards this solution. As described in 2.2.4, each linear actuator has a driver which controls the system using a Programmable Logic Controller (PLC) unit.

Here the controller is embedded, with all the typical limitations of this device: low computing potentialities that force the use of simplified code to run high frequency control loops (fast task loop 8 kHz). The code has been written in it with a specific format generically described as *IEC 61131- 3 programming languages*.

Future developing phases will consider the integration of an additional processing unit with high potentialities to solve this problem and to open up at the possibility to test other control methods, as those indicated above.

The final version of the algorithm is described in Figure 63: the feedforward term is fed by the measurements of rack speed and acceleration, given by the positioning sensor on the rack.

The feedback controller instead has in input the difference between the load cell force measurement and the target force sent by the vehicle model. To be more accurate, the load cell signal is amplified and read by each actuator's driver; the latter, which receives the target force via serial protocol, calculates the difference.

Although the selected method gave good chances to do a fine tuning directly at the test rig, a preliminary setting has been defined by means of a numerical model: this was necessary to make an initial selection of the possible setups.

Figure 64 describes the very last version of the numerical model used for the tuning, obtained after a long process of optimization to reach the most balanced combination between realistic behaviour and structural simplification. In the drawing, the system is schematised with two degrees of freedom: the first body (M) is the equivalent translating mass of the actuation system of one unit, the second one $(m\ /\ 2)$ represents half of the mass of the connecting bar (used to move together the two rockers) plus half of the load cell mass. Indeed, the structure recalls the layout visible in Figure 48, where one actuator is source of the displacement's profile $(\bar{x})$ and the other is activate and compensates.

Two different springs are inserted, one (k) that represents the equivalent stiffness of one unit up to the rocker, and the other (k_C) which is the load cell characteristic stiffness. To conclude the description, the two force components are the dissipative force (F_L) and the compensation force (F_C). The tuning process had the goal to nullify the force read by the load cell, with different source profiles.

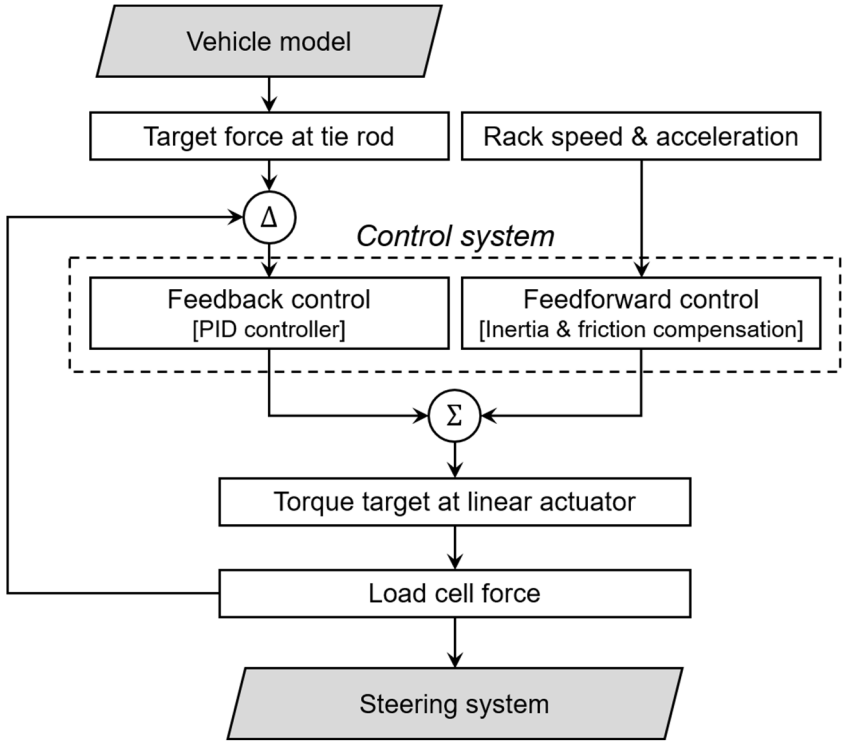

Figure 63 – Flow chart of the compensation algorithm

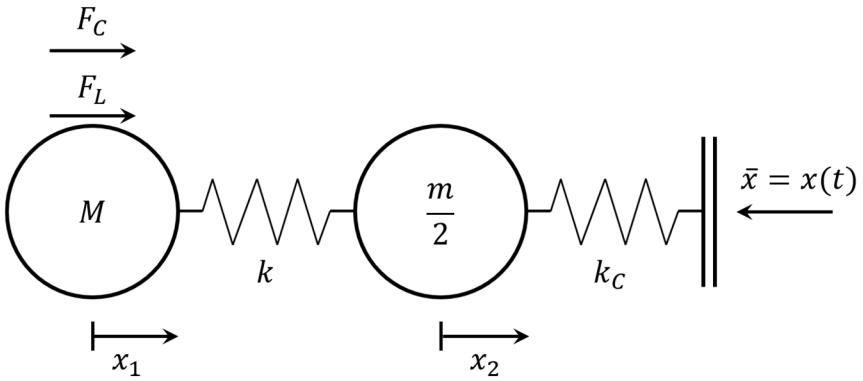

Figure 64 – Test rig scheme used for the compensation algorithm tuning (reference eq. (17))

$$M\ddot{x}_1 = F_C + F_L - kx_1 + kx_2 \tag{17}$$

$$\frac{m}{2}\ddot{x}_2 = kx_1 - kx_2 - k_c x_2 + k_c \bar{x}$$

As reference tests for the calibration can be mentioned weave and slow ramp steer manoeuvers, where the first one, with different amplitude and frequency combinations, helped to characterize the transient behaviour. In both the cases the target force for the load cell was zero, as the rack speed were moved without any connection to the upright.

The first analyses' campaign provided a set of values which guaranteed an optimal compensation with enough gain margin: it was considered the starting point for the experimental tests.

4.4.2. Compensation tests

Pre-test phase considered the implementation of the control law in the actuator driver. In this sense, a brief description of the machine's architecture is appropriate. The system is based on a Finite-State Machine (FSM), which is a mathematical model of computation that can be in one of a finite number of states at any given time. The changing from one state to another occurs in response to some external inputs: this is called transition. A FSM is characterized by a list of its states, its initial states and the conditions required for each transition.

The procedure chose is so structured: the two main state are indicated as 0 (idle) and 10 (activate). To pass from one to the other, several intermediate states are gone through considering a global counter as the trigger: these allow to check the values of each safety switch and of the external activation parameter. Whichever change brings back the machine to the idle state and the procedure must restart.

Referring to the code implementation, some specific precautions not necessary in the numerical model, were introduced. Firstly, the actuators current level was saturated to avoid unwanted and dangerous peak of force. Additionally, the input signals were undergone to a pre-process procedure, during which some of them were filtered. An example is the acceleration measurement, obtained deriving the rack displacement sensor, which is characterized by a certain level of noise.

It might be highlighted that the entire code was deployed in floating-point format because it simplified the parameters tuning; because of the nature of the PLC processor, the executable task can be speeded up using a fixed-point format, which however requires a precision knowledge of each variable range: this was not the main purpose of the current phase, which instead considered the investigation of the control potentialities. The planning foresees tests of other control techniques before the final version will be defined, as the mentioned SMC or MPC.

Once the implementation was concluded and verified, the tests started considering the best configuration obtained with the numerical model: obviously, the presence of other and not considered effects imposed a variation of the parameters. As reference test was considered a weave manoeuver: the steering wheel angle profile is shown in Figure 65.

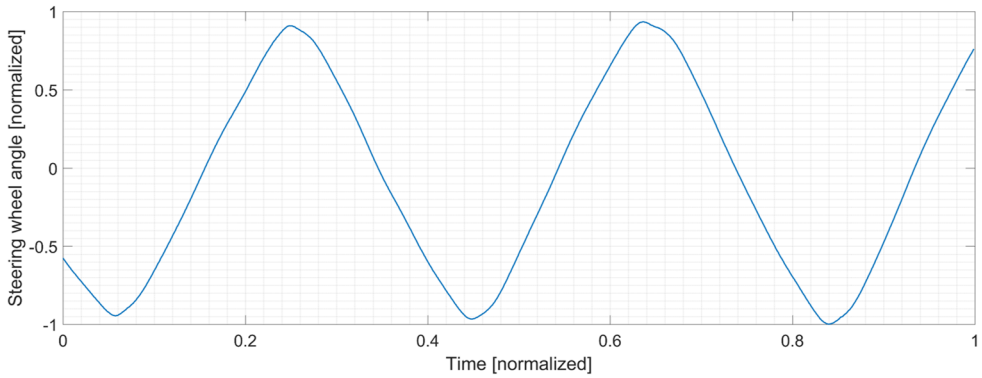

Figure 65 – Steering wheel angle profile for the weave test

The large amount of parameters to be set made difficult their adjustment, therefore a subdivision of the effects was necessary to understand on which terms operate. In this sense, the Figure 66 helped to understand the single effects and to define a target for each one during the calibration process.

In the top left corner, the load cell force is represented as a function of the rack speed, on the right side the same force is plotted versus the rack acceleration and in the bottom right corner it is represented versus the rack displacement. The fourth picture defines the dependency on the actuator's current.

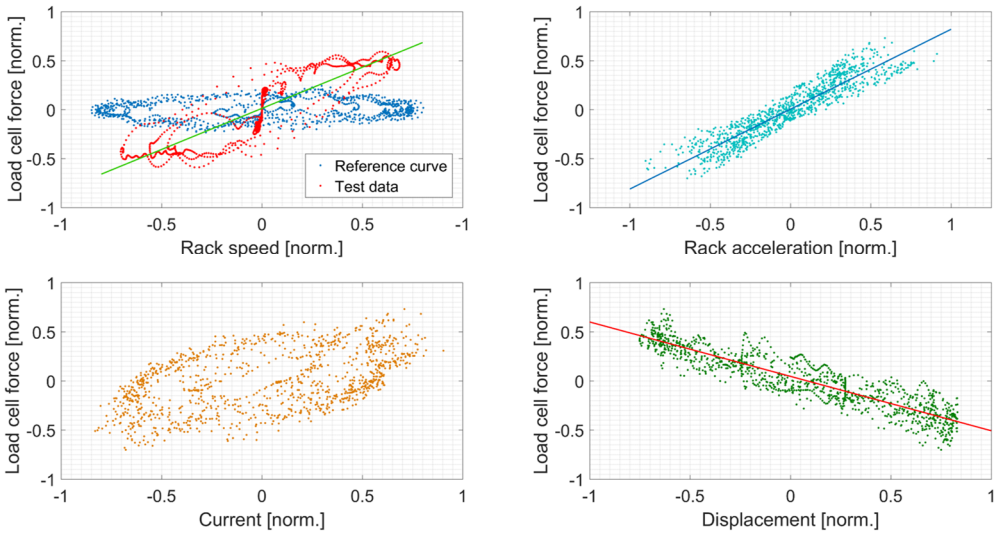

Figure 66 – Focus on the main components to be compensated

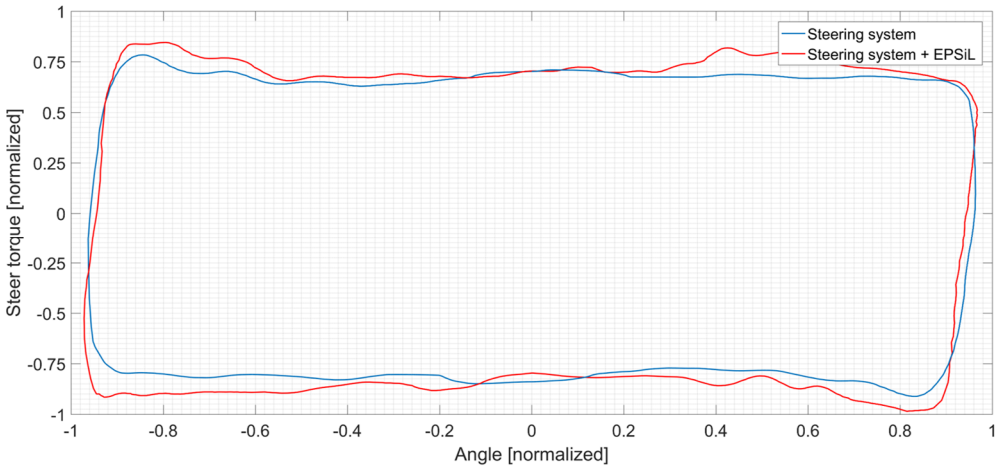

Figure 67 – The effect of the compensation algorithm

The good results of the controller are summarized in Figure 67, which shows the steering torque versus the steering angle of a weave test for two different configurations: in blue the behaviour of the steering system only, with the tie rod's ends disconnected from the test bench, in red with the steering system connected and the compensation algorithm activated. It might be noticed that the intermediate condition, with the steering system connected but the control disengaged is not shown because the values were out of the instrument range.

A careful analysis reveals that the compensation is well realized, with only little differences between the two curves. A greater error is measured for larger values of angle that is a sign of a worse compensation of the inertial term.

Additionally, the red line shows more oscillations: this is a particular effect noticed during the calibration. For its nature, the electric assistance system introduces an alternative component of resisting force: the reason is the mechanical connection between the EPS motor and the rack, realized by means of a ball screw and a belt gear. The result of the compensation algorithm, which considered as input the rack speed and acceleration, is an amplification of this effect.

However, the obtained results can be considered enough accurate to guarantee the use of the test bench in the loop with the driving simulator.

4.5. Inverted model

The last paragraph of this chapter deals with a subject conceptually well positioned here but that represents the last activity of this project from a chronological point of view.

It is based on a limit of the proposed solution: as illustrated, the possibility to enhance the steering feeling relies on the use of a real steering system installed on the test rig; it means that possible variations of its main parameters, except for the changing of the EPS control logic, are not possible in a reasonable amount of time, because it will entail hardware modifications. This is disadvantageous, especially for a preliminary phase of system definition.

Under these circumstances, to increase the potentialities of the test rig, it was conceived a possible solution based on the simple concept to modify the resisting force applied at the tie rods to change the steering system response.

4.5.1. Model inversion and layout

Referring to the scheme illustrated in Figure 68, normally the test rig has two interfaces. The first one with the driver, from which receives an angular profile and to which returns a feedback torque; the second one with the vehicle model, which requires the rack position measurement and that calculates the tie rods target forces.

The new features are obtained introducing two additional numerical blocks: a direct and an inverted steering model. The first one is exactly the model illustrated in paragraph 3.2; this receives the tie rod forces and the steering wheel angle and gives in output the rack position and the steering wheel torque. Populated with the new parameters, different from those of the actual steering system installed on the test rig, it has the main task to describe which behaviour would have the modified system.

The second one is basically the same, with inverted input-output. It is necessary to define the input modifications for the test rig, to have the same behaviour described by the direct model. Differently from the latter, the inverted model has to be parametrized with the same characteristics of the real steering unit installed.

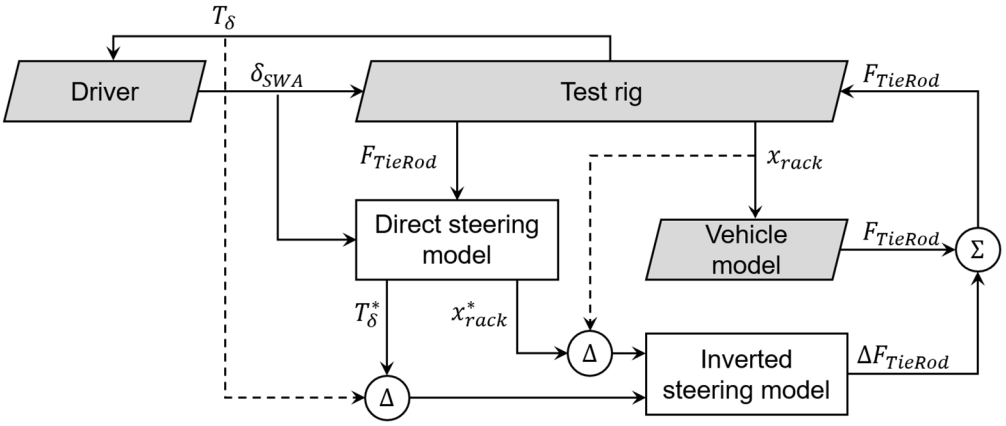

Figure 68 – Flow chart with the inverted steering model

The inverted model equations (18) directly descend from (3), written in accordance with different variables. As mentioned, in this case the steering wheel angle and the rack positioning are the output.

$$\ddot{\theta}_1 = \frac{1}{I_1}\left[T_{SW} + T_{f1} - c_1\left(\dot{\theta}_1 - \dot{\theta}_2\right) - k_1(\theta_1 - \theta_2) - c_0\dot{\theta}_1\right] \tag{18}$$

$$T_r = I_2\ddot{\theta}_2 + c_1\left(\dot{\theta}_2 - \dot{\theta}_1\right) + c_2\dot{\theta}_2 + k_1(\theta_2 - \theta_1) - T_{f2} - T_a - T_h$$

5. Results and discussion

The chapter 4 dealt with the installation of the test rig and the starting of activities. It required a long process of setup to guarantee the suitable behaviour, which began with an accurate characterization of test rig. The results led to the introduction of a control system, key requisite to reach the designed targets. Due to the high level of complexity, the procedure was split in two sub-tasks: a first release of the algorithm was defined in a numerical environment, after the description of the test bench functioning through a state-space equation. Afterward, this was implemented in the actuators' drivers and tested: only subtle variations were generated by the fine tuning. The results demonstrated a behaviour as desired in the designing requirements.

The present chapter shares the central idea with the previous one, being the natural consequence: as the main purpose it shows the good functioning of the proposed test rig during online simulations. The evaluation of the solution's benefits follows two criteria: an objective and a subjective one.

The first one is perfectly fit if the error between the target and the measured force at the tie rods is nullified: this is the only important feature to monitor. Indeed, as already mentioned, once the same force profiles are generated at the tie rods' end, since the steering system installed is a real one, the steering wheel behaviour would be the same.

More demanding is the second one. In literature different approaches are proposed, but in this work a skilled test driver was engaged to verify the main subjective differences between the feedback unit and the proposed solution.

5.1. Objective results

This first section is dedicated to define the objective qualities of EPSiL. During the experimental campaign several tests were selected and performed, to analyse the wider possible set of results. However, only few of these are here described and examined, to guarantee a structural order of the dissertation. Before the results are analysed, a premise is appropriate: as in the previous chapters, all the next graphs will show normalized values for confidentiality agreement.

The first two manoeuvers presented are standard tests already described above and in Appendix A: weave and slow ramp steer. Commonly used to characterize the steady state and transient behaviour of a vehicle, even in this case they have the capabilities to summarise the test rig functioning in the main working conditions.

During the weave test the driver maintained a constant speed of 60 kph and applied a sinusoidal steering profile with constant amplitude and frequency, as far as he was able to. Figure 69 shows the profile acquired using a specific encoder installed on the steering wheel.

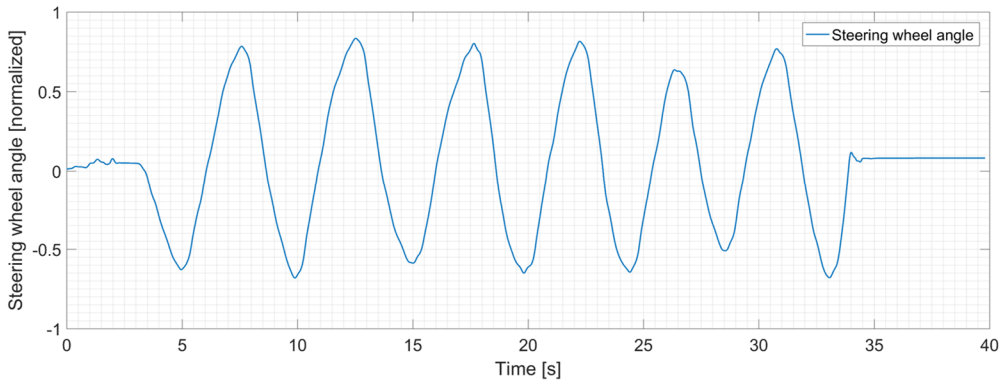

Figure 69 – Weave – Steering wheel profile

The behaviour is analysed considering the two graphs shown in Figure 70. For each actuator (on the left and right side of the structure) is reproduced the time history of the target force at the tie rods' end and of the load cell values. As might be seen, the two actuators have practically the same behaviour: this result was expected but not certain, however it is important to focus the attention on one graph only.

A preliminary analysis demonstrates how the two signals are well-phased: it means that the latency of the control process has a lower order compared to the characteristic effects of the mechanical system, therefore it does not affect the system response.

Additionally, a part from the peaks which are followed with a certain gap, the two curves are well overlapped, sign of a good tuning of the compensation algorithm. The force's peaks coincide in time with the peaks of the steering angle: since the latter profile is, almost, sinusoidal, the position peaks are equivalent to the acceleration peaks. Therefore, the main gaps are in correspondence of the maximum values of acceleration, where the rack inversions are placed.

This is a clue to identify a possible limit: the inertia is partially compensated but not completely. As said, this is only a clue, because to be sure the verification of other possible relations with the rack position and velocity is necessary.

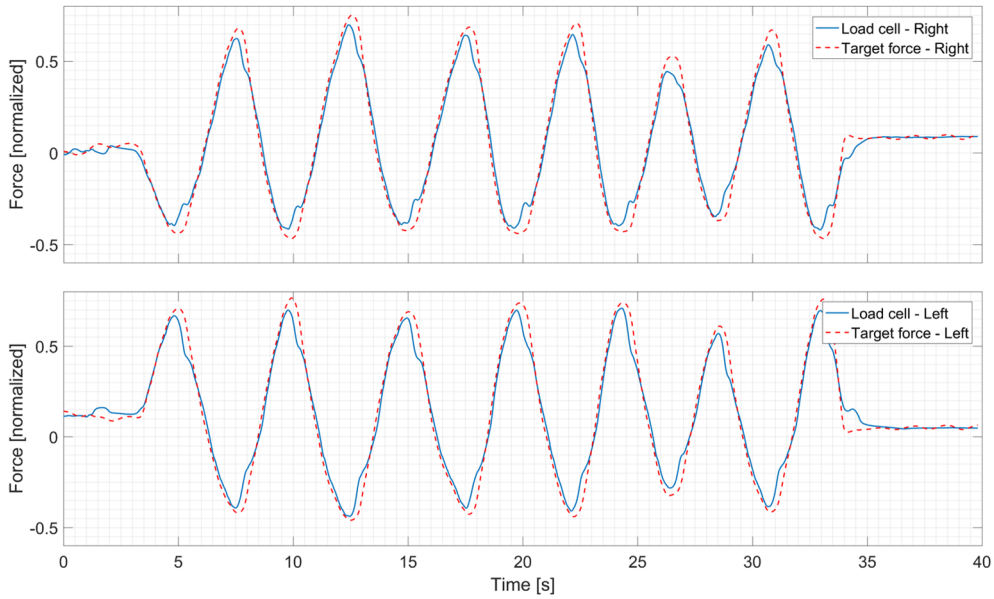

Figure 70 – Weave – Force profile at tie rods

The second manoeuver introduced is a slow ramp steer, made starting from a constant speed of the vehicle and keeping a constant throttle value during the manoeuver. Figure 71 illustrates the time history of the steer profile: in red are highlighted two ramp steer manoeuvers, performed in opposite directions for symmetry reasons.

The peak values were chosen to maintain the lateral acceleration within the linear range, but the remarkable point is that the chosen speed of the vehicle was limited to allow a wider range swept by the steer angle, which is the principal matter of the investigation.

Each section ended with an irregular and random slalom, anyway useful to characterize the system behaviour.

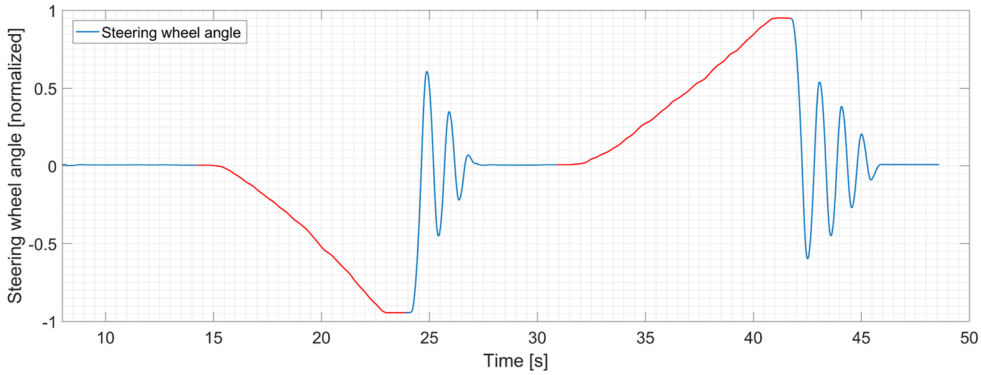

Figure 71 – Slow ramp steer – Steering wheel profile

As for the first test, the main results are described referring to the target and the load cell force profiles (Figure 72). In this case, Figure 73 magnifies the first part of the manoeuver, to better observe the relative difference between the curves.

Each slow ramp steer is identified by a higher level of force on the external wheel and a lower level on the internal one, justified by the vehicle dynamics and by the high level of lateral acceleration reached.

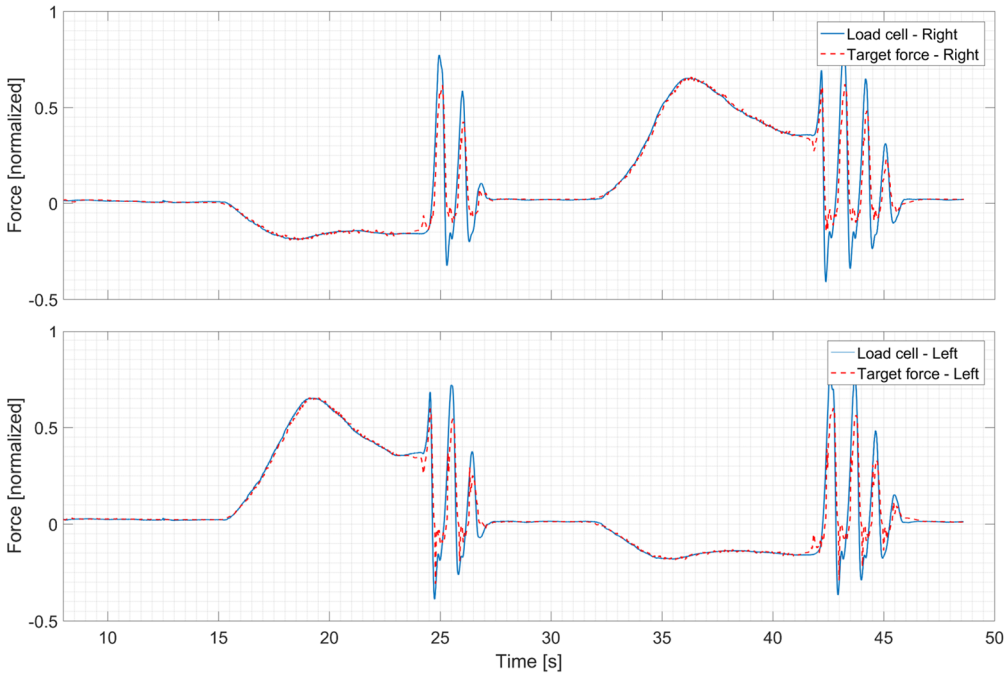

Figure 72 – Slow ramp steer – Force profile at tie rods

For what concerns the test rig behaviour, it may be highlighted the perfect functioning in quasi steady-state conditions, without any substantial difference between the two directions. Moreover, these results give the evidences that not any direct correlation between the force discrepancy and the rack position is describable. On the contrary, nothing can be claimed about the relation with the rack speed.

A part from the ramp steer areas, the outcomes show the same limits: the forces' peaks are smoothed down because of a not sufficient compensation of the inertia.

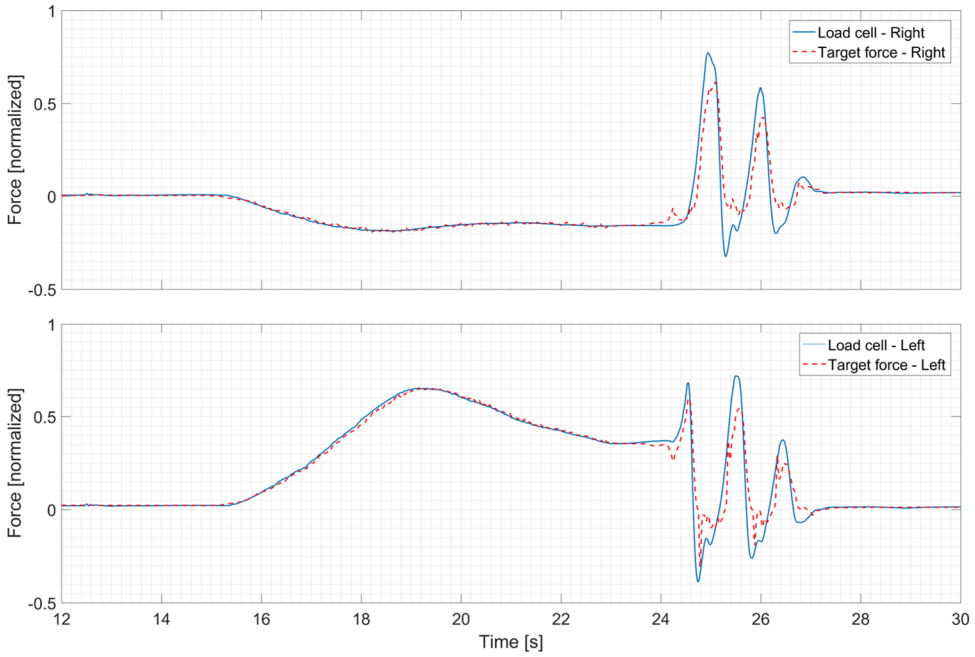

Figure 73 – Slow ramp steer – Force profile at tie rods (zoom)

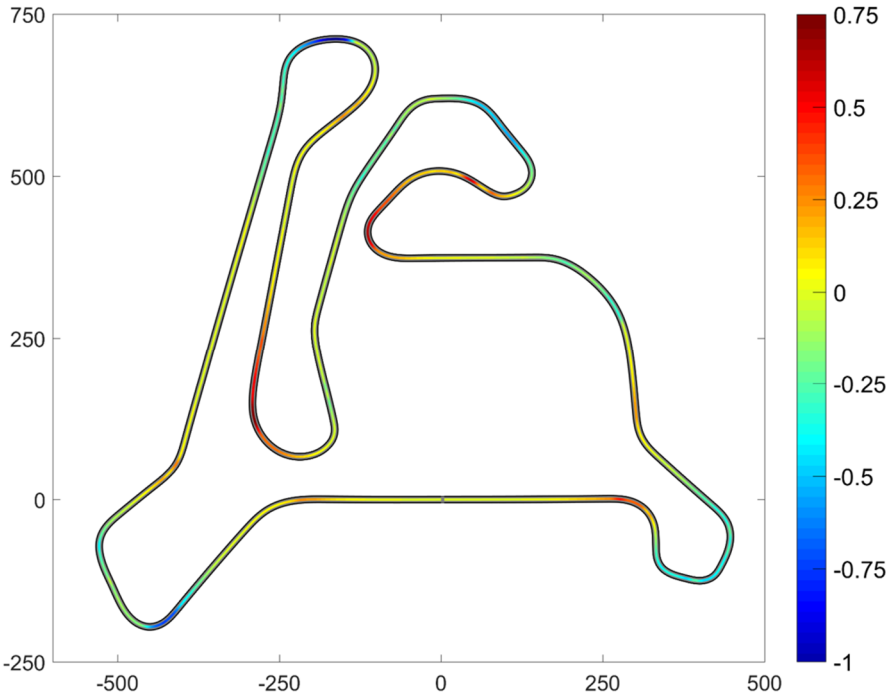

Figure 74 – Calabogie Motorsports Park circuit. The colorbar depicts the steering wheel angle

After two standard manoeuvers, to conclude this objective analysis a track lap was selected. Since the general steady-state and transient behaviour has been already classified, this one brings other benefits; firstly, several different conditions of operation are taken into account with a great saving of time: to obtain the same information with standard tests a long list of them should be done. Related to this point, there is the possibility to define some correlations between the force error and the rack displacement, speed and acceleration, which help to understand how operate to reduce the gap.

The chosen track is the Calabogie Motorsports Park circuit (Figure 74), one of the most advanced available for the driving simulator, characterized by a great number of corners with different curvature's radii. The results refer to a single flying lap ran by a professional driver, to exploit the maximum performance of the vehicle.

The results are summarized in Figure 75 that shows the difference between the target and the measured forces on the two sides together with the steering wheel profile. The latter is useful to verify the premises: the lap is demanding, from the steering point of view, and enough various too. Therefore, this track constitutes a perfect example to study the steering system.

However, as for the previous test, to appreciate the differences, only a part of the time history of these profiles is visible in Figure 76.

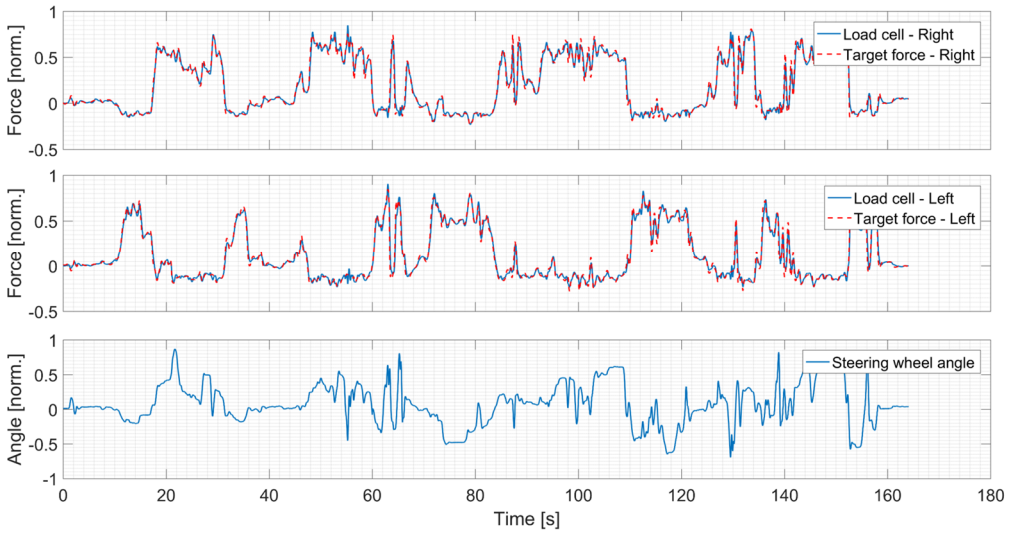

Figure 75 – Calabogie circuit – Steering wheel and force at tie rods profiles

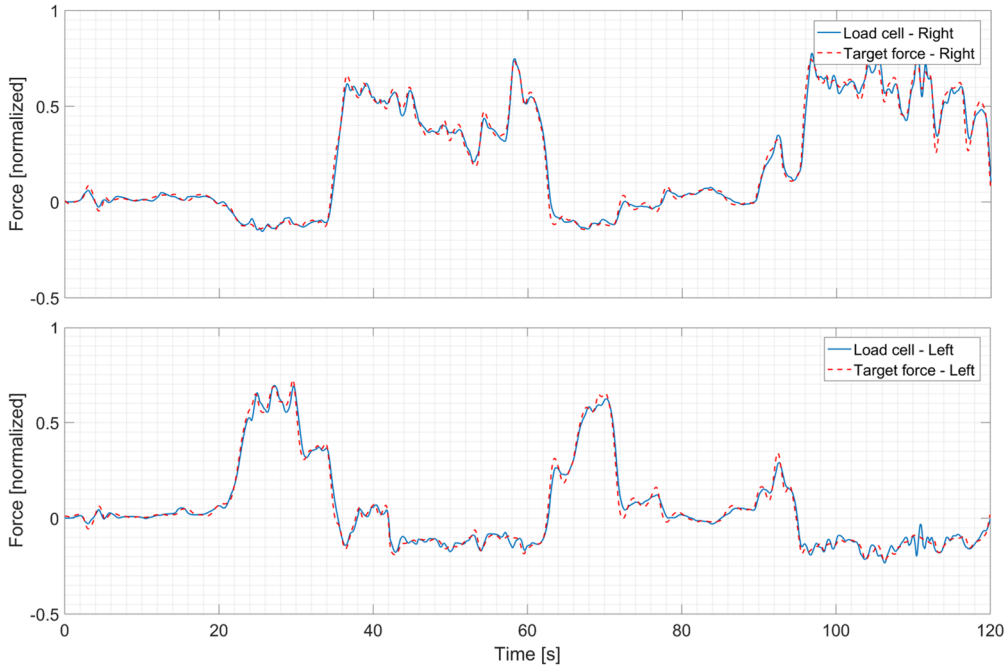

Figure 76 – Calabogie circuit – Force profiles at tie rods (zoom)

Differently from the graphs of the previous results, in this case the time history of forces are hardly understandable: it is difficult to divide the entire track in sectors, each one with a specific and easy to analyse feature. This is another strong incentive to pass to a selective study, not considering the time history.

To allow this, a previous stage was required to prepare the dataset: each channel, as the rack position, speed and acceleration or the load cell forces were filtered to cancel noise contributions and to raise the main characteristics.

The principal quantity considered in the plots is the relative error, measured as the difference between the target value and the actual value, normalized on the peak value of the target force (19).

$$Relative\ error = \frac{Target\ force - Load\ cell\ force}{\max(Target\ force)} \quad \textbf{(19)}$$

The first graph (Figure 77) identifies the relation between the relative error and the rack displacement. To be precise, the origin coincides with the centre position of the rack, considered as the idle position. A remarkable point, valid for the following plots as well, is the range of the error values, which is enough limited: it is well balanced across zero and barely overcomes the ten percent.

About the relation with the rack displacement, it might be identified a flat dependency: a part from a greater distribution around the idle position, the points are well distributed over a band with a quite constant height. In other words, the evidences confirmed what was theorized during the analysis of the previous test: there is not a direct implication among the

force error and the rack position. Therefore, not any specific source of resisting action related to the rack position is present.

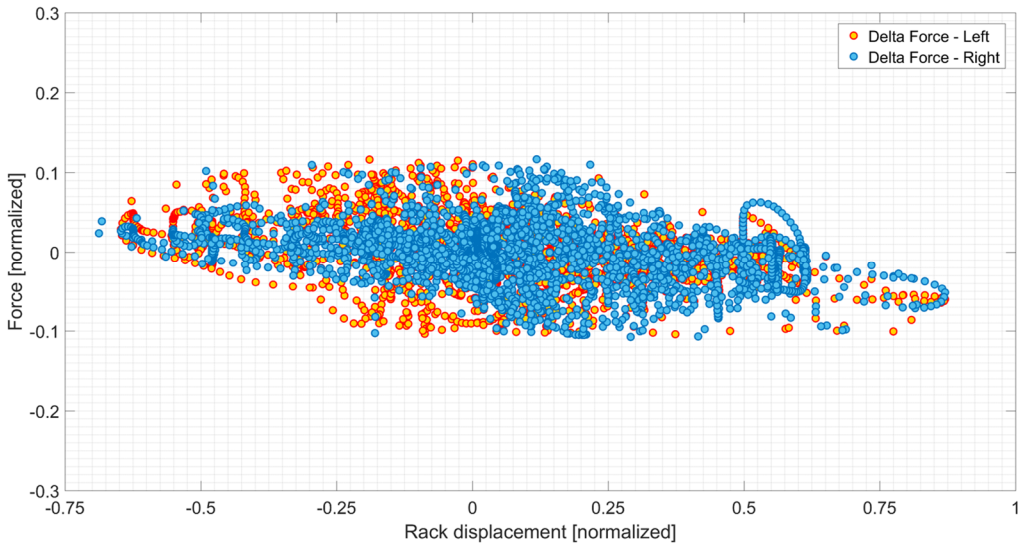

Figure 77 – Calabogie circuit – Force error versus rack displacement

At a first glance similar trends could be observed for the rack speed dependency (Figure 78), but actually this gives some food for thought.

The points are almost uniformly spread over the entire range, but defining a sort of diamond shape with the major diagonal aligned with the x-axis. This underscores the presence of a remarkable group of points around the null velocity. Partially this is justified by the effect of inertia: as already mentioned, some subtle lack in the compensation of the inertial term is present; since the worst condition coincides with the maximum acceleration that is reached with a speed inversion, it is clear how this effect should be more evident across the zero speed value. But this opens up to a second point: the friction in static conditions can generate the same effect.

This, generally known as stiction effect, characterizes the pre-sliding phase; also, it is hardly compensable without phase lag, so a small error is always present. This mix of effects complicates the compensation's method.

Finally, the dependency from the rack acceleration is shown in Figure 79. As before, the central zone is characterized by a more numerous cloud of points with a greater range along y-axis. The main reason is still the stiction effect already introduced and described above, as regards to the relation with the rack velocity.

Except for this part, an evident trend of the points, highlighted by the black dashed line, is visible. Since the trend is linear with the rack acceleration, the contribution is certainly due to a not complete compensation of the inertia. However, the angular coefficient of the straight line which passes from the origin is much less than the actual value of the equivalent mass: it is an evidence that the inertia is compensated but not completely.

Among the other changes, the future activities will consider a variation of the equivalent mass value used in the compensation algorithm to nullify the slope of this fitting curve.

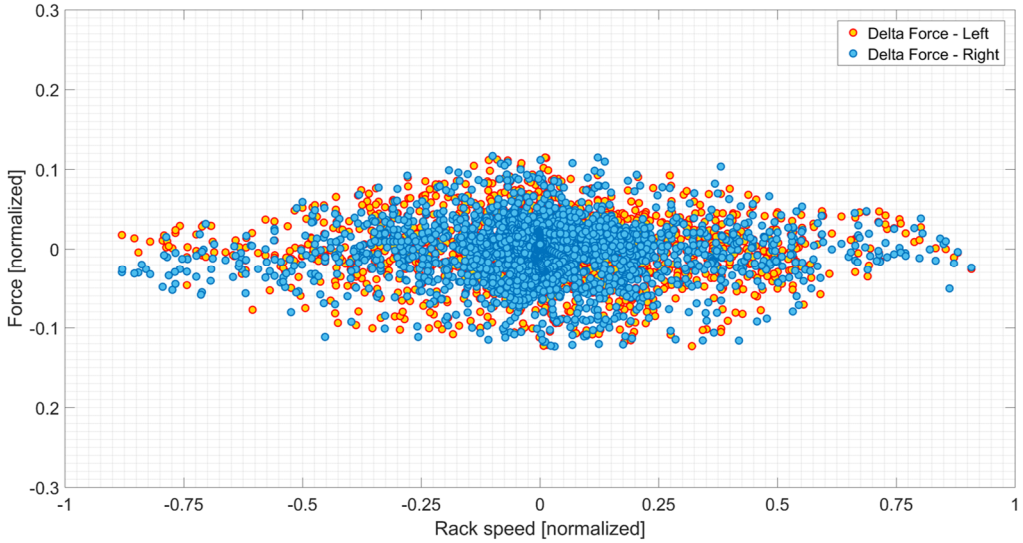

Figure 78 – Calabogie circuit – Force error versus rack speed

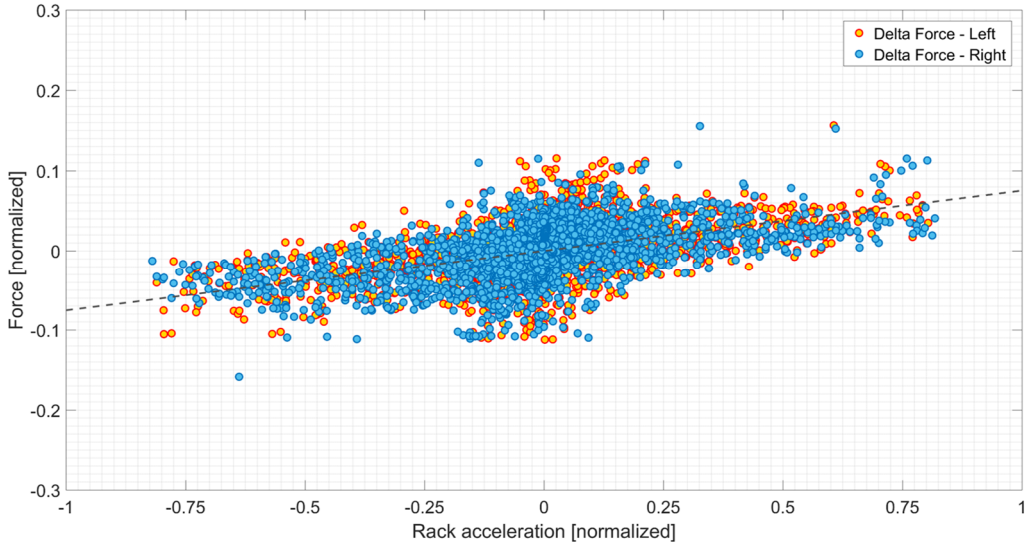

Figure 79 – Calabogie circuit – Force error versus rack acceleration

As already seen, the relative error is generally well distributed, but more exact comments require statistical tools. Figure 80 introduces the Probability Density Function (PDF) (20) of the relative error for both the actuators. The results were limited in the range $\pm$ 10%, given the few residual points.

$$v_i = \frac{c_i}{N w_i} \tag{20}$$

where:

v_i = bin value
c_i = number of elements in the bin
w_i = width of the bin
N = number of elements in the input data.

The histograms are almost overlapped, therefore to have a more direct view of the distributions the Kernel Density Estimation (KDE) curves were marked. KDE is a non-parametric way to estimate the probability density function of a random variable, basically used to smooth problems based on a finite data sample [55].

The plot gives some food for thought: both the actuators have a similar tendency, with a substantial superimposition of the columns. They appear to own an almost symmetrical shape.

Given that the distributions are similar, the left side was analysed more in depth as example. In Figure 81 the histogram is combined with the probability density of the normal distribution (21). It might be said that the PDF of the relative error does not draw a perfect normal distribution, hence only a central part (the orange one) is considered. In this region, it appears a slightly unbalanced disposition of the points towards the function tails to the detriment of the central zone.

However the values obtained give an idea about the error: the media is almost zero and the standard deviation is 0.14.

$$f(x|\mu, \sigma^2) = \frac{1}{\sqrt{2\pi\sigma^2}} e^{-\frac{(x-\mu)^2}{2\sigma^2}} \tag{21}$$

where:

μ = mean value or expectation of the distribution
σ = standard deviation.

A last index introduced is called Skewness: it is the measure of the asymmetry of the probability distribution of a real-valued random variable about its mean. The value for a normal distribution is zero, but applying this index to the original PDF, the value obtained is 0.4. Being positive, it indicates how the data are spread out more to the right side.

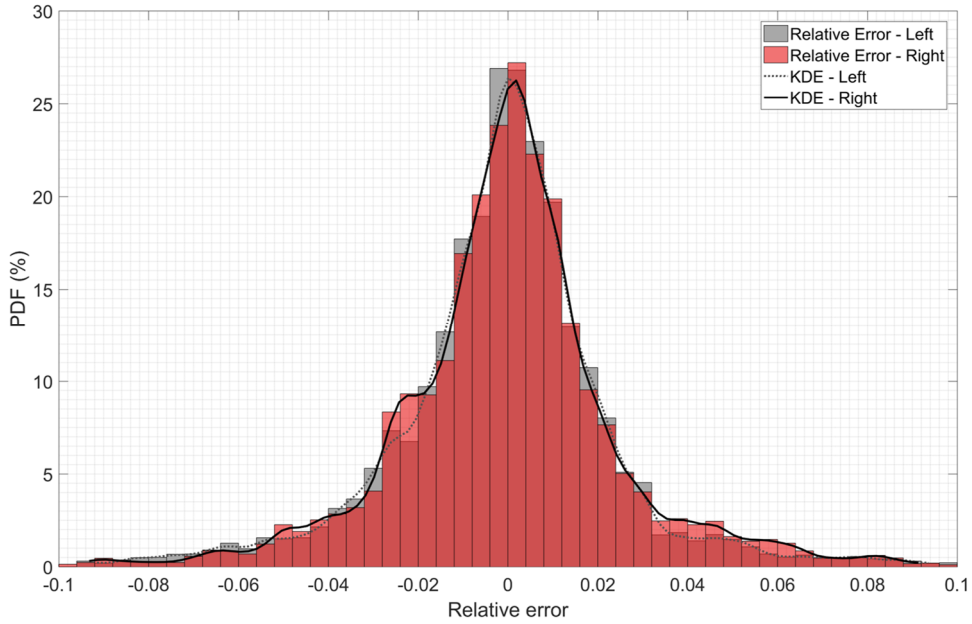

Figure 80 – Probability density function of the relative error

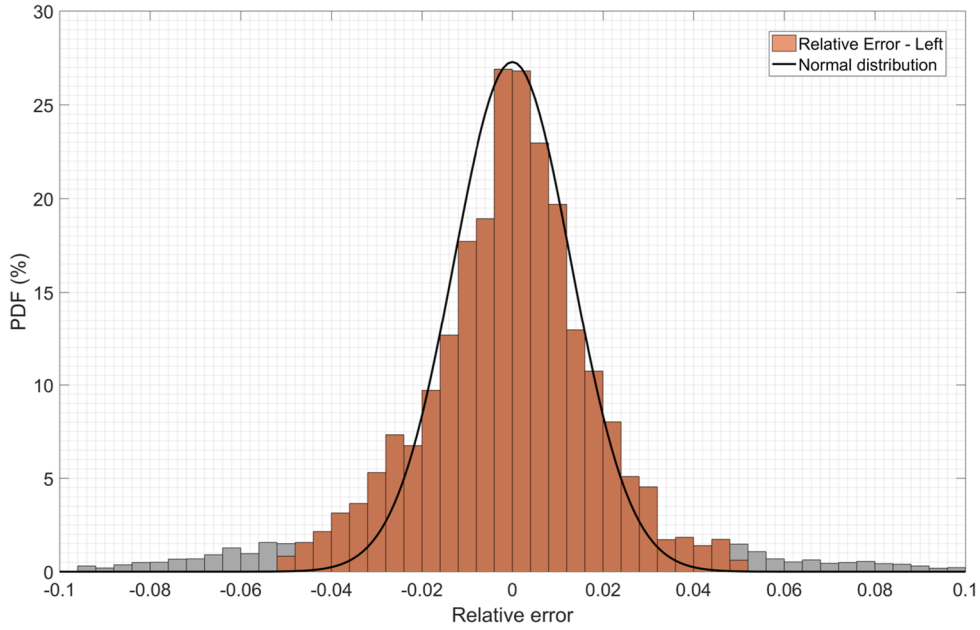

Figure 81 – Probability density of the normal distribution of the relative error

In conclusion, this paragraph presents the results of the objective investigation. The adopted method allows to understand and define the dependencies from each principal contribution, which help to judge the outcomes. The long process of calibration brings positive results: the unwanted and spurious contributions are correctly compensated with only few lacks related to some friction and partially to some inertial effects.

Furthermore, an additional verification has been carried out: using statistical tools, it has been possible to investigate more clearly the relative error's dispersion. The outcomes proved a significant symmetry of the distribution with an almost null mean value and a remarkable low value of standard deviation, in addition to a good superimposition of the two actuators, which excludes any local effects on one unit (Table 5).

Given that, the target to generate the same force profile has been achieved with a sufficient level of fidelity.

Table 5 – Objective results – Statistical parameters

Statistical parameter	Value
Mean value μ	0
Standard deviation σ	0.14
Skewness index	0.4

5.2. Quality profile

The objective qualification is followed by the subjective one and the latter is even more interesting from the project point of view, because the main purpose of this thesis is the proposition of an alternative solution compared to those already available from the state of the art, capable of enhancing the steering feeling in driving simulators. Indeed, this main point has several positive implications, from the development of new steering systems to the verification of ADASs interface with human beings and more.

From a brief review of the literature ([18], [56]–[59]), it is clear enough that the most common approaches adopted in these cases are based on statistical methods: a group of drivers, with different level of skills, is selected and undergone to the same test. A survey, accurately prepared and relevant for the information to acquire, is provided and the results are then processed: statistical tools are useful and can give a perfect idea about the average trend or the dispersion of the results. However, in all the mentioned cases the main purpose was slightly different: the most of the papers refer to a process to define relations between objective data and subjective feelings (obviously related to the steering system) or to describe the ideal targets for a perfect steering system. And it is obvious that a large assessment is required.

Instead, the main goal for this project is slightly different, therefore well-trained drivers are necessary to verify the small differences between the feedback unit and the test rig. Additionally, the selected test drivers should have experience at driving simulator, to be able to focus on steering characteristics only without lack of concentration due to other effects. These reasons, added to few resources dedicated to the project, led to the involvement of a single test driver only but used to work with driving simulators.

Concerning the evaluation method, a list of the main features to be analysed was defined. Table 6 introduces the principal quality indices, selected merging the industrial know-how of the partner company with the information available from ISO rules and specific journal articles as [27] or technical books as [8]. Also the judgment method is not casual: SAE J1441_201609 [60] defines a guide line to rate subjective evaluations for vehicle ride and handling. The score ranges from 1 to 10, but to be aligned with the entire dissertation, the values were normalized at one.

5.2.1. **Quality indices and results**

Before the discussion of the results, it is presented a brief explanation of the criteria adopted. It has to be noticed that different KPIs require different manoeuvers, as well reported in the second column of Table 6.

Basically, the driver has the capability to perceive directly the steering torque, while a feedback on the steering angle is provided by the vehicle dynamics. However, quite all the measurements are based on these two quantities: steer torque and angle.

A remarkable point consists in the characterization of the *steer torque* and *angle rate*, which is the analysis of their linear features. Referring to the first one, it is required a linear growth with the lateral acceleration, up to the 90% of the lateral grip limit; since the steering system is a great source of driver feedback, this ideal trend is important to transmit how the vehicle behaves during the manoeuver: the first part is characterized by a linear increment with the growth of lateral forces. Then, before the lateral acceleration limit, the steer torque slope reduces and inverts the trend, as a safety warning of the next loss of grip. In accordance with the torque, the steering wheel angle follows a similar tendency, with an initial linear slope and a following decrement around the peak value. For the evaluation of these factors, a slow ramp steer manoeuver is the best choice.

On-centre feeling refers to nominally straight-line driving conditions with large-radius bends at high speeds but low lateral accelerations [23]; a practical example is the lane change manoeuver on highway.

Referring to the passenger vehicles, this is a fundamental index representing daily driving conditions and being directly connected to the comfort perception. Translating the sensations in mathematical parameters, the dead-bands around zero (along the two axes) play a fundamental role: the angle dead-band is required to avoid a too much reactive behaviour of the vehicle, which is a negative quality that promotes the discomfort. On the contrary, a too large dead-band is badly felt, reducing the overall handling features of the vehicle and giving the undesired idea of backlash and hysteresis. Therefore, a good balance is required: the sharp value is a trademark feature.

Similar considerations can be done concerning the steering torque: the value should increase at the growing of the speed (and of the lateral force consequently) without leaving the idea of a too much greater effort. As highlighted by prof. P. Pfeffer in [22], the elastokinematics and the hysteretic effects have a crucial role to qualify this effect, therefore, a better behaviour of EPSiL is plausible.

Returnability test is commonly realized at different levels of velocity, because the behaviour could change a lot. Once a defined lateral acceleration limit is achieved and the vehicle is stable, which entails few seconds of constant steer angle, the steering wheel is

released. For this specific case, the results have been summarized in a single indicator, mainly because the values assigned at the three levels were coherent.

The spider plot shown in Figure 82 compares the subjective results of the feedback unit against those of EPSiL. The test driver made use of the same vehicle model and performed the same manoeuvres to provide information about its perceptions. Each test was repeated few times to gather the required data to judge the behaviour.

From a global point of view, the feedback unit lacks of subjective realism, having less points in each single field. According to the driver, the steer angle rate and the reversibility are comparable with the EPSiL's results, while the quantities related to the torque perception are less effective.

However, each single index deserves a specific explanation going further in detail. Starting from the reversibility, this has the lowest overall score, but the main issue is in the tyre modelling: a bad characterization of the self-aligned moment of the tire crucially influences the results. A part from that, in this case the advantages of EPSiL are limited, because it only depends on the torque profile generated.

Referring to the on-centre feeling, EPSiL does not guarantee a perfect behaviour mainly for some issues in compensating the stiction forces outside the steering system, because the on-centre feeling is deeply affected by the hysteretic effects.

However, for opposite reasons the feedback unit has a worse behaviour: in this case the problems are related to the difficulties in modelling these complex, almost nonlinear, effects. This is a remarkable point, because it is one of the main reason that justifies the use of EPSiL in the place of a feedback unit. Similar reflections can be done for the steer angle rate, although the score reached were greater for both the solutions.

EPSiL gained high scores for the indices related to the torque. The basic idea of the test rig rotates around the recreation of the real force profiles, therefore good values were expected. Additionally, the possibility to exploit the real assist system eliminates a great source of possible inaccuracies. In this specific case, during the population of the steer model great efforts were made to have at the driver's disposal the most accurate assist system; nevertheless, the characterization of the entire dynamic behaviour was hardly possible. Then a second key point is the description of the elastokinematics and hysterical effects, which in the on-centre zone have a fundamental importance.

Table 6 – Quality profile criteria

Performance indices	Manoeuvers	Evaluation criteria
Steer torque rate	Ramp steer till limit	At lateral acceleration between 0.3 g and 90% of the limit, the steering torque should rise gently with lateral acceleration without compromising the on centre response. Torque rate should be linear and to give a good understeer feeling in the linear range and thereafter a roll-off in torque before the grip limit to advise the driver.
Steer angle rate	Ramp steer till limit	In cornering, the steering sensitivity should remain constant in the linear, off-centre range and then reduce in a progressive fashion when approaching the limit in a way which is in harmony with the steering torque rate.
Steering effort progressivity	Weave	Torque rate variation has not to be excessive, giving bad feeling of slow damping effect at zero and a consequent excessive damping effect beginning new steering; the dead band has not to be much large neither too much narrow. Around 0 deg, no *spring effect* is admitted.
On-centre feeling	Highway	Evaluation of correct dead band around 0 deg. Evaluation of *boat effect*.
Reversibility at slow speed	Steering pad 10 m	Allow the vehicle and the steering angle to return to the zero condition with as little overshoot and as little oscillations as possible – Slow speed.
Reversibility at medium speed	Steering pad 20 m	Allow the vehicle and the steering angle to return to the zero condition with as little overshoot and as little oscillations as possible –Medium speed.
Reversibility at high speed	Ramp steer	Allow the vehicle and the steering angle to return to the zero condition with as little overshoot and as little oscillations as possible – High speed.

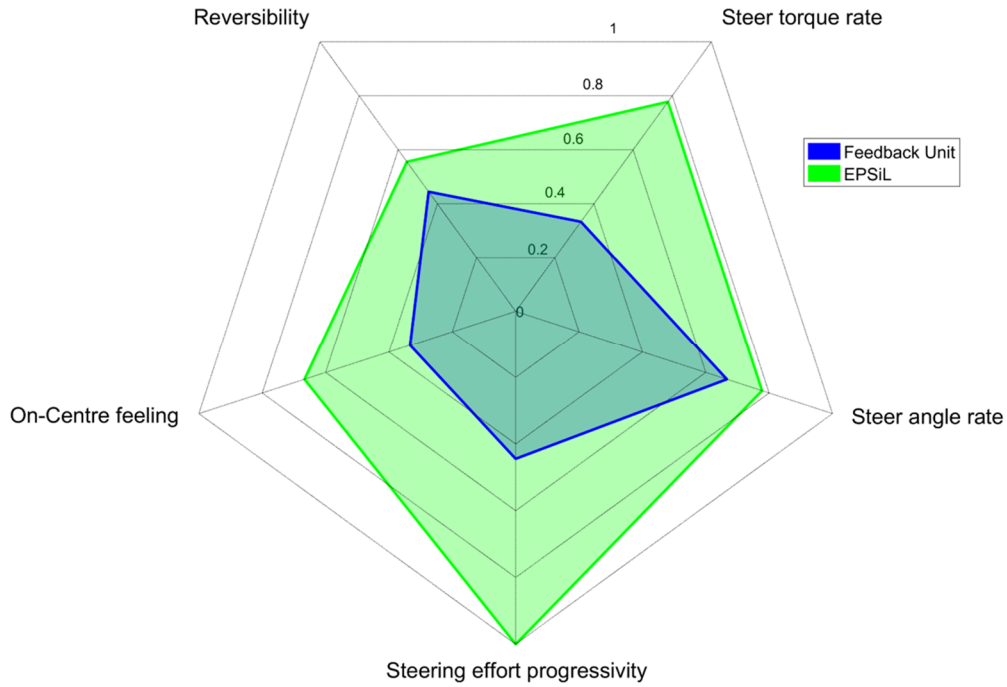

Figure 82 – Quality profile comparison: feedback unit vs EPSiL

This paragraph contains some of the key results that justify the project and therefore has to be considered among the principal ones. What should be gathered as fundamental information is that the proposed solution is able to generate with sufficient accuracy the force profile as required, guaranteeing a realistic response of the steering system as well as a controllable outcome.

The results are clear from a subjective point of view as well: the comparative promotes the experimental approach as the most precise, especially for the quite perfect generation of the feedback torque.

Nevertheless, a possible objection could be raised: the feedback unit's results derived from the steering system model deployed. Modifying the model, the results could improve. The truth is that the limits of the feedback units lie on the possibility to model all the effects active in a complex nonlinear system and, as mentioned above, even the most advanced steering models are not able to describe an optimal characteristic functioning.

5.3. Inverted model

In paragraph 4.5 has been presented the method designed to overcome a limit of EPSiL, which is the impossibility to easily test hardware modifications of the steering system. As described in Figure 68, this makes use of two numerical models of the steering system (one direct and one inverted) to change the system response.

The project's planning foresaw the implementation of the virtual part on a dedicated hardware of the driving simulator and a test campaign to prove its effectiveness directly at the test bench. Unfortunately, for partner company's decisions, the cited tests did not take place but they were postponed and will be subject of future activities.

Nevertheless, bringing some modifications to the original framework, it was possible to start up a virtual activity with the purpose of verifying the potentialities of this process.

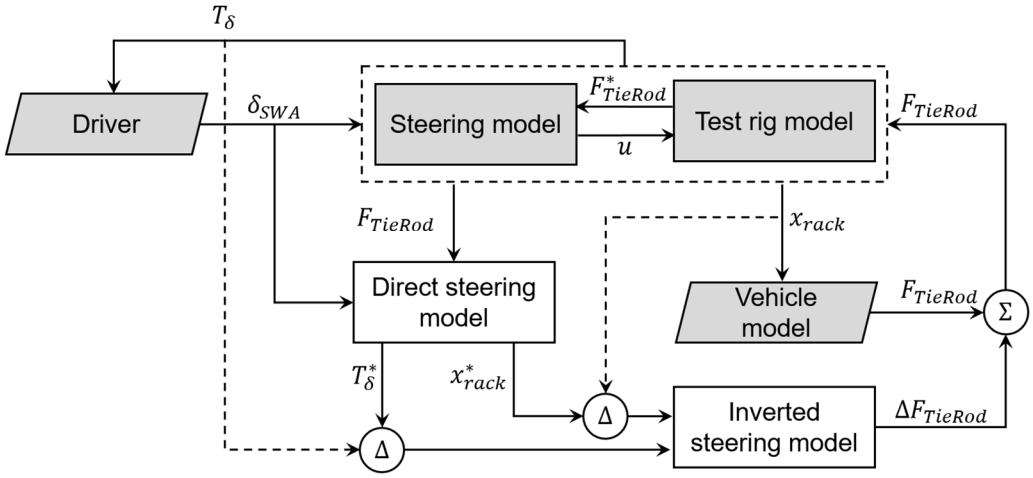

Figure 83 – Flow chart with the inverted steering model for numerical validation

The changes can be identified referring to Figure 83: the main difference lies in the replacement of the real test rig with a virtual block (the dashed rectangular in the figure). It is composed by two elements: the first one symbolizes the steering system and it is represented using the two degrees of freedom model above introduced. The other one instead reproduces the dynamic behaviour of the test rig, using a state space representation.

The latter is inspired by the scheme of Figure 64, with some modifications to better cover the real behaviour of the test rig. Before it was used for this application, the equation system was verified with experimental data.

Despite this variation, the functioning is globally the same, though the information in input are divided among the two blocks. The steering wheel angle profile is sent to the steering model, whilst the resisting force target is input to the test rig model.

The latter, acquiring information about the steering system state (u), defines the actual force profiles exerted at the tie rods' end (F^*_{TieRod}) which, in turn, are applied to the steering model. Finally, this can generate the steering torque felt by the driver.

From a structural point of view, this layout counts three different steering models: two direct and one inverted. Regarding the direct models, one is required to substitute and to replicate the behaviour of the real steering while the second one describes how the updated steering system (with all its modifications) would work. Differently, the inverted one, which belongs to the original layout, is necessary to provide the modifications of the tie rod forces.

5.3.1. Numerical results

To validate the potentialities of the method and comment its basic functioning, a simple open-loop manoeuver was chosen: a weave test, described in detail in Appendix A.

Referring to the possible modifications, it was hypothesized to analyse the effects of a crucial part as the torsion bar. The substitution of this component, which means a variation of the torsional stiffness, is plausible because it affects some macroscopic features. To give an example, a HPS with a stiffer torsion bar is characterized by an increment of the overall effort required at the driver, accompanied by a reduction of the total steering wheel angle and a consequent increase of the driving precision. In this specific case, the original torsion bar stiffness was increased by 20%.

Since the manoeuver is an open-loop, the steering wheel angle profile is equal for both the cases. Rather, the attention has to be given to two other quantities: the forces at the tie rods as input and the steering wheel torque as output.

Starting from the latter, the expected result for a stiffer torsion bar is an increment of the steering torque, due to a smaller force exerted by the assist system. Referring to the graph in Figure 84, the modified solution has greater values of feedback torque, as expected. Instead, the trend is similar without any significant variation of the effects.

To reach this reliable enhancement of the feedback torque, the system acted to change the target force required at the tie rods. In particular, the resisting action was increased consequently: as depicted in Figure 85, the peaks of tie rod forces has greater magnitude.

It has to be noticed the difference between the force profile required at the tie rods' end and the actual force exerted: obviously, in this case the major interest is captured by the request. Indeed, the actual force applied is a function of the control system's functioning and of the control logic utilized. Once this is considered well-functioning, there is not any substantial variation with different input.

In conclusion, although the impossibility to test the original methodology at the simulator, an alternative plan was scheduled to carry out a virtual analysis. Despite the ease of the test proposed, the results testify the potential functioning of this smart solution, which could be able to enlarge the system functionalities.

As will be described below, this is one of the main points to be developed in future works, with the planning of a testing phase at the driving simulator.

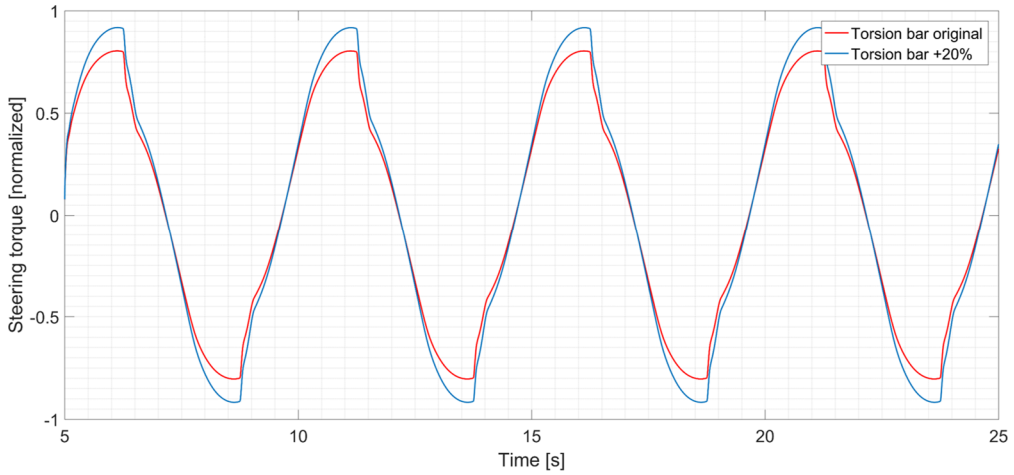

Figure 84 – Inverted model – Steering torque comparison

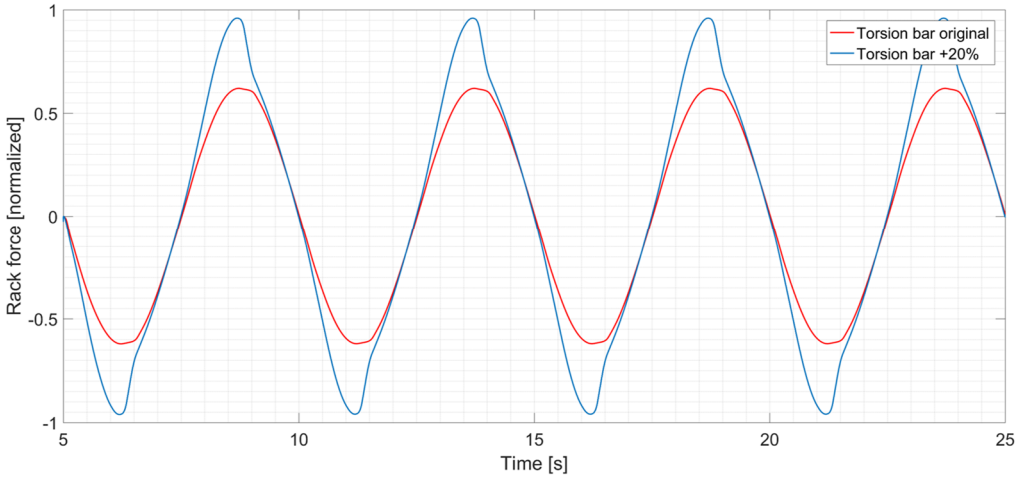

Figure 85 – Inverted model – Rack force comparison

6. Conclusions and final remarks

The function of the steering system to assess the vehicle performances is well witnessed in literature and in this context the steer torque covers a key role. Among the driver's perception paths, the haptic system has a quicker processing that helps the driver to provide a fast reaction; the steering feel is directly related to the subjective assessment of the lateral vehicle dynamics, therefore a proper steering behaviour is able to positively influence the general opinion about a vehicle. It is not the only reason, but it surely explains the industrial investments for a significant improvement of this assembly, even introducing new technologies.

Referring to the research question raised at the beginning, the automotive industry has improved the developing method exploiting new technologies and these benefits have been transferred to the steering systems as well. In detail, in the last decades, the research has met the potentialities of modern driving simulators, which nowadays are capable of a high level of realism both for static versions and moved-base ones. Introducing a real driver, not only they acquire the capability to test the vehicles with realistic human input that are difficult to be generated artificially, but provide a perfect environment to study the driver's behaviour and its perceptions.

In this context it is placed the current project, which attempts to solve a common drawback of driving simulators: these, typically equipped with feedback units, present difficulties of different nature in producing a realistic steering response. Therefore, this project aimed at proposing an alternative solution to create a more realistic steering behaviour and consequently a more genuine driving perception.

The research began with the definition of the key targets; once they were designated, a literature review helped in the identification of the possible solutions. Commonly, the main shortcoming of feedback units comes from the problems to represent a realistic and numerically stable steering model to emulate the feedback torque, consequently the idea considered the introduction of a real steering system to avoid problems in modelling all the effects. This included an experimental test bench designed to install a steering assembly and to apply at the tie rods the forces coming from the front wheels.

This option moves the main system's target: if the common solution pays attention to the steering torque, which is the term of comparison with real vehicles, with this test rig only the tie rod forces have to be matched. In this sense, the control task is easier.

The first part of the process considered a careful investigation of the actual performances of real steering systems in different driving conditions. Making use of

instrumented test vehicles, the main quantities were acquired and then processed to obtain the characteristic force and speed profiles. Besides an identification of the working range for the actuation system, it supported the designing phase. The resultant load cases were helpful to validate the stiffness of the overall structure in the following validation phases, while the information about the influence of the vertical displacement on the friction effects were crucial to select the structure's layout.

In reference to this, an accurate evaluation of pros and cons of all the versions brought to the use of a simple one: the final layout is distinguished by a common base frame on which two symmetrical units are installed and fixed. Each unit owns an actuation system based on an electric linear actuator that transforms the engine torque in a linear thrust applied to the tie rods. However, they do not have any mechanical system to emulate the wheels' heave.

Basically, considering that the friction effects due to the vertical movement of the wheel are limited, it was preferred a simpler version but able to be controlled easily. Moreover, with few variations, this structure will host the additional mechanism necessary to create the wheels movement.

The installation phase included the integration of the test bench with the driving simulator. In this sense, the layout was conceived to respect volume constraints; furthermore, the necessity to keep a high level of realism, has pushed towards a compact solution to avoid any interference with the driver's visual field.

This first phase was then followed by a longer stage necessary to identify the system's properties: the main aim was the classification of the unwanted components of forces coming from the test bench capable to affect the force profiles. As hypothesized at the beginning, to achieve an accurate functioning, a control system is required to compensate these effects. The investigation's outcomes were crucial to describe and tune an efficient controller solution. In this sense, the tuning process was boosted by a numerical model, which helped to select the most suitable parameters.

Currently, the control algorithm is based on two contributions: a feedforward and a feedback part. The first one allows the compensation of the friction and inertial contributions, while the second attempts to compensate the error between the forces' request and the load cell measurements using a PID controller. As indicated in the following, investigations on alternative controllers will be subject of future works.

The validation considered two phases: an objective and a subjective comparatives, both important to utilize the system.

Referring to the first one, several of the typical manoeuvers were analysed: since the crucial point for this test rig is to guarantee the same force profiles at the tie rods, the tests focused the attention on the difference between the request of force and the actual force measured.

A more detailed study was applied to the results of a track lap: all the contributions of the relative error, calculated considering the two quantities above cited, were extrapolated and commented, using statistical tools as well. The results prove a good overall functioning of the system: the curves are almost overlapped and only few lacks are mainly related to the inertial compensation and stiction effects.

The subjective investigation faced other issues: the definition of the procedure to follow and the identification of the comparison term. Starting from a literature review, the main methodologies adopted for these analyses were selected: in the end, it was decided to adopt a

single test driver to compare the effectiveness of the test rig. Principally, the reasons lay on the necessity to have a skilled driver with a previous expertise of driving simulators but also on the limited budget allocated for this specific activity.

Referring to the comparison term instead, it was decided to realize a custom steering model to be used together with the feedback unit of the driving simulator. The necessity of a specific model was prescribed by the required balance between model's accuracy and stability. The resulting layout consists in a two degrees of freedom model, supplied with advanced friction and assist models.

The subjective campaign referred to some quality indices among the most favourite for subjective surveys, based on the perception of the steering behaviour. Again, the results demonstrated the undeniable advantages of the proposed solution to recreate a more realistic response.

Combining the results of the two campaigns, the global judgement about the test rig is positive, despite some limitations. The main one concerned the difficulties to test steer's modifications: for the test bench nature, the entire steering assembly has to be changed with a consequent waste of time.

A possible solution to this issue has been theorized during the creation of the steering model: using a specific framework it is possible to modify, via software, the system response as a hardware modification has occurred. This method, completely new for the state of the art, has already proved its potentialities.

In conclusion, the results certify that this solution can improve the steering feel in driving simulators, simplifying the development process and speeding up the parameter's tuning. In light of the results, the proposed solution responds to the research question raised at the beginning and addressed to the project. The test rig can bring the realism of the driving simulator to an upper level, facilitating the test driver role. Therefore, it can be considered as a novel contribution to the development of the state of the art.

Nevertheless, the current work produces an additional scientific contribution from a methodological point of view. The same approach adopted for the steering assembly, can be extended to any other mechatronic system of a vehicle, following the same framework. Therefore, the benefits are rather related to the enhancement of the virtual simulation with the introduction of the human factor.

6.1. Outlook for future work

The outcomes of the current work opened at several developing points, which could be subjects of future projects. As already described in the dissertation, a suggestion is to operate on the control algorithm: the objective results have already reached a good level, but the revealed limits highlight the necessity to move in different directions.

More in detail, the friction model is enough accurate to foresee the hysteretic behaviour of the system, but with some residual limitations. As an alternative, the friction effects could be calculated starting from the load cell measurements, instead of the rack speed values. Otherwise, the stiction forces could be estimated with a neural-network based approach.

Regarding the compensation algorithm, the idea is to exploit the peculiarities of advanced controllers: among these, the MPC and SMC can be listed. Briefly, the MPC attempts to foresee the system evolution using an appropriate model: the possible changes in

the controlled variable can be caused by the control action (actuators) or by some disturbances. The controller's optimization algorithm calculates the actuators' action that minimizes the error evolution between the target and the system response [61].

On the contrary, the SMC is a nonlinear control method that alters the system dynamics applying a discontinuous signal that brings the system to work on a *sliding* surface, target of the control system. For this application, a continuous controller based on the measurements at the test rig is supported by the discontinuous action of the SMC to compensate the uncertainties.

Referring to the subjective analysis, an interesting point is the planning of a more complete and extended driver's campaign. The promising results obtained with the test driver could be verified with a larger group of people with different driving preparation.

Similar considerations have to be done about the activity on the inverted model: for strategic reasons of the company, there was only the possibility to virtually validate the process. Despite the good premises, there is anyway the necessity to plan an experimental campaign to evaluate the effectiveness of the proposed method at the test rig.

As fourth point, the positive outcomes could encourage the structural modification of the layout to integrate the vertical movement of the wheels. An increment of the performances is not sure, due to the higher level of complexity, but some additional investigations could assure this idea.

Furthermore, as mentioned above, this project brings contributions related to the methodology, therefore another interesting future activity could consider the extension of the method to other areas of the vehicle, for a larger and more complete validation.

Acknowledgements

This long journey has revealed that continuous discussions and ideas sharing are crucial for a personal and professional growth, therefore I wish to thank all the people I met and who have given me a precious contribution.

First and foremost I would like to express my sincere gratitude to Prof. R. Capitani for the incredible opportunity conceded and the wise help. I also want to thank Ph.D. Ing. C. Annicchiarico for the technical and personal support, and the fruitful discussions and exchange of ideas we had.

A deserved thanks to the doctoral committee for the feedback and help to define a strong research path. Additionally, I want to give my personal thanks to Prof. Gobbi and Prof. Guiggiani, reviewers of my dissertation, for their availability and their precious comments to improve the document's quality.

A special thanks to Danisi Engineering that supported the activity and made the static driving simulator available to me for this project.

Finally, a very special thought to all the former and current colleagues: Amedeo, Cesare, Lorenzo and especially Tommaso, continuous source of inspiration during technical discussions.

References

[1] I. Riches, "Electronic steering system market development EPS dominates growth", www.strategyanalytics.com, 2011.

[2] Y. Jiang, W. Deng, S. Zhang, and H. Zheng, "Modeling and verification of steering torque feedback system for driving simulator", *17th International IEEE Conference on Intelligent Transportation Systems (ITSC)*, 2014.

[3] J. Kale, S. Kumar, P. Lavangare, and A. Subramaniam, "Development of Road to Lab Steering Test Rig (ROLAST) ", *SAE Technical Paper Series*, 2017.

[4] L. Nehaoua, A. Marouf, J. J. Santin, P. Pudlo, and M. Djemai, "Towards An Electrical Power-Assisted Steering Simulator : Modeling Specifications", *IFAC Proceedings*, 2010.

[5] L. Yu, H. Zheng, and C. Zong, "The Design of Electrically Controlled Steering System Hardware-In-the-Loop Test Bench", *SAE Technical Paper Series*, 2014.

[6] F. Vinattieri, T. Wright, R. Capitani, C. Annicchiarico, and G. Danisi, "Target setting and structural design of an EPS-in-the-Loop test bench for steering feeling simulation", *SAE Technical Paper Series*, 2016.

[7] F. Vinattieri, L. Morrocchi, R. Capitani, and C. Annicchiarico, "Sviluppo di un'apparecchiatura sperimentale per l'integrazione del sistema di sterzo in un simulatore di guida statico", *Proceedings of the 46th Convegno Nazionale AIAS*, 2017 (in Italian).

[8] M. Harrer and P. Pfeffer, Eds., *Steering Handbook*, Cham: Springer International Publishing, 2017.

[9] M. Harrer, "Steering System Development in Premium Car Segment", *SAE Technical Paper Series*, 2006.

[10] H. H. Braess, "Steering System, Steering System Properties, Vehicle Dynamics-The Progress of the Last 50 Years, an Outlook into the Future", *VDI Berichte*, 2001.

[11] E. Fiala, *Mensch und Fahrzeug*. Springer - Verlag, 2006 (in German).

[12] S. Grüner, T. Werner, and B. Käpernick, "Objectification of steering feel and application in the context of virtual steering feel tuning", *Proceedings of 8th International Munich Chassis Symposium,* 2017.

[13] M. Decker, "Zur Beurteilung der Querdynamik von Personenkraftwagen", Ph.D. dissertation, TU Münch (Germany), 2009 (in German).

[14] H. J. Wolf, "Ergonomische Untersuchung des Lenkgefühls an Personenkraftwagen", Ph.D. dissertation, TU Münch (Germany), 2010 (in German).
[15] G. Gil Gómez, "Towards efficient vehicle dynamics development: From subjective assessments to objective metrics, from physical to virtual testing", Ph.D. dissertation, Kungliga tekniska högskolan (Sweden), 2017.
[16] M. Harrer, "Characterisation of steering feel", Ph.D. dissertation, University of Bath (United Kingdom), 2007.
[17] K. D. Norman, "Objective Evaluation of On-Center Handling Performance", *SAE Technical Paper Series*, 1984.
[18] M. Rothhämel, J. IJkema, and L. Drugge, "A method to find correlations between steering feel and vehicle handling properties using a moving base driving simulator", *Vehicle System Dynamics*, 2011.
[19] Y. Jiang, W. Deng, S. Zhang, S. Wang, Q. Zhao, and B. Litkouhi, "Studies on Influencing Factors of Driver Steering Torque Feedback", *SAE Technical Paper Series*, 2015.
[20] M. Schlager, *Hardware-in-the-loop simulation of real-time systems*, VDM Verl. Müller, 2008.
[21] M. Bacic, "On hardware-in-the-loop simulation," *Proceedings of the 44th IEEE Conference on Decision and Control*, 2005.
[22] P. E. Pfeffer, "Interaction of vehicle and steering system regarding on-centre handling", Ph.D. dissertation, University of Bath (United Kingdom), 2006.
[23] *ISO 13674:2016 - Road vehicles — Test method for the quantification of on-centre handling*, International Organization for Standardization, Geneva, Switzerland, 2016
[24] J. Kim, "Objectification of on-center handling characteristics based on spring-mass-damper system", *International Journal of Automotive Technology*, 2011.
[25] P. E. Pfeffer, M. Harrer and D. Johnston, "Interaction of vehicle and steering system regarding on-centre handling", *Vehicle System Dynamics*, 2008.
[26] K. T. R. van Ende, F. Küçükay, R. Henze, F. K. Kallmeyer, and J. Hoffmann, "Vehicle and steering system dynamics in the context of on-centre handling", *International Journal of Automotive Technology*, 2015.
[27] A. Balachandran and J. C. Gerdes, "Designing Steering Feel for Steer-by-Wire Vehicles Using Objective Measures", *IEEE/ASME Transactions on Mechatronics,* 2015.
[28] *ISO 3888-1:1999 - Passenger cars -- Test track for a severe lane-change manoeuvre -- Part 1: Double lane-change*, International Organization for Standardization, Geneva, Switzerland, 1999
[29] *ISO 7401:2003 Road vehicles - Lateral transient response test methods - Open-loop test methods*, International Organization for Standardization, Geneva, Switzerland, 2003.
[30] *ISO 8855:2011 - Road vehicles — Vehicle dynamics and road-holding ability — Vocabulary*, International Organization for Standardization, Geneva, Switzerland, 2011.

[31] F. Gustafsson, "Determining the initial states in forward-backward filtering", *IEEE Transaction Signal Processing,* 1996.
[32] F. Ambrogi, F. Cianetti, L. Fabellini, and V. Formica, "Sviluppo e validazione di un modello semplificato di sterzo automobilistico", *Proceedings of the 45th Convegno Nazionale AIAS*, 2016 (in Italian).
[33] F. Ambrogi, F. Cianetti, L. Fabellini, and V. Formica, "Definizione e verifica di una tecnica di identificazione sperimentale di sterzi", *Proceedings of the 45th Convegno Nazionale AIAS*, 2016 (in Italian).
[34] U. Neureder, "Investigation into steering wheel nibble", *Proceedings of the Institution of Mechanical Engineers, Part D: Journal of Automobile Engineering,* 2002.
[35] T. Dietz, "Model-based Friction Compensation for the Furuta Pendulum using the LuGre Model", MSc thesis dissertation, University of Lund (Sweden), 2006.
[36] Y. F. Liu, J. Li, Z. M. Zhang, X. H. Hu, and W. J. Zhang, "Experimental comparison of five friction models on the same test-bed of the micro stick-slip motion system", *Mechanical Sciences,* 2015.
[37] T. Piatkowski, "Dahl and LuGre dynamic friction models — The analysis of selected properties", *Mechanism and Machine Theory,* 2014.
[38] D. D. Rizos and S. D. Fassois, "Friction Identification Based Upon the LuGre and Maxwell Slip Models"*, IEEE Transactions on Control Systems Technology,* 2009.
[39] S. Zschäck, S. Büchner, A. Amthor, and C. Ament, "Maxwell Slip based adaptive friction compensation in high precision applications", *IECON 2012 - 38th Annual Conference on IEEE Industrial Electronics Society,* 2012.
[40] V. Lampaert, F. Al-Bender, and J. Swevers, "A generalized Maxwell-slip friction model appropriate for control purposes", *Physics and Control, Proceedings of IEEE International Conference*, 2003.
[41] C. C. De Wit, H. Olsson, K. J. Astrom, and P. Lischinsky, "A new model for control of systems with friction", *IEEE Transaction on Automatic Control*, 1995.
[42] K. Johanastrom and C. Canudas-de-Wit, "Revisiting the LuGre friction model", *IEEE Control Systems*, 2008.
[43] I. J. M. Besselink, A. J. C. Schmeitz, and H. B. Pacejka, "An improved Magic Formula/Swift tyre model that can handle inflation pressure changes", *Vehicle System Dynamics*, 2010.
[44] E. G. Papadopoulos and G. C. Chasparis, "Analysis and Model-Based Control of Servomechanisms With Friction", *Journal of Dynamic Systems, Measurement and Control,* 2004.
[45] M. Gobbi, G. Mastinu, and G. Previati, "A method for measuring the inertia properties of rigid bodies", *Mechanical Systems and Signal Processing*, 2011.
[46] R. Kloepper and M. Okuma, "Experimental identification of rigid body inertia properties using single-rotor unbalance excitation", *Proceedings of the Institution of Mechanical Engineers, Part K: Journal of Multi-body Dynamics*, 2009.

[47] R. A. B. Almeida, A. P. V. Urgueira, and N. M. M. Maia, "Identification of rigid body properties from vibration measurements", *Journal of Sound and Vibration,* 2007.
[48] G. Legnani, M. Tiboni, R. Adamini, and D. Tosi, *Meccanica degli azionamenti*, Società Editrice Esculapio, 2016 (in Italian).
[49] M. R. Popovic and A. A. Goldenberg, "Friction diagnostics and modeling using DFT analysis", *Proceedings of International Conference on Robotics and Automation*, 1997.
[50] D. Putra, L. Moreau, and H. Nijmeijer, "Observer-based compensation of discontinuous friction", *43rd IEEE Conference on Decision and Control (CDC),* 2004.
[51] R. W. Daniel, "Control of machines with friction: Brian Armstrong-Hélouvry", *Automatica*, 1992.
[52] S. T. Godley, T. J. Triggs, and B. N. Fildes, "Driving simulator validation for speed research", *Accident Analysis & Prevention*, 2002.
[53] B. Bona and M. Indri, "Friction Compensation in Robotics: an Overview", *44th IEEE Conference on Decision and Control (CDC) and European Control Conference (ECC), 2005.*
[54] P. Bolzern, R. Scattolini, and N. Schiavoni, *Fondamenti di controlli automatici*, McGraw-Hill Education, 2015 (in Italian).
[55] R. Davis, K. Lii and D. Politis, "Remarks on Some Nonparametric Estimates of a Density Function", *Selected Works of Murray Rosenblatt*, 2011.
[56] J. Dang, H. Chen, Q. Li, T. Watanabe, R. Hayama, and L. Lou, "A method to set the target on-centre steering force characteristic", *Proceedings of the Institution of Mechanical Engineers, Part D: Journal of Automobile Engineering*, 2016.
[57] J. Black, E. Iyasere, and J. Wagner, "Creation of a driver preference objective metric to evaluate ground vehicle steering systems", *American Control Conference (ACC),* 2011.
[58] J. Pelikan, P. Steinbauer, M. Valasek, and J. Ulehla, "Correlation of objective and subjective evaluation of vehicle handling by neural networks", *Bulletin of Applied Mechanics*, 2011.
[59] J. Black, P. T. Freeman, J. R. Wagner, E. Iyasere, D. M. Dawson, and F. S. Switzer, "Evaluation of driver steering preferences using an automotive simulator", *International Journal of Vehicle Design*, 2014.
[60] *J1441: Subjective Rating Scale for Vehicle Ride and Handling*, Vehicle Dynamics Standards Committee, SAE International, 2016.
[61] F. Borrelli, A. Bemporad, and M. Morari, *Predictive control for linear and hybrid systems*, Cambridge University Press, 2017.
[62] W. F. Milliken and D. L. Milliken, *Race car vehicle dynamics*, Society of Automotive Engineers, 1995.
[63] H. B. Pacejka, *Tire and vehicle dynamics*, Elsevier Science, 2012.
[64] M. Guiggiani, *The science of vehicle dynamics: handling, braking, and ride of road and race cars*, Springer Science & Business Media, 2014.

[65] M. Schlager, R. Obermaisser, and W. Elmenreich, "A Framework for Hardware-in-the-Loop Testing of an Integrated Architecture", *Software Technologies for Embedded and Ubiquitous Systems*, 2007.

[66] B. Heißing and M. Ersoy, *Chassis Handbook Fundamentals, Driving Dynamics, Components, Mechatronics, Perspectives*, Springer Science & Business Media, 2011.

[67] B. A. M. van Daal, "Friction and compliance identification in a vehicle's steering system", *Extern Traineeship Report Eindhoven,* 2007.

[68] E. Ueda, E. Inoue, Y. Saki, M. Hasegawa, H. Takai, and S. Kimoto, "The development of detailed steering model for on-center handling simulation", *Proceedings of the International Symposium on Advanced Vehicle Control (AVEC)*, 2002.

[69] A. Wohnhaas and U. Essers, "Nonlinear modeling and simulation of a rack and pinion steering", *Proceedings of International Symposium on Advanced Vehicle Control*, 1992.

[70] M. H. Lee, S. K. Ha, J. Y. Choi, and K. S. Yoon, "Improvement of the steering feel of an electric power steering system by torque map modification", *Journal of Mechanical Science and Technology*, 2005.

[71] V. D. Mills and J. R. Wagner, "Behavioural modelling and analysis of hybrid vehicle steering systems", *Proceedings of the Institution of Mechanical Engineers, Part D: Journal of Automobile Engineering*, 2003.

[72] S. Sugita, M. Tomizuka, and A. El-Shaer, "Human-machine interaction in vehicle steering", *SAE Technical Paper Series*, 2009.

[73] P. E. Pfeffer, M. Harrer, and D. N. Johnston, "Interaction of vehicle and steering system regarding on-centre handling", *Vehicle System Dynamics*, 2008.

Appendix A

Testing manoeuvers

1. Double Lane Change – Severe Double Lane Change

This two maneuvers, both defined in [28] (Double Lane Change : 3888-1, Severe Double Lane Change: 3888-2), are similar with the exception of the longitudinal speed and the path followed by the vehicle, which characterized the intensity. The different trajectories are illustrated in Figure 86 where it might be seen the disposition of the cones on the track: the path is composed of three straight legs. The first and the last ones are aligned, while the second one is shifted aside as a function of the vehicle width.

ISO norm requires the vehicle starts the test at a constant speed on a straight direction. Once the first gate of the path is reached, the driver fixes the throttle position and acts the steering wheel to maintain the vehicle among the cones. Therefore, this is a closed-loop test, where the driver affects the results. All the tests are performed with different longitudinal speeds: from 50 to 200 kph.

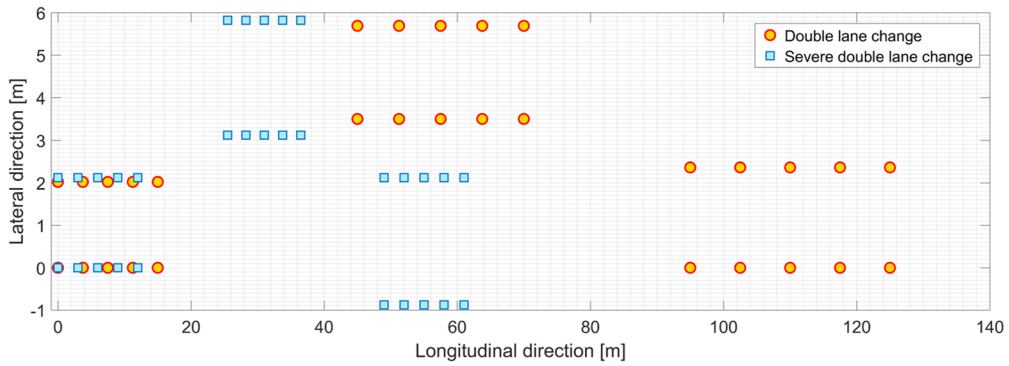

Figure 86 – Double lane change & Severe double lane change path

2. Sine sweep

Sine sweep manoeuver is an open-loop test: once the desired vehicle speed is reached, the throttle valve is set and the steering wheel follows a sinusoidal profile with a constant amplitude and an increasing frequency. Normally, the frequency ranges from 0.2 Hz to 2 Hz (for passenger cars) and up to 4 Hz for high performance cars [29].

Figure 87 shows the steering wheel profile of one test analysed: it is evident that the manoeuvers were not done using a steering robot (that is a common procedure) because the amplitude varies and the frequency rate has an oscillation. However, the variation is within the range considered as acceptable.

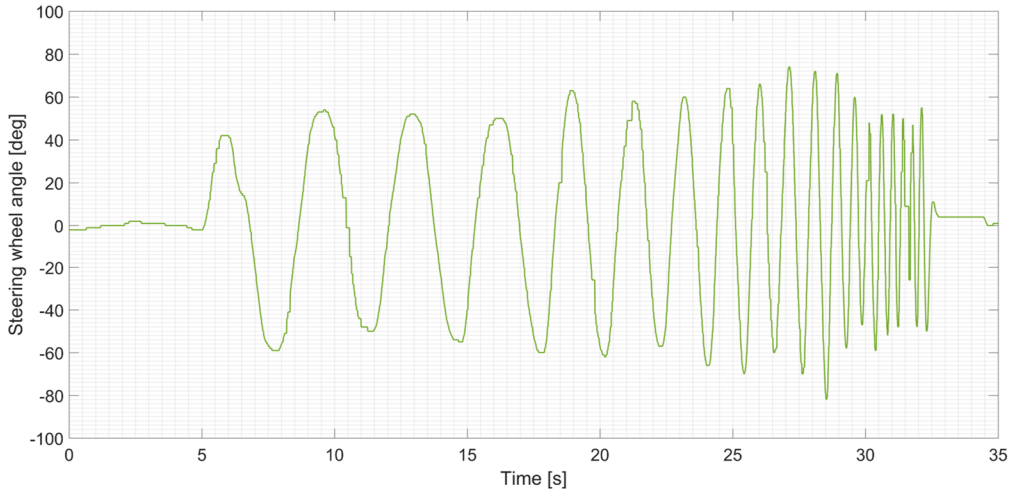

Figure 87 – Steering wheel profile in sine sweep manoeuver

3. Step steer

This represents a second open-loop manoeuver, widely used to characterize the transient behaviour of road vehicles. As the previous one, this is described by ISO 7401 [29]. The initial conditions are the same: the vehicle is brought to a specified level of longitudinal velocity with straight-ahead steer position.

When the starting line is reached, the driver executes the manoeuver keeping the accelerator pedal fixed and acting on the steering wheel to follow a quick step profile. The final value is established to achieve a desired level of lateral acceleration in steady-state in the steady-state conditions. Often, it is used as an alternative to slow ramp steer test, to characterize the steady-state behaviour using the values acquired after the transient phase. Indeed, when a steer robot is not available, the step steer tests are more feasible for test drivers.

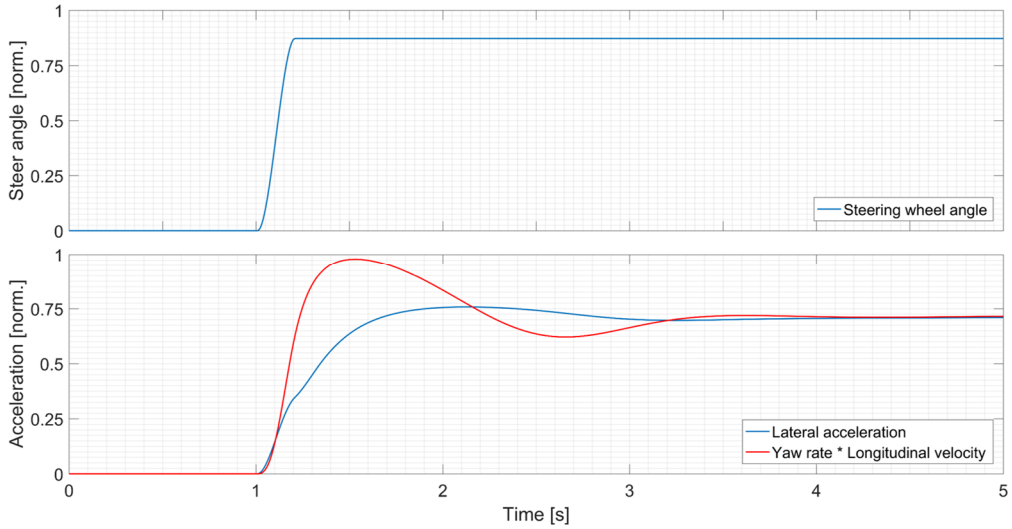

Figure 88 – Step steer manoeuver

Appendix B

The purpose of this appendix is the detailed description of the relations that characterized the advanced steering model proposed by prof. P. Pfeffer. As mentioned, the model has five degrees of freedom and it is divided in two main part: the mechanical and the hydraulic one.

The mechanical part is described by the following system of equations (here in matrix format).

$$\begin{pmatrix} I_1 & 0 & 0 & 0 & 0 \\ 0 & I_2 & 0 & 0 & 0 \\ 0 & 0 & I_3 & 0 & 0 \\ 0 & 0 & 0 & I_4 & 0 \\ 0 & 0 & 0 & 0 & I_5 \end{pmatrix} \begin{pmatrix} \ddot{\theta}_1 \\ \ddot{\theta}_2 \\ \ddot{\theta}_3 \\ \ddot{\theta}_4 \\ \ddot{\theta}_5 \end{pmatrix} + \begin{pmatrix} c_a + c_b & -c_b & 0 & 0 & 0 \\ -c_b & c_b + c_c & -c_c & 0 & 0 \\ 0 & -c_c & c_c + c_d & -c_d & 0 \\ 0 & 0 & -c_d & c_d + c_e & -c_e \\ 0 & 0 & 0 & -c_e & c_e + c_f \end{pmatrix} \begin{pmatrix} \dot{\theta}_1 \\ \dot{\theta}_2 \\ \dot{\theta}_3 \\ \dot{\theta}_4 \\ \dot{\theta}_5 \end{pmatrix} + \begin{pmatrix} k_a + k_b & -k_b & 0 & 0 & 0 \\ -k_b & k_b + k_c & -k_c & 0 & 0 \\ 0 & -k_c & k_c + k_d & -k_d & 0 \\ 0 & 0 & -k_d & k_d + k_e & -k_e \\ 0 & 0 & 0 & -k_e & k_e + k_f \end{pmatrix} \begin{pmatrix} \theta_1 \\ \theta_2 \\ \theta_3 \\ \theta_4 \\ \theta_5 \end{pmatrix} = \begin{pmatrix} M_s + F_1 \\ F_2 \\ F_3 \\ F_4 \\ M_R + M_A + F_5 \end{pmatrix} \tag{22}$$

where:

I_i	= inertia of i-th body
θ_i	= rotation angle of the i-th body
c_a, c_f	= damping coefficient between the first/last body and a fixed frame of reference
$c_b - c_e$	= damping coefficient among the bodies
k_a, k_f	= stiffness between the first/last body and a fixed frame of reference
$k_b - k_e$	= stiffness among the bodies
M_s	= torque applied at the steering wheel
M_A	= assist torque
M_R	= resisting torque from the tires
F_i	= friction force on the i-th body.

The following equations characterize the hydraulic system, where (23) is the turbulent flow for the right chamber. This describes the difference between the reference quasi-static value of pressure and the actual value considering the liquid flow. This, together with (24) that describes the compressibility, leads to (25), which describes the real pressure profile as a function of time.

The total assistance force acting on the rack is the result obtained integrating equation (25) both for the right and left chambers, calculating the difference and multiplying the value for the piston area.

$$|p_{r_s} - p_r| = \frac{\rho}{2}\left(\frac{Q_r}{C^* A_0}\right)^2 \tag{23}$$

$$\frac{V}{\beta_f}\frac{\mathrm{d}p_r}{\mathrm{d}t} = Q_r - Q_{out} = Q_r - \dot{s_r} A_p \tag{24}$$

$$\frac{\mathrm{d}p_r}{\mathrm{d}t} = \frac{\beta_f}{V}\left(\mathrm{sgn}(p_{r_s} - p_r) C \sqrt{\frac{2A}{\rho}|p_{r_s} - p_r|} - \dot{s_r} A_p\right) \tag{25}$$

To conclude, it is interesting to notice how in the final equation (25) appears C and A in the place of C^* and A_0 of (23). Indeed, these formulations are equivalent if (26) is valid: it is convenient because a generic area can be used in the place of the actual section of the valve, whose value is often not available.

$$\sqrt{C^* A_0} = C\sqrt{A} \tag{26}$$

where:

Q_r = right chamber flow rate
p_r = right chamber pressure
p_{r_s} = right chamber static pressure (reference value)
ρ = liquid density
A_0 = valve section area
C^* = scaling factor
V = right chamber volume
β_f = liquid bulk modulus
$\dot{s_r}$ = rack velocity
A_p = piston area.

As an evidence of the good functioning of the system, Figure 89 describes a test presented in [39]. It is a micro-weave test at 120 kph with steering wheel angle of 5 deg and steering frequency of 0.5 Hz.

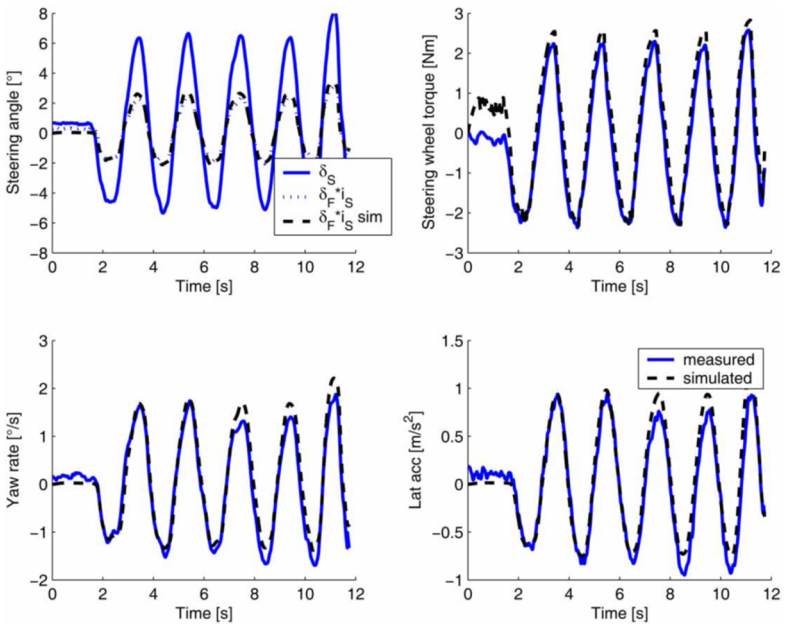

Figure 89 – Micro-Weave test - top left: simulation input steering wheel angle δ_s; measured and simulated mean steering angle at front wheels δ_S times overall steering ratio. Figure on the bottom right proves the good correlation between the simulated model and the actual results [73]

Appendix C

This appendix describes the structure of the two degrees of freedom model introduced in chapter 3.

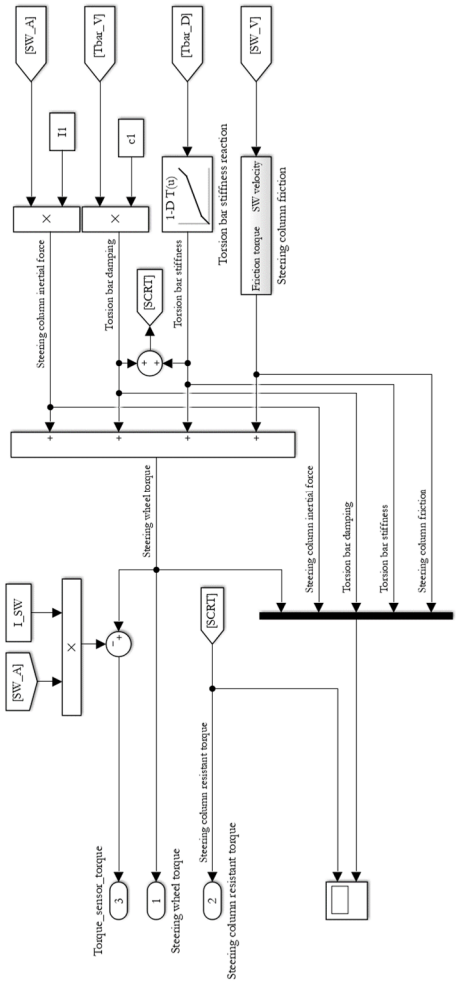

Figure 90 – First body equation

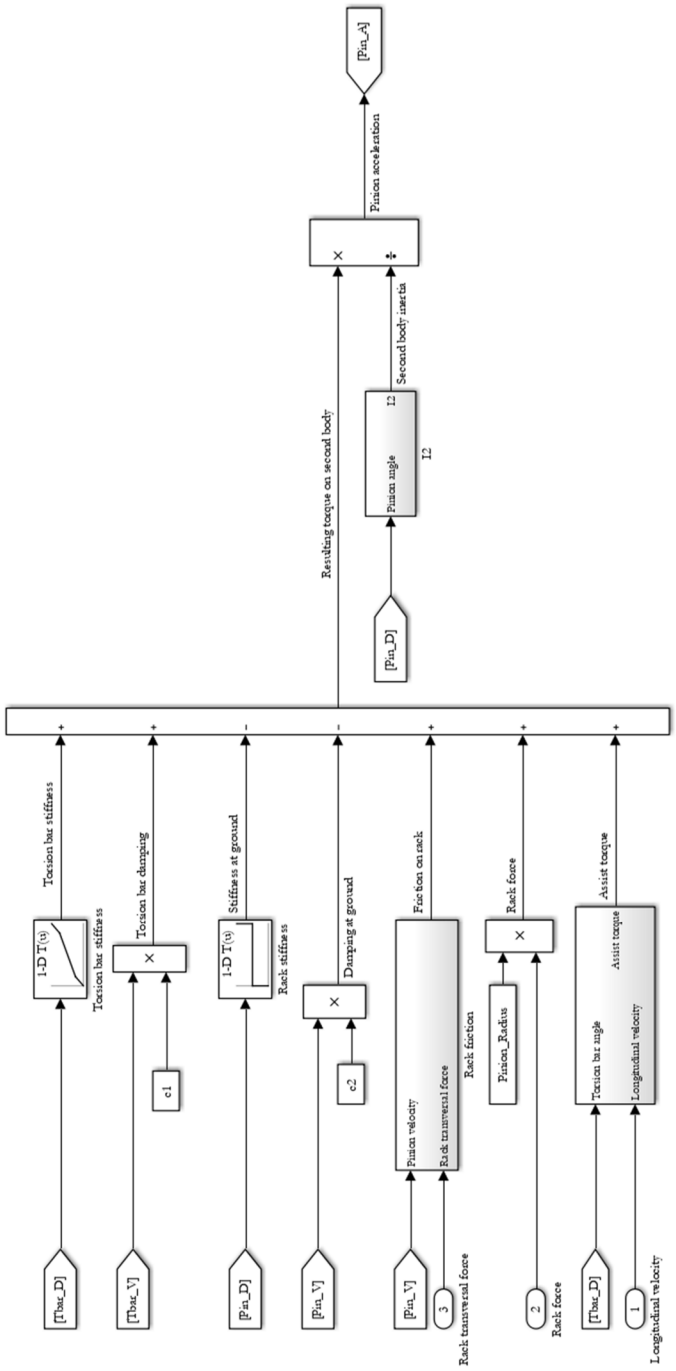

Figure 91 – Second body equation

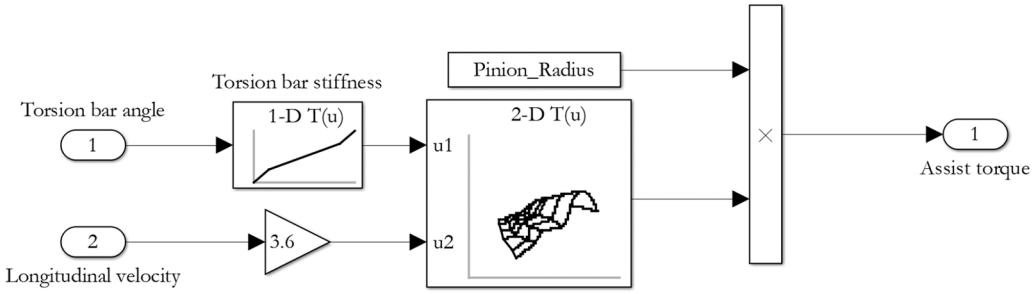

Figure 92 – Assist pressure module

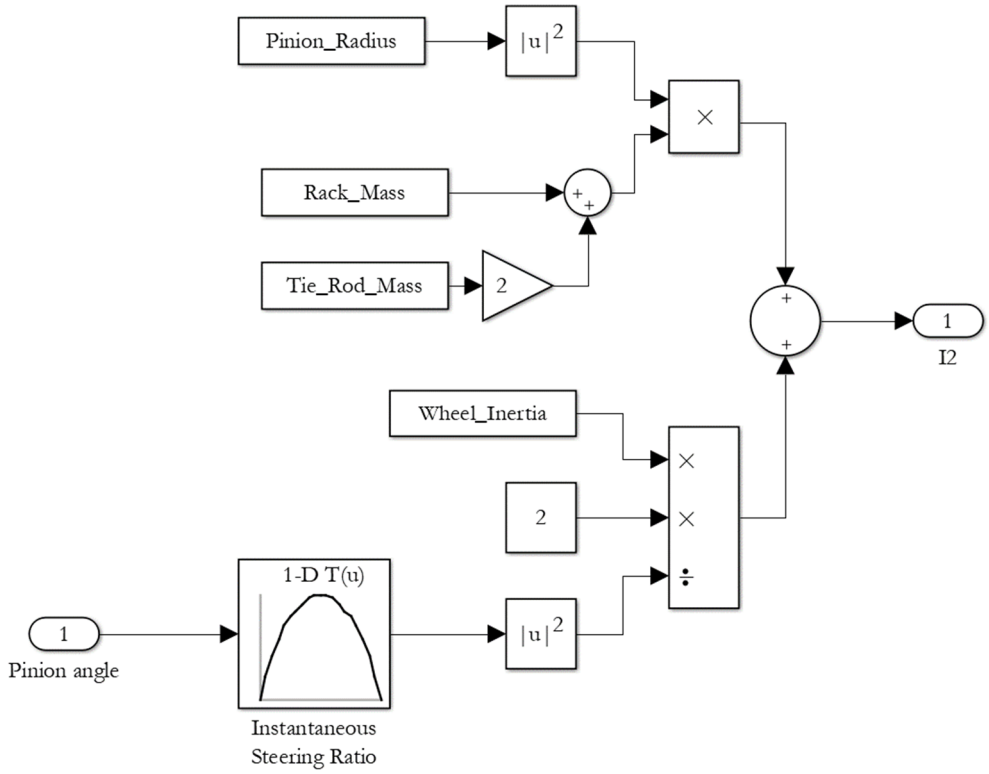

Figure 93 – Second body inertia

Appendix D

This appendix is dedicated to the description of the main sensor used on EPSiL.

- **Tie rod load cell**

Nominal force (kN)	20
Nominal output (mV/V)	1.5
Actual sensitivity $(kN/(mV/V))$	13.26
Linearity error (%)	0.06
Standard deviation (%)	0.02

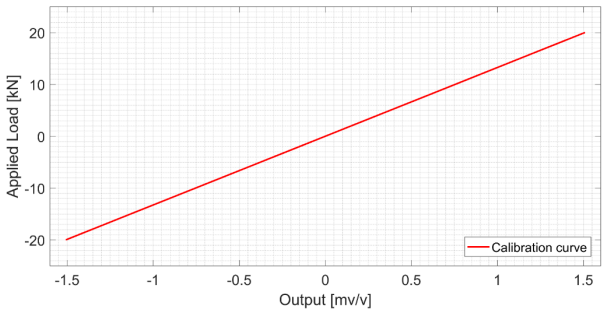

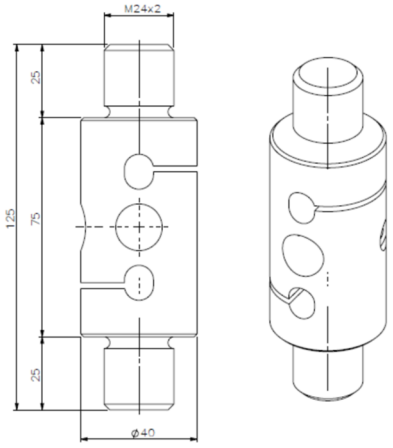

- **Measurement Steering Wheels**

Measurement frequency (Hz)	1000
Torque range (Nm)	$\pm$ 50
Torque accuracy (% FSO)	$\pm$ 0.15
Torque linearity deviation (% FSO)	$\pm$ 0.15
Angle range (deg)	$\pm$ 1250
Speed range (deg/s)	$\leq$ 2000
Angle resolution (deg)	0.015
Angle accuracy (deg)	$\pm$ 0.1

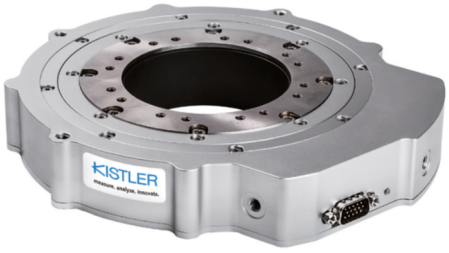

- **Rack position optical sensor**

Sampling rate (kHz)	$\leq$ 8
Measurement range (mm)	$\leq$ 350
Resolution (mm)	0.1
Linearity (%)	$\pm$ 0.2
Light source	Laser
Analogue output (V)	0 ÷ 10